2017

Reconstructing Coastal Forest Retreat and Marsh Migration Response to Historical Sea Level Rise

Nathalie Schieder
College of William and Mary - Virginia Institute of Marine Science, nathalie.schieder@freenet.de

Reconstructing coastal forest retreat and marsh migration response to historical sea level rise

A Thesis

Presented to

The Faculty of the School of Marine Science

The College of William and Mary in Virginia

In Partial Fulfillment

of the Requirements for the Degree of

Master of Science

by

Nathalie Wilhelmine Schieder

January 2018

APPROVAL PAGE

This thesis is submitted in partial fulfillment of

the requirements for the degree of

Master of Science

Nathalie Wilhelmine Schieder

Approved by the Committee, December 2017

Matthew L. Kirwan, Ph.D.
Committee Chair / Advisor

Christopher J. Hein, Ph.D.

William Reay, Ph.D.

James E. Perry, III, Ph.D.

TABLE OF CONTENTS

ACKNOWLEDGEMENTS

First, I would like to thank my advisor, Dr. Matthew Kirwan, for his outstanding advice, guidance and enthusiasm during my time at VIMS. Thank you for your endless support and encouragement, not only as a scientist but also as a person. I would also like to thank my committee members Dr. Christopher Hein, Dr. James Perry, and Dr. William Reay for their critique, discussions and advice throughout this project. You helped me a lot to successfully finish my project.

A special thank you to the members of my lab group, Ellen Herbert, Dan Coleman, Orencio Duran, David Walters, Tyler Messerschmidt, Josh Himmelstein, and David Nicks who helped me a lot with my field and lab work, and data analyses. Thank you for your patience when I struggled with language or cultural differences. I couldn't have felt more at home and welcomed.

I would like to thank Derek Loftis, David Wilcox, Madison Clapsaddle, VIMS Center for Coastal Resources Management and VIMS Shoreline Studies Programs, and the Chesapeake Bay National Estuarine Research Reserve System for assistance with GIS analyses. I would also like to thank Rebecca Harrison, Pete Campbell, and Michelle Chappell for helping me to organize my field work. A special thank you to Lennert Schepers, Dr. Benjamin Poulter, and Doug Newcomb for sending me historic aerial images that I could not have found without their help. I would like to thank Dr. Robert Young and Dr. Martin Rabenhorst for their guidance in finding transect locations.

I would especially like to thank my close friends and boyfriend for supporting me throughout my time at VIMS and for giving me place to be myself. You reminded to take a break and rest sometimes, and you made me fall in love with the U.S., Gloucester, and VIMS. Thank you for many beautiful hours that I got to spend with you.

Finally, I would especially like to thank my parents who always supported me and all of my decisions, even though we were thousands of miles apart. I would not be here if you hadn't encouraged me to always be the best of myself. Also, a special thank you to my sister who spent hours teaching me about presentations, and never hesitated to give me advice and support in every stage of my life. Thank you for your continuous support and love.

LIST OF TABLES

LIST OF FIGURES

CHAPTER 1:

CHAPTER 2:

THESIS ABSTRACT

Climate change assessments predict that rates of relative sea level rise will increase in the future, leading to enhanced inundation of low-lying coastal regions and a 20 – 50 % decline in salt marsh area by 2100. Global sea level rise began accelerating in the late 19th to early 20th century, and local rates along the U.S. mid-Atlantic coast are twice as fast as global estimates. Frequent flooding and salt stress associated with sea level rise lead to coastal transgression, and the survival of ecosystems depends on their ability to migrate inland faster than they erode and submerge. Here, I compared aerial imagery analyses and field measurements to test the hypothesis that marsh migration into retreating terrestrial forests is fundamentally tied to sea level rise, and that sea level rise does not necessarily lead to overall habitat loss.

For my first chapter, I compared the areal salt marsh extent between historical topographic maps and modern aerial imageries across the entire Chesapeake Bay, and found that marsh migration into terrestrial forests largely compensated for marsh erosion at the seaward edge during the last century. This emphasizes that the location of coastal ecosystems changes rapidly on centennial timescales, and that sea level rise does not necessarily lead to overall habitat loss. For my second chapter, I reconstructed the position of coastal treelines through time at five study sites along the U.S. mid-Atlantic coast to identify long- and short- term drivers of coastal forest retreat. My findings suggest that 20th century migration rates greatly exceed pre-industrial rates (< 1875 CE), and have generally accelerated throughout the last century in parallel with accelerating rates of relative sea level rise.

Previous work predicts widespread marsh loss as a response to sea level rise, but underestimates the potential for marshes to migrate inland. Although anthropogenic barriers may locally prevent marsh migration into retreating coastal forests, my work finds that about 400 km^2 (100,000 acres) of uplands have converted to marshes in the Chesapeake region since the late 1800s, and that this process was responsible for the formation of about 1/3 of all marsh area. Beyond the Chesapeake, my work reveals that forest retreat is fundamentally tied to the rate of sea level rise, and is accelerating through time. Therefore, management efforts that allow marshes to migrate into adjacent uplands may help preserve marshes by exploiting their ability to quickly adapt to environmental change.

Reconstructing coastal forest retreat and marsh migration response to historical sea level rise

CHAPTER 1

Massive upland to wetland conversion compensated for historical marsh loss in Chesapeake Bay, USA[1]

[1] Published as

Schieder, N.W., D.C. Walters, and M.L. Kirwan. 2018. Massive upland to wetland conversion compensated for historical marsh loss in Chesapeake Bay, USA. *Estuaries and Coasts.* In press. https://doi.org/10.1007/s12237-017-0336-9.

ABSTRACT

Sea level rise leads to coastal transgression, and the survival of ecosystems depends on their ability to migrate inland faster than they erode and submerge. We compared marsh extent between 19th century maps and modern aerial photographs across the Chesapeake Bay, the largest estuary in North America, and found that Chesapeake marshes have maintained their spatial extent despite relative sea level rise rates that are among the fastest in the world. In the mapped region (i.e. 25 % of modern Chesapeake Bay marshland), 94 km^2 of marsh was lost primarily to shoreline erosion, whereas 101 km^2 of marsh was created by upland drowning. Simple projections over the entire Chesapeake region suggest that approximately 400 km^2 (100,000 acres) of uplands have converted to wetlands, and that about a third of all present-day marsh was created by drowning of upland ecosystems since the late 19th century. Marsh migration rates were weakly correlated with topographic slope and amount of development of adjacent uplands, suggesting that additional processes may also be important. Nevertheless, our results emphasize that the location of coastal ecosystems changes rapidly on century timescales, and that sea level rise does not necessarily lead to overall habitat loss.

INTRODUCTION

Sea level rise leads to coastal transgression, and the survival of ecosystems depends on their ability to migrate inland faster than they erode and submerge (Brinson et al. 1995; FitzGerald et al. 2008; Curray 2016). Global sea level rise rates began accelerating sharply in the late 19th or early 20th century, with an approximate tripling in sea level rise rates in the last 150 years in many parts of the world (Kemp et al. 2009; Church et al. 2013). Late 20th century relative sea level rise rates are 3-4 times higher along the U.S. mid-Atlantic coast than the global average due to changes in the Gulf Stream and spatial variability in subsidence (Ezer and Corlett 2012; Sallenger et al. 2012). When those changes exceed the ability of marshes and other coastal systems to adapt, ecosystems will be forced to migrate inland or submerge (Brinson et al. 1995; FitzGerald et al. 2008; Craft et al. 2009; Kirwan and Megonigal 2013). Accelerated sea level rise therefore threatens tidal marshes and other coastal environments, which are well known for ecosystem services such as carbon sequestration, storm protection, and nutrient transformation (Barbier et al. 2011).

Feedbacks between flooding, plant growth, and sediment deposition allow marshes to adapt to changes in sea level in the vertical dimension. Increases in flooding duration tend to enhance sediment deposition on the marsh surface, plant productivity, soil building, and marsh elevation gain (Reed 1995; Friedrichs and Perry 2001; Cahoon et al. 2006; Kirwan and Megonigal 2013; Kirwan et al. 2016a). However, the strength of this feedback depends fundamentally on the availability of mineral sediments, so that marshes in sediment deficient areas remain vulnerable to sea level rise (Kirwan et al. 2010; Day et al. 2011; D'Alpaos et al. 2012; Weston 2014). Marshes are fundamentally unstable in the lateral dimension, where erosion of marsh edges is a primary contributor to marsh loss even in the absence of sea level rise (Fagherazzi et al. 2013). Marsh erosion rates typically vary between ~0.1 - 3 m yr^{-1}, depending

on wave power, the elevation of marsh relative to water level, and vegetation-mediated soil strength (Schwimmer 2001; Mariotti and Fagherazzi 2010; Gedan et al. 2011; Fagherazzi et al. 2013; McLoughlin et al. 2015; Ford et al. 2016; Silliman et al. 2016). Accelerations in the rate of sea level rise potentially enhance erosion rates by increasing water depth, wave height, and the height of the marsh-tidal flat scarp (Mariotti and Fagherazzi 2010; Marani et al. 2011).

Marshes also respond to sea level rise by migrating inland and replacing terrestrial ecosystems (Brinson et al. 1995; Raabe and Stumpf 2016; Kirwan et al. 2016a). Progressive flooding leads to the development of wetland soils and vegetation (Hussein 2009; Anisfeld et al. 2017). In coastal forests, inundation and salt stress lead to seedling mortality so that forests do not regenerate following the death of adult trees during storms or other events (Clark 1986; Williams et al. 1999; Kirwan et al. 2007). These processes allow new marshes to form along a moving upland boundary as a function of the rate of sea-level rise and upland slope (Brinson et al. 1995; Hussein 2009; Smith 2013; Raabe and Stumpf 2016). Upland-to-wetland conversion has been described along the margin of many marshes throughout North America, and is thought to be important to future marsh survival at regional scales along the Gulf and mid-Atlantic coasts (Doyle et al. 2010; Feagin et al. 2010; Morris et al. 2012; Smith 2013; Raabe and Stumpf 2016; Clough et al. 2016; Enwright et al. 2016). However, steep topography and anthropogenic barriers commonly limit marsh migration in other places (Feagin et al. 2010; Kirwan and Megonigal 2013; Torio and Chmura 2013; Wasson et al. 2013; Enwright et al. 2016; Field et al. 2016).

The vulnerability of marshes to sea level rise therefore depends at least in part on the competition between erosion and migration, but it is unclear how the balance between these processes has changed historically, or will change under accelerated rates of sea level rise in the future. Previous work focuses largely on either erosion or migration alone, and suggests that both

processes may accelerate in parallel with sea level rise (Hussein 2009; Mariotti and Fagherazzi 2010; Kirwan et al. 2016b). Recent work along a portion of the Florida Gulf Coast suggests migration into uplands has exceeded historical erosion rates (Raabe and Stumpf 2016), and modeling proposes that marsh migration rates are more sensitive to sea level rise than edge erosion rates (Kirwan et al. 2016a). These observations suggest a counter-intuitive expansion of marshes with sea level rise along undeveloped coasts, but this idea remains largely untested, especially at regional scales with large human populations that may present barriers to migration. Here, we compare the extent of marshes from 19th century maps of the Chesapeake region to modern imagery, and find that marsh migration into adjacent uplands has allowed Chesapeake marshes to survive the fastest relative sea level rise rates on the Atlantic coast.

METHODS

Regional setting

This study concentrates on the marshes and low-elevation coastal region surrounding the Chesapeake Bay, the largest coastal-plain estuary in North America (Fig. 1). Chesapeake Bay is a classic, drowned river valley estuary, with microtidal tides, and a total watershed area of approximately 166,000 km^2 (Perry et al. 2001; Chesapeake Bay Program 2015). Marshes occupy about 1,200 km^2 of the Chesapeake region (Stevenson et al. 1985; Chesapeake Bay Program 2015), including approximately 20 % of the Chesapeake Bay shoreline (Rosen 1980). Typical vegetation communities in regularly flooded marshes include *Spartina alterniflora* and *Schenoplectus americanus*, and irregularly flooded marshes include *Spartina patens, Distichlis spicata,* and *Juncus romerianus.* Adjacent low-gradient uplands are dominated by *Pinus taeda*

and *Juniperus virginiana*, and the marsh-forest transition zone typically includes *Phragmites australis*, *Iva frutescens*, and *Myrica cerifera* (Perry et al. 2001; Kirwan et al. 2007).

Historical relative sea level rise rates in the Chesapeake Bay range between 3 and 6 mm yr^{-1} (http://tidesandcurrents.noaa.gov/sltrends/sltrends.html) and are about twice as fast as eustatic sea level rise rates as a result of subsidence (1.6 – 2.0 mm yr^{-1}) (Engelhart et al. 2009). Relative sea level rise in the Chesapeake Region has accelerated from 1 – 3 mm yr^{-1} in the 1930's to 4 – 10 mm yr^{-1} in 2011 due to climate warming, changes in ocean currents, and groundwater withdrawal (Ezer et al. 2012; Sallenger et al. 2012). Coastal ecosystems are rapidly transgressing in response to sea level rise, characterized by erosion of salt marsh edges, mortality of low elevation forests, and migration of marshes into adjacent uplands (Brinson et al. 1995; Hussein 2009).

Habitat mapping

To determine how the size and location of marshes in the Chesapeake region have responded to historical sea level rise, we compared the spatial distribution of marshes from 19th century era maps to modern aerial photographs (Fig. 2). We located 66, 1:20,000 scale NOS topographic sheets ("T-sheets") from the years 1846 to 1912 that included information on simple land types (e.g. marsh, farmland, forests) from the tidal portions of the Chesapeake Bay and its tributaries (NOAA Shoreline Website 2015). T-sheets from this time period were created by plane tables and focused on the coastline as well as its plane geometry (Shalowitz 1964). We discarded 26 maps that did not clearly distinguish between marsh and forested areas due to poor map quality, inconsistent symbology, and ambiguous treatment of forested wetlands. To build consistency between different standards of individual surveyors, we did not include maps with no clear

delineation between upland and marsh. We georeferenced each historical T-sheet to modern aerial photographs in ArcGIS by locating approximately 10 control points (e.g. road intersections, creeks) that were visible in both sets of images, and fitting with 1^{st} or 2^{nd} order polynomial. We calculated the root mean square error (RMSE) associated with georeferencing by calculating the distance between the same control points on historic and modern image sources, and discarded maps with RMSE greater than 15 m. Average RMSE of the remaining 40 maps was 6-7 m. This error is similar to that reported for T-sheets in previous work (Raabe and Stumpf 2016). The remaining historical maps represented all sections of the bay, though maps were most abundant in the southwestern portion of the bay (Fig. 1).

We compared the T-sheets with six-inch resolution orthoimagery from Maryland collected in 2013 (Eastern Shore of Chesapeake Bay) and 2014 (Western Shore) (Maryland's Mapping & GIS Data Portal) and orthoimagery from Virginia collected in spring 2013 (ArcGIS server gismaps.vita.virginia.gov). Tidal marshes were digitized by hand by tracing the boundary between marsh and open water and the boundary between marsh and upland. The marsh-forest boundary was identified as the line between the dense tree canopy and marsh, and the marsh-water boundary was identified as the line between open water and adjacent land excluding beaches. Because the resolution of the modern photographs was significantly better than the T-sheets, we delineated the modern marsh at the same scale as the historical T-sheets (1:20,000). This treatment eliminated interior ponds and many narrow (< 15 m) fringe marshes that were discernable along channels in modern imagery but not in the T-sheets. The minimum size of marshes and forest patches delineated on the T-sheets was about 350 m^2, and we were careful to delineate patches of similar minimum size on the modern imagery. This approach allows marsh delineation over large spatial scales, builds consistency between high-resolution modern imagery

and low-resolution historical maps, and ensures that measured changes in marsh area are not an artifact of changes in map quality.

Analytical methods

To summarize changes in marsh area through time, we calculated historic and modern marsh area for each T-sheet individually, where rates refer to the change in area divided by the number of years between 2013 and the year of the T-sheet. We derived linear rates of change by dividing the area of marsh change by the modern shoreline length, defined as the length of the water-marsh boundary for edge erosion rates, and the length of the marsh-forest boundary for migration rates. The shoreline length was calculated directly from previously established marsh polygons, and was therefore determined at the same scale (1:20,000) so that it included only large creeks (> 30 m wide). Finally, we summarized changes in marsh area across watersheds of the major river systems in the Chesapeake region defined by USGS HUC 4 watershed boundaries (USGS Watershed Boundary Dataset: http://nhd.usgs.gov/wbd.html). For portions of the watershed with overlapping T-sheets, we generally used the T-sheet with the lowest georeferencing error. Changes in marsh area by watershed were aggregated to determine total, bay-wide changes.

Our methods explicitly calculate areas of marsh gain and loss along the seaward and landward margins of the historic and modern marsh extent, and assume that positive changes in marsh area at the upland boundary are due to migration into retreating uplands, whereas negative changes in marsh area at the seaward boundary are due to marsh-edge erosion. Total net change in marsh size is calculated as the difference between the area of marsh migration and marsh shoreline erosion. Thus, our approach focuses on large-scale drivers of marsh gain and loss, rather than more subtle changes such as expansion of small, interior ponds. We tested these key

assumptions by re-mapping 4 randomly selected, but representative, map units in different portions of the Chesapeake region [T02957, T01534I, T00199, T00686 in Table 1]. For each map, we manually compared the causes of marsh loss and gain. On average, 96% of marsh gain resulted from marsh migration into adjacent uplands, whereas 4% resulted from progradation into open water. 98% of marsh loss resulted from marsh edge erosion, whereas 2% resulted from woody encroachment and conversion to anthropogenic land uses. Total marsh loss across the 4 map units did not depend on the spatial resolution of mapping (61.4 km^2 at 1:20,000; 62.8 km^2 at 1:1,000) because small interior ponding visible on the modern imagery was only responsible for about 2% of total marsh loss. Since the vast majority of marsh gain and loss was caused by migration and shoreline erosion, those terms are hereafter used interchangeably.

We characterized the slope and land cover of uplands within a 100 m buffer of delineated marshes in an effort to understand potential factors influencing rates of marsh migration. The slope of adjacent uplands was determined from digital elevation models derived from bare-earth LIDAR flown between 2010 and 2012 at a resolution of 2.5x2.5 ft (Virginia Lidar 2015) and between 2014 and 2015 at a resolution of 1x1 m (ESRGC 2015). For each pixel within the buffered upland region, we extracted elevation from the digital elevation model and used the Euclidean Distance tool in ArcGIS to determine distance from the modern marsh-upland boundary and then used linear regression to calculate an average upland slope. We used the NLCD 2011 Land Cover map (Multi-Resolution Land Characteristics Consortium 2016) to estimate potential anthropogenic barriers to marsh migration. Typical anthropogenic barriers to wetland migration in the Chesapeake region include roads, bulkheads, and small berms and revetments. These features are not consistently identifiable near the upland boundary, so we assume that the fraction of developed land is a proxy for anthropogenic barriers, where highly

developed land would have more extensive barriers to marsh migration. Landscape-scale models of marsh migration commonly assume that migration will only occur into forested uplands. Therefore, we defined developed uplands as land that was classified as urban or agricultural, and calculated the ratio of developed land to total land area within the buffered upland region. Rates of marsh migration were then compared to characteristics of the adjacent uplands (i.e. slope and degree of development) for each map, using linear and multiple regression.

RESULTS

The total extent of tidal marshes in the studied portion of the Chesapeake Bay region was nearly identical in 19th century historical maps and modern aerial photographs. The 19th century T-sheet maps included 311 km^2 of tidal marshes, and the same mapping area included 318 km^2 of marshes in 2013 (Table 1). Marsh area change at the marsh-water boundary was negative in each map unit (defined as the extent of individual T-sheets), indicating that erosion was greater than marsh progradation into open water, and is likely the dominant driver of marsh loss in our study (Table 1). Marsh area change at the marsh-upland boundary was positive in each map unit, indicating that marsh migration into uplands was greater than apparent woody encroachment into marshes that could potentially result from classification errors in the 19th century maps (Table 1). Marsh gain slightly exceeded loss in the James River and Eastern Shore watersheds, whereas loss slightly exceeded gain in the York River watershed (Fig. 3). Summed across the entire mapped area, new marsh created at the migrating upland edge (101 km^2) compensated for marsh loss at the marsh-water boundary (94 km^2), resulting in a total net marsh expansion of about 7 km^2 or 2% (Fig. 3). The total mapped area represents 24% of all marshes in the Chesapeake Bay and its tributaries (1,200 km^2 (Stevenson et al. 1985; Chesapeake Bay Program 2015)). The slope

of the upland topography within a 100 m buffer of marshes in the mapped area (0.03 ± 0.02) is similar to the slope of adjacent uplands in the entire Chesapeake region (0.05 ± 0.08), suggesting that our upland submergence rates may be generally representative. Therefore, simple projections across the entire Chesapeake region imply that more than 400 km^2 (100,000 acres) of uplands have converted to wetlands over the last century.

Despite little net change in marsh area summed across the entire Chesapeake region, net change in marsh extent differed widely between individual map units (Table 1). For example, a maximum loss of ~90% of marshes was observed for the Cape Charles, VA T-sheet extent, and a maximum gain of ~400% was observed for the Potomac River, MD T-sheet extent. 16 of 40 maps had marsh loss rates exceeding 10%, 15 maps had expansion rates exceeding 10%, and only 10 maps showed net change rates of less than 10%. The average rate of marsh migration for individual map units was 0.49 ± 0.36 m yr^{-1} (SD), with the highest migration rates occurring on the eastern shore of the Chesapeake Bay and the mouth of the York River (Fig. 4a). The lowest marsh migration rates appear along the Chesapeake tributaries and in the middle fractions of the bay. The average erosion rate was 0.53 ± 0.42 m yr^{-1} (SD), with the fastest rates peaking along the Rappahannock River as well as the Choptank River area and the lowest rates appearing along the eastern shore of Virginia and the Chickahominy River (Fig. 4b). In general, net marsh expansion occurred primarily in the southern part of the Chesapeake Bay, whereas marsh contraction occurred mostly in the mid and northern Bay and on islands with limited potential for marsh migration (Fig. 4c). These results are broadly consistent with previous work demonstrating marsh loss in the mid Bay (e.g. Stevenson et al. 1985; Kearney et al. 1988; Schepers et al. 2017), rapid erosion of Chesapeake Bay islands (Kearney and Stevenson 1991), and localized marsh expansion in the lower bay (Kirwan et al. 2016b).

Marsh migration rates were weakly correlated with characteristics of adjacent uplands. The average upland slope within 100 m of the modern marsh was 0.03 and varied between 0.004 and 0.1 between map units (Table 1). Low upland slopes were located along the eastern shore of Virginia (e.g. Nandua Creek map = 0.003), and the highest slopes were generally located near the heads of rivers (e.g. Choptank River map = 0.1). Simple linear regression indicated a weak relationship between rate of marsh migration and upland slope (r^2=0.16; $p<0.05$) (Fig. 5a).

The average land use within 100 m of the modern marsh was 41% forest, 26% urban, and 22% agriculture. Developed land (urban plus agriculture) averaged over individual map units ranged from 3% developed to 79% developed within the buffer. Simple linear regression indicated a weak relationship between marsh migration rate and the fraction of uplands developed (r^2= 0.09; p=0.05) (not shown), and that migration rate was weakly related to upland slope even in the most undeveloped uplands (development < 10%) (r^2=0.19; p=0.07) (Fig. 5b).

DISCUSSION

Reliability of historical maps

19th century T-sheet maps are commonly used to reconstruct changes in the position of shorelines, barrier islands, marshes, mangroves, and coastal forests, where they are considered to be an effective baseline dataset on which to measure subsequent change (e.g. Douglas and Crowell 2000; Moore 2000; Krauss et al. 2011; Raabe and Stumpf 2016). Delineation of the marsh-upland boundary on T-sheets is more uncertain than delineation of shorelines, as it depended on site accessibility and interpretations of individual surveyors (Shalowitz 1964; Moore 2000). Nevertheless, historical changes in the position of the marsh-upland boundary have been reconstructed on the basis of 19th century T-sheet maps, where previous work noted that maps were generally consistent with aerial imageries and soil samples (Collins and Sheikh

2005; Raabe and Stumpf 2016). The average RMSE of the 40 maps analyzed here (6-7 m) is similar to that reported in other T-sheet based studies of marsh extent (e.g. ~8 m (Wrayf et al 1995), 6-20 m (Collins and Sheikh 2005) and 4.6 m (Raabe and Stumpf 2016)). The combined error in the x and y directions (7m x 7m = $4.9x10^{-5}$ km^2) is several orders of magnitude less than observed changes in marsh area for an individual T-sheet (~1 km^2) (Table 1), and changes in land type are generally parallel to shorelines or elevation contours, rather than the type of systematic offset that might be expected for a georeferencing error.

Several observations suggest 19th century T-Sheets are suitable for reconstructing historical marsh change, and the position of the marsh-upland boundary, in the Chesapeake region. Rates of erosion and marsh migration into uplands at Goodwin Island, VA (lower Chesapeake Bay) based on aerial photographs are similar to rates determined from T-sheets at the same location. Aerial photograph analysis indicates erosion and migration rates of 0.25 m yr^{-1} and 0.5 m yr^{-1} from 1937 to 2011 (Kirwan et al. 2016b), and the T-sheet analysis indicates erosion and migration rates of 0.26 m yr^{-1} and 0.35 m yr^{-1} between 1853 and 2013 (this study). The slight difference in migration rate reflects increasing migration rates through time in response to accelerated sea level rise (Kirwan et al. 2016b). The location of the forest-marsh boundary on T-sheets is also consistent with historical maps and sediment cores from a site in the upper Chesapeake Bay. Figure 6 shows the position of the historical forest-marsh boundary near Hell Hook marsh from multiple map sources, which is a site where forest retreat has been independently reconstructed through sediment coring (Hussein 2009). The resulting map shows the expected gradual inland migration of the marsh-forest boundary through time. The marsh-forest boundary in the 1848 T-sheet is similar to an 1864 map, and slightly seaward of the 1898 and 1905 maps. Dated sediment cores show the same gradual inland migration of the marsh-

forest boundary (Hussein 2009). The sediment core with a dated 1848 forest-marsh transition is located approximately 58 m inland of the 1848 T-sheet boundary, but the two metrics are perhaps consistent given that sediment cores reflect the development of wetland soils that may occur under living trees, and therefore pre-date the retreat of mapped forests. In any case, migration rates over century timescales (1848-1905 to 2013) are similar whether derived from boundaries inferred from the 1848 sediment core (2.1 m yr^{-1}), the 1848 T-sheet (2.4 m yr^{-1}), or maps from 1864 (2.8 m yr^{-1}), 1898 (2.8 m yr^{-1}) or 1905 (2.1 m yr^{-1}). Therefore, multiple lines of evidence in two disparate locations within the Chesapeake study region all suggest that T-sheets are reliable for mapping century-scale forest retreat.

Finally, we note that inconsistent mapping of the marsh-upland boundary is not itself a critical issue for our goal of resolving total changes in marsh area across the entire Chesapeake region because errors in one direction on some maps would be balanced by errors in the other direction on other maps. A much more serious problem would be consistent, systematic error (i.e. the marsh-upland boundary consistently mapped too far inland or too far seaward) in every T-sheet. Our observation of no upland encroachment into marshes (Table 1) helps rule out systematic error associated with mapping the boundary too far inland, while our observation of gradual upland retreat through time (Fig. 6) helps rule out systematic error associated with mapping the boundary too far seaward. Though these observations suggest that historical T-sheets are generally reliable, we caution that it may be difficult to distinguish between no net change and slight marsh expansion summed across the entire Chesapeake Bay.

Chesapeake Bay marsh erosion and migration

Our finding that marshes have historically maintained or slightly increased their spatial extent in response to rapid sea level rise (Fig. 3) contrasts with previous work that identifies Chesapeake marshes as highly vulnerable to sea level rise. Expansive marshland along the Blackwater River, for example, is well recognized to be submerging and eroding (Stevenson et al. 1985; Kirwan and Guntenspergen 2012; Ganju et al. 2013; Schepers et al. 2017), with a total loss of about 20 km^2 since the 1930s within the Blackwater National Wildlife Refuge (Stevenson et al. 1985; Scott et al. 2009). Extensive marsh loss has also been reported along the Nanticoke River (Kearney et al. 1988). There are no T-sheets of suitable quality along the Blackwater River, which means our analysis likely underestimates historical marsh loss. However, 4 T-sheets located in similar areas on adjacent rivers, including the Nanticoke River, actually show net marsh expansion despite substantial erosion because upland drowning is rapid in this low relief region (Table 1; 17 km^2 erosion; 23 km^2 upland drowning; T00270, T00268-1, T00255, T00266). Aerial photograph analysis within the Blackwater National Wildlife Refuge indicates net marsh loss since 1938, but that marsh migration into drowned uplands (12 km^2) compensated for more than half of the marsh area that was lost due to conversion to open water (20 km^2) (Scott et al. 2009).

Across the entire Chesapeake region, remote sensing suggests that approximately 70% of marshes are currently degraded (Kearney et al. 2002). Expert opinion assessments predict major loss of Chesapeake marshes even for slight increases in sea level rise rates (Reed et al. 2008), and SLAMM modeling predicts a 36% loss of marshes with a 0.69 m SLR by 2100 (Glick et al. 2008). More generally, Chesapeake marshes are considered highly vulnerable to sea level rise because marshes in low tidal range estuaries have a narrow range of elevations that vegetation

can survive and low maximum rates of vertical accretion (Kirwan et al. 2010; D'Alpaos et al. 2012; Balke et al. 2016).

Important limitations of this study and previous studies likely explain why historical mapping reveals regional stability of Chesapeake marshes in a system well recognized to be vulnerable to sea level rise. Previous work along the Blackwater and Nanticoke rivers identifies rapid marsh loss that occurs primarily by the expansion of interior ponds (Stevenson et al. 1985; Kearney et al. 1998; Schepers et al. 2017). However, our T-sheet-based reconstructions measure the overall size of marshes between uplands and major water features such as a bay or channel, and cannot capture the loss of interior marshland due to ponding. Therefore, it is entirely possible that expanding marshes are simultaneously becoming more dissected with ponds and small tidal creeks, so that marsh size is not necessarily an indicator of vegetated area or marsh health. On the other hand, the large spatial domain of our study uniquely indicates that marsh loss in some parts of the Chesapeake region (e.g. Blackwater and Nanticoke rivers (Stevenson et al. 1985; Kearney et al. 1988; Beckett et al. 2016)) has been at least partially compensated by the creation of new marsh elsewhere (e.g. southwestern Bay) (Fig. 4). Site specific research focused on hotspots of marsh loss, and vulnerability assessments based on rates of vertical soil building, therefore underestimate the major contribution upland migration makes to marsh stability in the face of sea level rise.

Our regional-scale estimates of Chesapeake Bay marsh erosion (0.53 m yr^{-1}) and migration (0.49 m yr^{-1}) rates are similar to reported rates. Reported rates of erosion from individual marshes typically vary from ~ 0.1 to > 3 m yr^{-1}. At the regional scale, average shoreline erosion rates have been reported for the Virginia portion of the Chesapeake Bay (0.21 m yr^{-1} (Byrne and Anderson 1978); 0.54 m yr^{-1} (Rosen 1980)), Albemarle-Pamlico Sounds (0.3

m yr^{-1} (Corbett et al. 2008), 0.91 m yr^{-1} (Soil Conservation Service 1975), 1 m yr^{-1} (Riggs, 2001)), the Delaware Bay (3.21 m yr^{-1} (Phillips 1986)), and the Big Bend region of the Florida Gulf Coast (1.2 m yr^{-1} (Raabe and Stumpf 2016)). Although many differences between methods and study sites could be responsible for the disparity, our reported erosion rates are likely lower than the majority of previously estimated rates because we include many marshes adjacent to tidal channels with fetches that are too small to generate wave driven erosion, whereas most previous work focused on erosion along the estuary edge and major tributaries. Reported rates of marsh migration into uplands vary from about 0.5-6.8 m yr^{-1} (Hussein 2009; Smith 2013; Raabe and Stumpf 2016; Kirwan et al. 2016a). The highest rates (3.5-6.8 m yr^{-1} (Hussein 2009)) are calculated from individual transects in locations selected specifically to study rapid marsh migration, whereas our rates also include large parts of the landscape with no migration. At the regional scale, our reported migration rates are likely lower than those observed along the Florida Coast (2.3 m yr^{-1}) because we measured the length of the marsh-upland boundary at the 1:20,000 scale and therefore included crenulations, islands, and many other features that would have been excluded in a more generalized approach (Raabe and Stumpf 2016). Nevertheless, linear rates of marsh erosion and migration are highly sensitive to the complexity of the topography and the scale at which shoreline length is measured.

Broader implications

Marsh migration rates into adjacent uplands are widely considered to be proportional to topographic slope and the rate of sea level rise (Brinson et al. 1995; Hussein 2009; Doyle et al. 2010; Raabe and Stumpf 2016; Kirwan et al. 2016b). We found that historical marsh migration rates were weakly correlated with slope, and were highly variable compared to the migration rate

that would be predicted on the basis of slope (m) and historical sea level rise rate (R) (i.e. migration = R / m) (Fig. 5a). Ecological lags and/or interactions with human development may explain the weak correlation. Adult trees are resilient to sea level impacts, so that retreat of coastal forests takes place only after punctuated disturbance events such as major hurricanes (Clark 1986; Williams et al. 1999; Kirwan et al. 2007; Poulter et al. 2008; Field et al. 2016). Even if marsh vegetation were colonizing under live trees, marsh migration could not be measured from aerial photographs until the death of canopy trees, which introduces a lag between sea level rise and observed marsh migration. Migration rates may also be weakly correlated with slope because anthropogenic barriers commonly prevent migration. Previous work focused on sections of the coast with very little urban and agricultural land (Hussein 2009; Smith 2013; Raabe and Stumpf 2016), whereas we mapped migration across the entire Chesapeake Bay region including areas that are highly urbanized. For example, the lowest marsh migration rates were observed for the Cape Charles map, where direct loss to coastal development negated any potential gains from migration. We found a weak relationship between migration rate and slope in uplands with minimal development (Fig. 5b). LiDAR-derived slope estimates may not be sufficiently accurate to identify correlations between slope and migration rate. In particular, our slope estimates are based on the slope of adjacent uplands, rather than the actual submerged upland over which the marshes have historically migrated. Nevertheless, regional-scale projections of marsh migration often rely on coarse elevation datasets, and the assumption that migration occurs as soon as topography is inundated (Feagin et al. 2010; Morris et al. 2012; Clough et al. 2016; Enwright et al. 2016; Kirwan et al. 2016b). Our findings therefore suggest that there are important limitations to simple topographic inundation models,

and that more process-based studies are needed to discern the role of coastal development and ecological lags in marsh migration.

Observations of historical marsh stability in the Chesapeake region contribute to the growing body of evidence that migration into uplands is a primary component of marsh response to sea level rise at regional scales. Previous studies, for example, found that historical migration into uplands exceeded edge erosion for a section of the Florida Gulf coast (Raabe and Stumpf 2016). The area of land that could be inundated by 1 m of sea level rise is similar to the existing area of coastal wetlands in the coterminous U.S. (Morris et al. 2012), and modeling studies suggest that in the absence of anthropogenic barriers to migration, a moderate acceleration in sea level rise could actually lead to overall marsh expansion (Feagin et al. 2010; Cadol et al. 2016; Clough et al. 2016; Kirwan et al. 2016a). Our work is consistent with these studies, but uniquely suggests that when integrated over a region with both anthropogenic and topographic barriers, migration has allowed marshes to survive but not expand substantially.

Simple extrapolation of our results from the study area to the entire Chesapeake region suggests that sea level rise has led to massive and widespread drowning of uplands, which has created more than 100,000 acres (400 km^2) of new marsh over the last century. Marsh migration into these drowned uplands has created about one third of all the marsh in the mapped region (marsh migration = 101 km^2; total 2013 marsh area = 318 km^2). Moreover, about one third of all marshes mapped in the late 19^{th} century (311 km^2) were lost by 2013, presumably due to edge erosion (94 km^2). These observations of rapid marsh change emphasize the disparity between marsh instability in the lateral dimension, and marsh stability in the vertical dimension where marshes have survived low rates of sea level rise for thousands of years (Fagherazzi et al. 2013; Kirwan and Megonigal 2013). Traditional approaches to predicting and mitigating marsh

vulnerability to sea level rise focus on the survival of existing marsh. However, our results indicate that sea level rise itself creates new marsh through upland drowning, and that marsh size can be maintained despite substantial loss of existing marsh. Averaged across the Chesapeake Bay region, widespread upland drowning has historically compensated for marsh edge erosion, and allowed Chesapeake Bay marshes to maintain their spatial extent despite relative sea level rise rates that are among the fastest in the world. There are real concerns over the ability of marshes to survive sea level rise in the Chesapeake and beyond (Kearney et al. 2002; Beckett et al. 2016; Crosby et al. 2016; Schepers et al. 2017; Watson et al. 2017), and our study focuses simply on the broad spatial extent of marshes rather than any indicator of their health. Nevertheless, our results emphasize that the location of coastal ecosystems changes rapidly on century timescales, and that sea level rise does not necessarily lead to overall habitat loss.

LITERATURE CITED

Anisfeld, S.C., K.R. Cooper, and A.C. Kemp. 2017. Upslope development of a tidal marsh as a function of upland land use. *Global Change Biology 23:* 755-766.

Balke, T., M. Stock, K. Jensen, T.J. Bouma, and M. Kleyer. 2016. A global analysis of the seaward salt marsh extent: The importance of tidal range. *Water Resources Research* 52: 3775-3786.

Barbier, E.B., S.D. Hacker, C. Kennedy, E.W. Koch, A.C. Stier, and B.R. Silliman. 2011. The value of estuarine and coastal ecosystem services. *Ecological Monographs* 81: 169-193.

Beckett, L.H., A.H. Baldwin, and M.S. Kearney. 2016. Tidal marshes across a Chesapeake Bay subestuary are not keeping up with sea-level rise. *PLoS ONE* 11(7): e0159753. doi:10.1371/journal.pone.0159753.

Brinson, M.M., R.R. Christian, and L.K. Blum. 1995. Multiple states in the sea-level induced transition from terrestrial forest to estuary. *Estuaries* 18: 648-659.

Byrne, R.J., and G.L. Anderson. 1978. Shoreline erosion in tidewater Virginia. Special Report in Applied Marine Science and Ocean Engineering 111, Virginia Institute of Marine Science, Gloucester Pt, VA, 102 p.

Cadol, D., A. Elmore, S. Guinn, K.A.M. Engelhardt, and G. Sanders. 2016. Modeled tradeoffs between developed land protection and tidal habitat maintenance during rising sea levels. *PLoS ONE* 11(10): e0164875. Doi:10.1371/journal.pone.0164875.

Cahoon, D.R., P.F. Hensel, T. Spencer, D.J. Reed, and N.S. McKee. 2006. Coastal vulnerability to relative sea-level rise: Wetland elevation trends and process controls. *Ecological Studies* 190: 271-292.

Chesapeake Bay Program: Tidal Wetland Abundance.2015.

http://www.chesapeakebay.net/indicators/indicator/tidal_wetlands_abundance.

Church, J.A., P.U. Clark, A. Cazenave, J.M. Gregory, S. Jevrejeva, A. Levermann, M.A. Merrifield, G.A. Milne, R.S. Nerem, P.D. Nunn, A.J. Payne, W.T. Pfeffer, D. Stammer and A.S. Unnikrishnan. 2013. Sea level change. In: Climate Change 2013: The Physical Science Basis. Contribution of Working Group I to the Fifth Assessment Report of the Intergovernmental Panel on Climate Change [Stocker, T.F., D. Qin, G.-K. Plattner, M. Tignor, S.K. Allen, J. Boschung, A. Nauels, Y. Xia, V. Bex and P.M. Midgley (eds.)]. Cambridge University Press, Cambridge, United Kingdom and New York, NY, USA.

Clark, J.S. 1986. Coastal forest tree populations in a changing environment, southeastern Long Island, New York. *Ecological Monographs* **56,** 259-277.

Clough, J., A. Polaczyk, and M. Popato. 2016. Modeling the potential effects of sea-level rise on the coast of New York: Integrating mechanistic accretion and stochastic uncertainty. *Environmental Modelling & Software* 84: 349-362.

Collins, B.D., and A.J. Sheikh. 2005. Historical reconstruction, classification and change analysis of Puget Sound tidal marshes. Puget Sound River History Project Report to: Washington Department of Natural Resources. www.pudgetsoundnearshore.org/supporting_documents/historical/shoreline/dnr.pdf

Corbett, D.R., J.P. Walsh, S.R. Riggs, D.V. Ames, and S.J. Culver. 2008. Shoreline change within the Albemarle-Pamlico estuarine system, North Carolina. 1907-2007 Centennial. www.ecu.edu/cs-acad/icsp/upload/EstuarineShorlineChangeDec2008.pdf

Craft, C., J. Clough, J. Ehman, S. Joye, R. Park, S. Pennings, H. Guo, and M. Machmuller. 2009. Forecasting the effects of accelerated sea-level rise on tidal marsh ecosystem services.

The ecological society of America. *Frontiers in Ecology and the Environment* 7(2): 73-78.

Crosby, S.C., D.F. Sax, M.E. Palmer, H.S. Booth, L.A. Deegan, M.D. Berness, and H.M. Leslie. 2016. Salt marsh persistence is threatened by predicted sea-level rise. *Estuarine, Coastal and Shelf Science* 181: 93-99.

Curray, J.R. 2016. Transgressions and regressions, in Miller, R.L., ed., Papers in *Marine Geology*: New York, Macmillan, 175-203.

D'Alpaos, A., C. Da Lio, and M. Marani. 2012. Biogeomorphology of tidal landforms: Physical and biological processes shaping the tidal landscape. *Ecohydrology* 5: 550-562.

Day, J., C. Ibáñez, F. Scarton, D. Pont, P. Hensel, J. Day, and R. Lane. 2011. Sustainability of Mediterranean deltaic and lagoon wetlands with sea-level rise: The importance of river input. *Estuaries and Coasts* 34: 483-493.

Douglas, B., and M. Crowell. 2000. Long-term shoreline position prediction and error propagation. *Journal of Coastal Research* 16(1): 145-152.

Doyle, T.W., K.W. Krauss, W.H. Conner, and A.S. From. 2010. Predicting the retreat and migration of tidal forests along the northern Gulf of Mexico under sea-level rise. *Forest Ecology and Management* 259: 770-777.

Engelhart, S.E., B.P. Horton, B.C. Douglas, W.R. Peltier, and T.E. Törnqvist. 2009. Spatial variability of late Holocene and 20th century sea-level rise along the Atlantic coast of the United States. *Geology* 37: 1115-1118.

Enwright, N.M., K.T. Griffith, and M.J. Osland. 2016. Barriers to and opportunities for landward migration of coastal wetlands with sea-level rise. *Frontiers in Ecology and the Environment* 14(6): 307-316.

ESRGC: Eastern Shore Regional GIS Cooperative LiDAR Services. 2015. http://lidar.salisbury.edu/arcgis/rest/services/DEM_ft.

Ezer, T., and W.B. Corlett. 2012. Is sea level rise accelerating in the Chesapeake Bay? A demonstration of a novel new approach for analyzing sea level data. *Geophysical Research Letter* 39: L19605. doi:10.1029/2012GL053435.

Fagherazzi, S., G. Mariotti, P. Wiberg, and K. McGlathery. 2013. Marsh collapse does not require sea level rise. *Oceanography* 26: 70-77.

Feagin, R., M. Martinez, G. Mendoza-Gonzalez, and R. Costanza. 2010. Salt marsh zonal migration and ecosystem service change in response to global sea level rise: A case study from an urban region. *Ecology and Society 15(4): 14.* www.ecologyandsociet.org/vol15/iss4/art14.

Field, C.R., C. Gjerdrum, and C.S. Elphick. 2016. Forest resistance to sea-level rise prevents landward migration to tidal marsh. *Biological Conservation* 201: 363-369.

FitzGerald, D., M. Fenster, B. Argow, and I. Buynevich. 2008. Coastal impacts due to sea-level rise. *Annual Review of Earth and Planetary Sciences* 36: 601-647.

Ford, H., A. Garbutt, C. Ladd, J. Malarkey, and M.W. Skov. 2016. Soil stabilization linked to plant diversity and environmental context in coastal wetlands. *Journal of Vegetation Science* 27(2): 259-268.

Friedrichs, C.T., and J.E. Perry. 2001. Tidal salt marsh morphodynamics: A synthesis. *Journal of Coastal Research* 27: 7-37.

Ganju, N.K., N.J. Nidzjeko, and M.L. Kirwan. 2013. Inferring tidal wetland stability from channel sediment fluxes: Observations and a conceptual model. *Journal of Geophysical Research Earth Surface* 18: 2045-2058.

Gedan, K.B., M.L. Kirwan, E. Wolanski, E.B. Barbier, and B.R. Silliman. 2011. The present and future role of coastal wetland vegetation in protecting shorelines: answering recent challenges to the paradigm. *Climatic Change* 106(1): 7-29.

Glick, P., J. Clough, and B. Nunley. 2008. Sea-level rise and coastal habitats in the Chesapeake Bay region. Technical Report. National Wildlife Federation. www.nwf.org/~/media/PDFs/Global-Warming/Reports/SeaLevelRiseandCoastalHabitats?ChesapeakeRegion.ashx

Hussein, A.H. 2009. Modeling of sea-level rise and deforestation in submerging coastal ultisols of Chesapeake Bay, *Soil Science Society of America Journal* 73(1): 185.

Kearney, M.S., E.G. Russell, and J.C. Stevenson. 1988. Marsh Loss in Nanticoke Estuary, Chesapeake Bay. *Geographical Review* 78(2). 205-220.

Kearney, M.S., and J.C. Stevenson. 1991. Island land loss and marsh vertical accretion rate evidence for historical sea-level changes in Chesapeake Bay. *Journal of Coastal Research* 7(2): 403-415.

Kearney, M.S., A.S Rogers, J.R.G. Townshend, E. Rizzo, and D. Stutzer. 2002. Landsat imagery shows decline of coastal marshes in Chesapeake and Delaware Bays. *Eos, Transactions American Geophysical Union* 83(16): 173-184.

Kemp, A.C., B.P. Horton, S.J. Culver, D.R. Corbett, O. van de Plassche, W.R. Gehrels, B.C. Douglas, and A.C. Parnell. 2009. Timing and magnitude of recent accelerated sea-level rise (North Carolina, United States). *Geology* 37: 1035-1038.

Kirwan, M.L., and J.P. Megonigal. 2013. Tidal wetland stability in the face of human impacts and sea-level rise. *Nature* 504: 53-60.

Kirwan, M.L., S. Temmerman, E. Skeehan, G. Guntenspergen, and S. Fagherazzi. 2016a. Overestimation of marsh vulnerability to sea level rise. *Nature Climate Change* 6: 253-260.

Kirwan, M.L., G.R. Guntenspergen, A. D'Alpaos, J.T. Morris, S.M. Mudd, and S. Temmerman. 2010. Limits on the adaptability of coastal marshes to rising sea level. *Geophysical Research Letters* 37(23): L23401. doi:10.1029/2010GL045489.

Kirwan, M.L., J.L. Kirwan, and C.A. Copenheaver. 2007. Dynamics of an estuarine forest and its response to rising sea level. *Journal of Coastal Research* 232: 457-463.

Kirwan, M.L., and G.R. Guntenspergen. 2012. Feedbacks between inundation, root production, and shoot growth in a rapidly submerging brackish marsh. *Journal of Ecology* 100: 764-770.

Kirwan, M.L., D.C. Walters, W.G. Reay, and J.A. Carr. 2016b. Sea level driven marsh expansion in a coupled model of marsh erosion and migration. *Geophysical Research Letters* 43: 4366-4373.

Krauss, K.W., A.S. From, T.W. Doyle, T.J. Doyle, and M.J. Barry. 2011. Sea-level rise and landscape change influence mangrove encroachment onto marsh in the Ten Thousand Islands region of Florida, USA. *Journal of Coastal Conservation* 15: 629-638.

Marani, M., A. D'Alpaos, S. Lanzoni, and M. Santalucia. 2011. Understanding and predicting wave erosion of marsh edges, *Geophysical Research Letters* 38: L21401. doi:10.1029/2011GL048995.

Mariotti, G., and S. Fagherazzi. 2010. A numerical model for the coupled long-term evolution of salt marshes and tidal flats. *Journal of Geophysical Research* 115: F01004. doi:10.1039/2009JF001326.

Maryland's Mapping & GIS Data Portal. Maryland Digital High-Resolution Aerial Photography Products. 2015. http://imap.maryland.gov/Pages/imagery-products.aspx.

McLoughlin, S.M., P.L. Wiberg, I. Safak, and K.J. McGlathery. 2015. Rates and Forcing of Marsh Edge Erosion in a Shallow Coastal Bay. *Estuaries and Coasts* 38(2): 620-638.

Moore, L. 2000. Shoreline mapping techniques. *Journal of Coastal Research* 16(1): 111-124.

Morris, J.T., J. Edwards, S. Crooks, and E. Reyes. 2012. Assessment of carbon sequestration potential in coastal wetlands. In recarbonization of the biosphere, Lal, R., K. Lorenz, R.F. Hüttl, B.U. Schneider, and J. von Braun (eds.) (Dordrecht: Springer Netherlands): 517-531.

Multi-Resolution Land Characteristics Consortium. 2016. http://www.mrlc.gov/nlcd2011.php.

NOAA. NOAA Shoreline Website: NOAA Historical Surveys (T-Sheets). 2015. https://shoreline.noaa.gov/intro/.

Perry, J.E., T.A. Barnard, JR., J.G. Bradshaw, C.T. Friedrichs, K.J. Havens, P.A. Mason, W.I. Priest, III, and G.M. Silberhorn. 2001. Creating tidal salt marshes in the Chesapeake Bay. *Journal of Coastal Research* 27: 179-191.

Phillips, J.D. 1986. Spatial analysis of shoreline erosion, Delaware Bay, New Jersey. *Annals of the Association of American Geographers* 76(1): 50-62.

Poulter, B., N. Christensen, and S. Qjian. 2008. Tolerance of *Pinus taeda* and *Pinus serotine* to low salinity and flooding: Implications for equilibrium vegetation dynamics. *Journal of Vegetation Science* 19(1): 15-22.

Raabe, E.A., and R.P. Stumpf. 2016. Expansion of tidal marsh in response to sea-level rise: Gulf Coast of Florida, USA. *Estuaries and Coasts* 39(1): 145-157.

Reed, D.J. 1995. The response of coastal marshes to sea-level rise: Survival or submergence? *Earth Surface Processes and Landforms* 20: 39-48.

Reed, D.J., D.A. Bishara, D.R. Cahoon, J. Donnelly, M. Kearney, A.S. Kolker, L.L. Leonard, R.A. Orson, and J.C. Stevenson. 2008. Site-specific scenarios for wetlands accretion as sea level rises in the Mid-Atlantic region. Section 2.1 in: Background Documents Supporting Climate Change Science Program Synthesis and Assessment Product 4.1., Titus, J.G., and Strange, E.M. (eds.). EPA 430R07004. U.S. EPA, Washington, DC.

Riggs, S.R. 2001. Shoreline Erosion in North Carolina Estuaries: the Soundfront Series UNC-SG_01-11. North Carolina Sea Grant, Raleigh, N.C.

Rosen, P.S. 1980. Erosion susceptibility of the Virginia Chesapeake Bay shoreline. *Marine Geology* 34: 45-59.

Sallenger, A.H.S., K.S. Doran, and P.A. Howd. 2012. Hotspot of accelerated sea-level rise on the Atlantic coast of North America, *Nature Climate Change* 2: 884-888.

Schepers, L., M.L. Kirwan, G. Guntenspergen, and S. Temmerman. 2017. Spatio-temporal development of vegetation die-off in a submerging coastal marsh. *Limnology and Oceanography* 62: 137 – 150.

Schwimmer, R.A. 2001. Rates and processes of marsh shoreline erosion in Rehoboth Bay, Delaware, U.S.A. *Journal of Coastal Research* 17(3): 678-683.

Scott, M., L. McDermott, E. Silva, and E. Watson. 2009. Digital spatial data capture of marsh extent in Blackwater National Wildlife Refuge, 1938 and 2006. *Eastern Shore GIS Cooperative at Salisbury University*.

Shalowitz, A.L. 1964. *Shore and Sea Boundaries*. Washington, DC: U.S. Government Printing Office.

Silliman, B., P. Dixon, C. Wobus, Q. He, P. Daleo, B. Hughes, J. Willis and M. Hester. 2016. Thresholds in marsh resilience to the Deepwater Horizon Oil Spill. *Scientific Reports* 6: 32520. https://doi.org/10.1038/srep32520.

Smith, J.A.M. 2013. The role of *Phragmites australis* in mediating inland salt marsh migration in a Mid-Atlantic Estuary. *PLoS ONE* 8: e65091. https://doi.org/10.1371/journal.pone.0065091.

Soil Conservation Service. 1975. Estuarine Shoreline Erosion Inventory, North Carolina. Raleigh, North Carolina: U.S. Soil Conservation Service, 71p.

Stevenson, J.C., M.S. Kearney, and E.C. Pendleton. 1985. Sedimentation and erosion in a Chesapeake Bay brackish marsh system. *Marine Geology* 67: 213-235.

Torio, D.D., and G.L. Chmura. 2013. Assessing coastal squeeze of tidal wetlands. *Journal of Coastal Research* 29(5): 1049-1061.

Virginia Lidar. 2015. http://virginialidar.com/index-3.html#.V_-Z1vkrKUk.

Wang, Y., and T.R. Allen. 2008. Estuarine shoreline change detection using Japanese ALOS PALSAR HH and JERS-1 L-HH SAR data in the Albemarle-Pamlico Sounds, North Carolina, USA. *International Journal of Remote Sensing* 29(15): 4429-4442.

Wasson, K., A. Woolfolk, and C. Fresquez. 2013. Ecotones as indicators of changing environmental conditions: Rapid migration of salt marsh-upland boundaries. *Estuaries and Coasts* 36: 654-664.

Watson, E.B., K.B. Raposa, J.C. Carey, C. Wigand, and R.S. Warren. 2017. Anthropocene survival of southern New England's salt marshes, *Estuaries and Coasts* 40: 617-625.

Weston, N.B. 2014. Declining sediments and rising seas: An unfortunate convergence for tidal wetlands. *Estuaries and Coasts* 37: 1-23.

Williams, K., K.C. Ewel, R.P. Stumpf, F.E. Putz, and T.W. Workman. 1999. Sea-level rise and coastal forest retreat on the West Coast of Florida, USA. *Ecology* 80: 2045-2063.

Wrayf, R.D., S.P. Leatherman, and R.J. Nicholls. 1995. Historic and future land loss for upland and marsh islands in the Chesapeake Bay, Maryland, U.S.A. *Journal of Coastal Research* 11(4): 1195-1202.

FIGURES

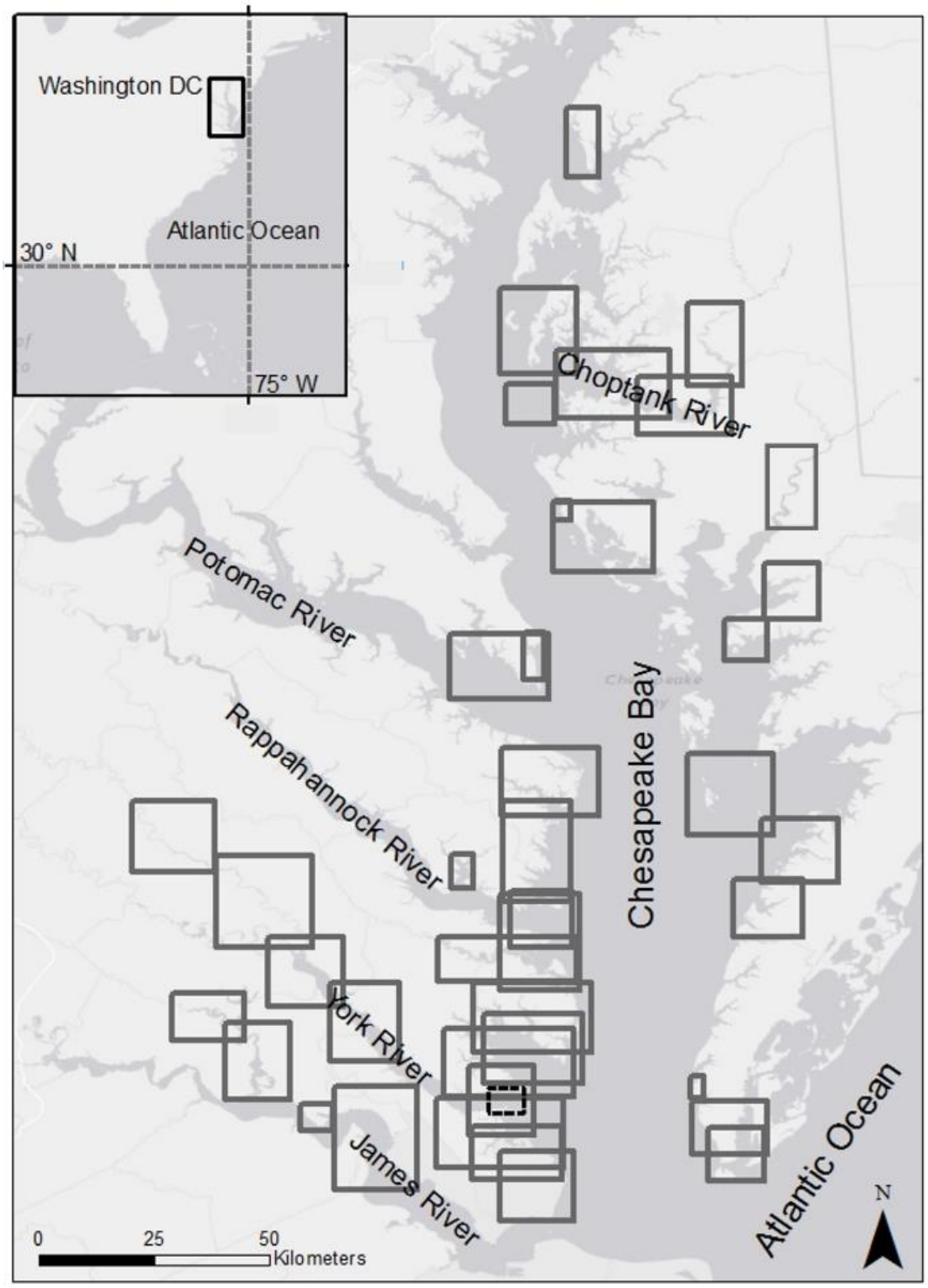

Fig. 1 *Study area map of the Chesapeake Bay region showing the major rivers, the extent of individual T-Sheets used in the analysis (grey rectangles), and area displayed in figure 2 (dashed rectangle)*

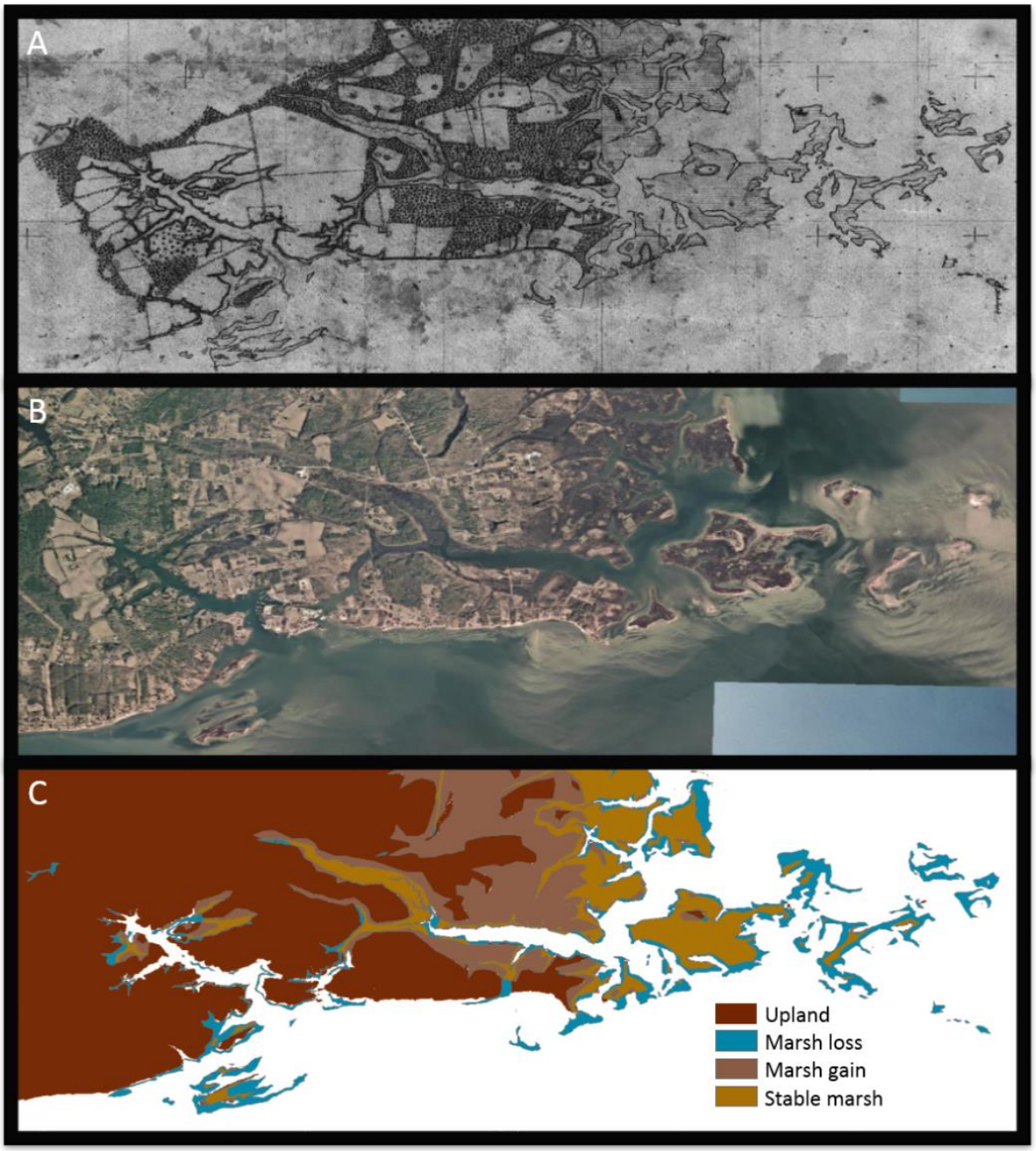

Fig. 2 *Example of land type delineation and change analysis. (A) T-sheet from the mouth of the York River from 1853 (T00496) showing water, marsh, forest, agriculture and developed upland land types. (B) Aerial photograph from 2013 was compared to historical maps to determine the amount of marsh area lost due to edge erosion and gained due to upland retreat. (C) Simplified map representing the historical change in marsh area*

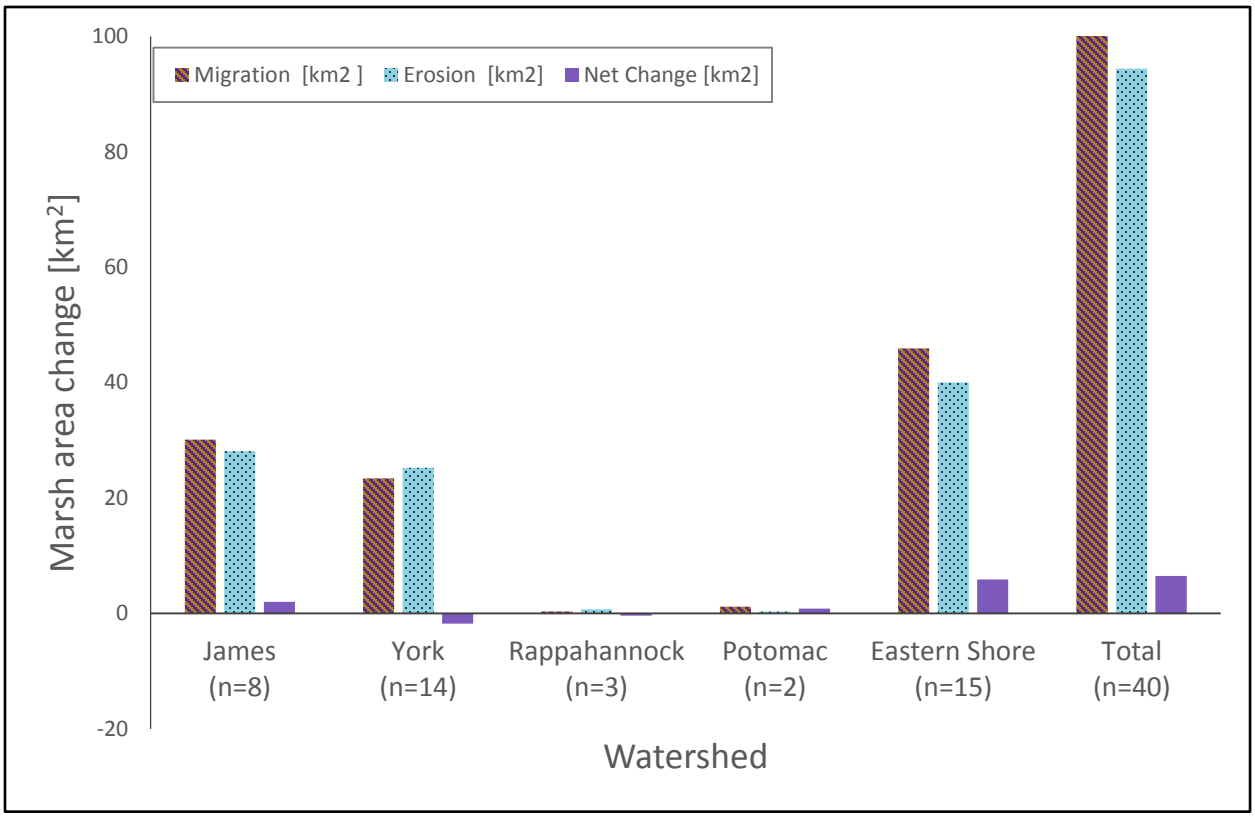

Fig. 3 *Changes in marsh area resulting from marsh migration into drowned uplands (stripes), edge erosion (dots) and net change (migration minus erosion) (solid fill) summarized by watershed*

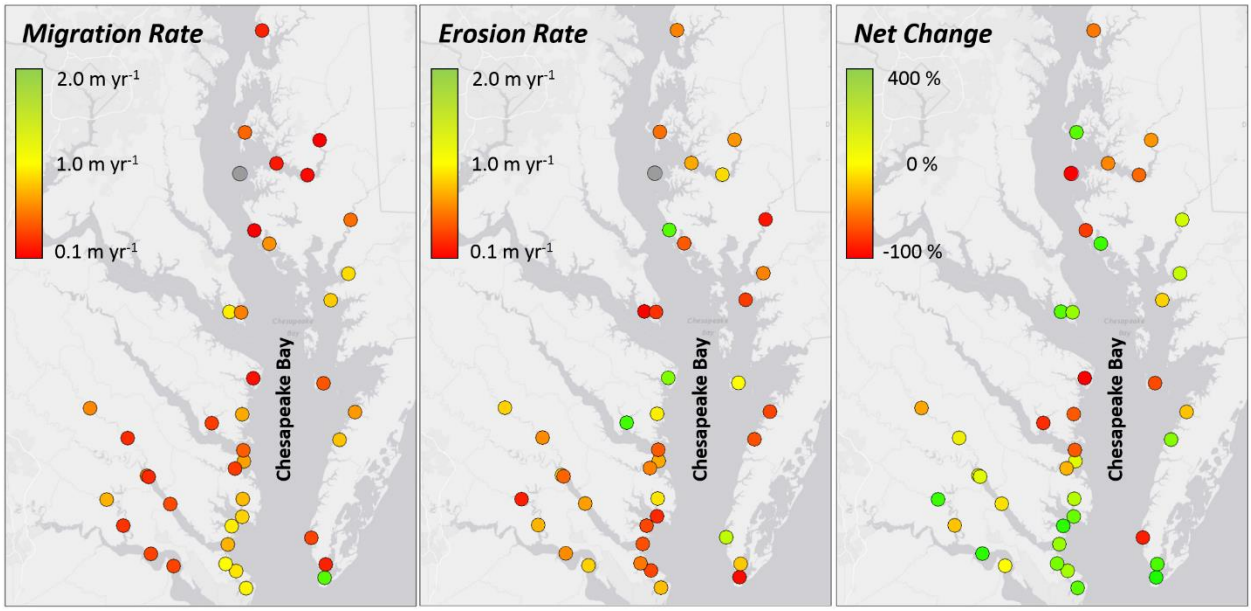

Fig. 4 *Marsh migration rates (m yr^{-1}), erosion rates (m yr^{-1}) and net change in area (%) along the Chesapeake Bay. Each circle represents an individual T-sheet, where reported values represent the change averaged over the entire T-sheet extent. Green colors denote rapid change and red colors denote slow change, except for in the "Net Change" panel where green indicates net marsh expansion (migration > erosion) and red indicates net marsh loss (erosion > loss). The gray dot represents Sharps Island, and does not have a migration or erosion rate because complete land loss occurred prior to 2013.*

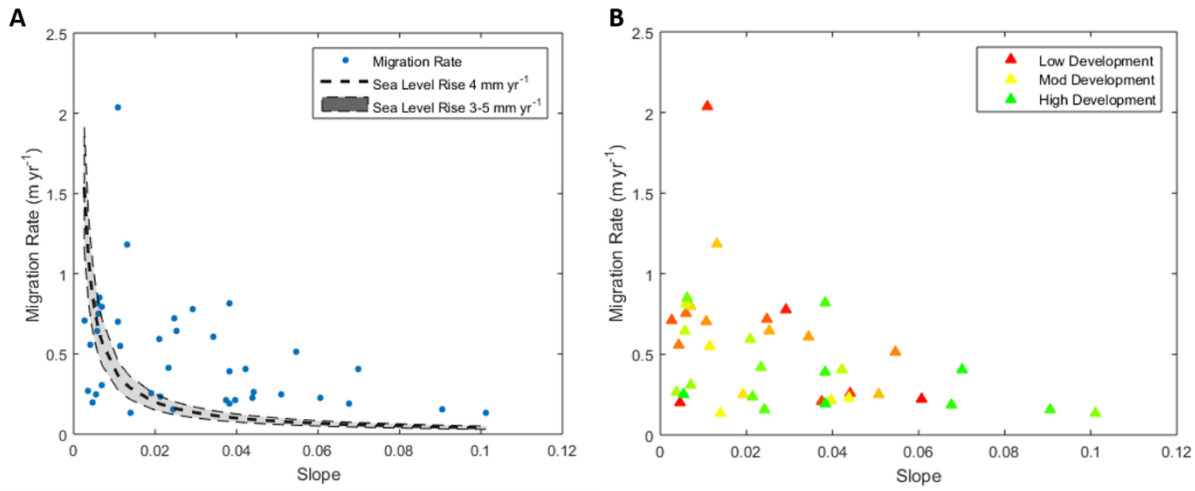

Fig. 5 *Historical marsh migration rate versus characteristics of adjacent uplands, where each marker represents the average migration rate and topographic slope across an individual T-sheet extent. Characterization of adjacent uplands is restricted to a 100 m buffer around the modern marsh-upland boundary. (A) Observed migration rates (blue markers) compared to expected migration rates for historical relative sea level rise rates of 3, 4, and 5 mm* yr^{-1} *(gray envelope). Observed migration rates are less than the expected migration rate, which is defined as the sea level rise rate divided by slope (i.e. y = R/m). Observed migration rates are weakly correlated with topographic slope (y = -6.0034x + 0.6673,* r^2 *= 0.16, p<0.05) and are not significantly correlated with expected migration rates (y =0.2206x + 0.4195,* r^2 *= 0.04, p>0.1). (B) Observed migration rates as a function of topographic slope and intensity of coastal development in adjacent uplands. Coastal development includes agricultural and urban land uses, and colors reflect a gradient in development from low (red) to high (green). There is a weak correlation between slope and migration rate in uplands with lowest development (< 10%) (y = -10.233x + 0.8828, p=0.07,* r^2 *= 0.19)*

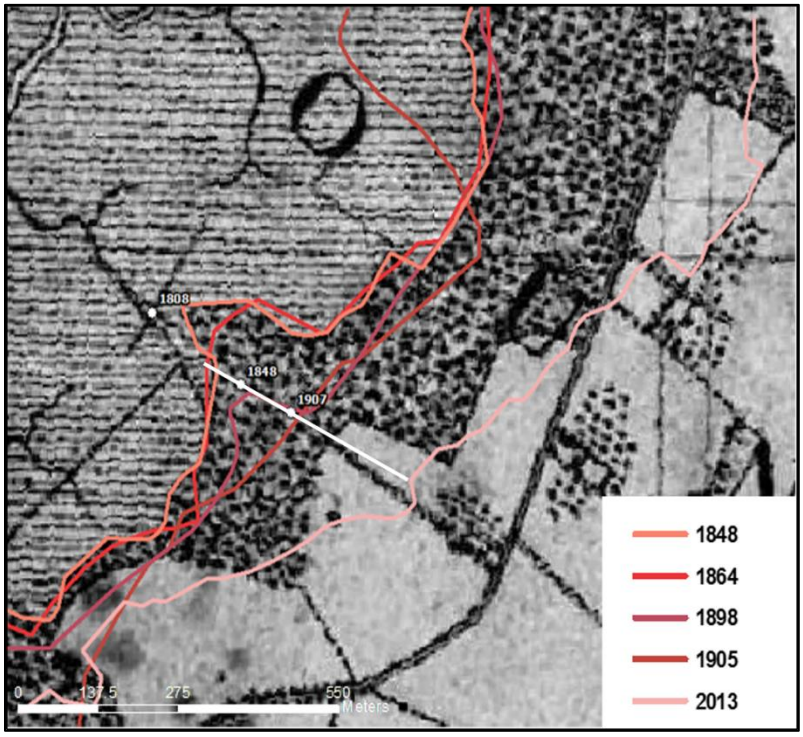

Fig. 6 *Movement of the marsh forest boundary derived from historical maps and sediment cores (lines = maps, dots = sediment cores). The 1848 line represents the T-sheet boundary [T00255] used in the analysis. The 1898 and 1905 lines are from USGS topographic maps, and the 1864 line is from the US Coast Survey, Coast Chart Number 33. The dots represent the location of the marsh-forest boundary inferred from dated sediment cores (Hussein, 2009), and the white line indicates a transect over which forest retreat rates were measured*

Table 1| *Summary of changes in marsh area between historical maps and modern aerial imagery. Results are summarized by individual T-sheet and ordered numerically starting with T-sheets along the western shore of the Chesapeake Bay. Characteristics of uplands (e.g. slope and land use) are calculated for the area within 100 m of the modern marsh. "Simple average" refers to the arithmetic mean of each column, whereas "total" refers to the sum of each column after redundant portions of overlapping maps were eliminated. Geospatial data will be archived with Dr. Matthew Kirwan, and eventually archived with the VIMS Shoreline Studies Program.*

T-sheet #	T-sheet Name and Year	Marsh Area in T-sheet (km^2)	Marsh Area in Modern (km^2)	Migration (km^2)	Migration (%)	Erosion (km^2)	Erosion (%)	Net Change (km^2)	Net Change (%)	Slope	Urban Area (%)	Agriculture Area (%)	Forested Area (%)	Shoreline length (marsh-water) (km)	Shoreline length (marsh-forest) (km)
T00458-2	Mouth of the Potomac River (1849-1850)	1.08	1.20	0.87	81.03	0.75	69.27	0.13	11.76	0.02	35.75	22.74	33.51	16.67	12.87
T00496	Mouth of the York River (1853-1854)	8.00	9.02	4.64	58.02	3.63	45.35	1.01	12.67	0.01	58.99	10.50	18.42	73.56	45.53
T00499	Black & Pocosin Rivers (1853-1854)	20.17	21.58	6.11	30.30	4.70	23.32	1.41	6.98	0.01	75.32	2.36	15.26	97.84	48.48
T00500	Little & Great Wicomico Rivers (1850-1856)	1.79	0.29	0.22	12.13	1.71	95.75	-1.49	-83.62	0.02	19.69	25.64	42.68	6.6	8.77
T00504	New Point Comfort to Wolf Trap (1853)	8.78	10.31	5.36	61.01	3.82	43.52	1.54	17.49	0.01	24.72	18.33	23.11	92.96	44.76
T00521	Mouth of the Rappahannock River (1851-1856)	0.78	0.53	0.30	38.40	0.56	71.39	-0.26	-32.99	0.01	43.42	1.54	43.14	11.11	6.15
T00661	Corrotoman River (1857)	0.28	0.07	0.04	15.44	0.25	90.14	-0.21	-74.70	0.02	3.33	63.33	28.89	0.96	1.18
T00686	York River from Clay Bank to Mount Folly (1857-1858)	9.03	8.24	2.09	23.18	2.88	31.94	-0.79	-8.77	0.04	15.36	6.79	69.72	40.16	51.18
T00722	York River from Mount	12.27	11.90	2.42	19.77	2.79	22.75	-0.37	-2.99	0.04	28.27	12.63	53.56	52.71	73.7

T-sheet #	T-sheet Name and Year	Marsh Area in T-sheet (km^2)	Marsh Area in Modern (km^2)	Migration (km^2)	Migration (%)	Erosion (km^2)	Erosion (%)	Net Change (km^2)	Net Change (%)	Slope	Urban Area (%)	Agriculture Area (%)	Forested Area (%)	Shoreline length (marsh-water) (km)	Shoreline length (marsh-forest) (km)
	Folly to West Point (1858)														
T01100	Piankatank River (1869)	0.46	0.40	0.30	66.03	0.36	78.57	-0.06	-12.54	0.04	9.55	11.61	68.91	6.27	9.35
T01289	James River VA - Burwell's Bay to College Creek (1873)	14.99	13.93	5.30	35.37	6.37	42.47	-1.06	-7.10	0.05	19.19	4.79	68.89	85.82	153.49
T01337a	Chickahominy River VA (1873-1874)	24.81	22.07	4.22	17.01	6.97	28.09	-2.75	-11.08	0.06	4.68	6.83	81.30	100.14	136.49
T01337b	Chickahominy River VA (1874-1875)	8.63	11.40	4.44	51.48	1.68	19.45	2.77	32.03	0.03	18.58	28.52	42.88	55.18	50.16
T02693	Jamestown Island (1905)	4.07	4.51	1.22	29.84	0.78	19.26	0.43	10.58	0.02	31.23	8.57	57.99	17.92	44.7
T02715	Mobjack Bay to Milford Haven (1905-1906)	10.32	10.41	5.30	51.37	5.21	50.51	0.09	0.86	0.01	15.60	20.75	37.50	81.29	70.73
T02716	Mobjack Bay (1905-1906)	11.56	16.15	9.10	78.75	4.50	38.97	4.60	39.79	0.01	38.75	24.22	21.36	138.53	104.57
T02747	Potomac River - Point lookout to Piney Point (1905)	0.32	1.66	1.50	464.01	0.16	50.17	1.34	413.84	0.04	36.25	41.01	17.44	20.95	17.07
T02749	Back River to Yorktown (1906)	17.40	20.26	6.88	39.55	4.14	23.81	2.86	16.45	0.01	69.20	2.61	19.69	104.93	54.55

T-sheet #	T-sheet Name and Year	Marsh Area in T-sheet (km^2)	Marsh Area in Modern (km^2)	Migration (km^2)	Migration (%)	Erosion (km^2)	Erosion (%)	Net Change (km^2)	Net Change (%)	Slope	Urban Area (%)	Agriculture Area (%)	Forested Area (%)	Shoreline length (marsh-water) (km)	Shoreline length (marsh-forest) (km)
T02801	Hampton to Back River (1906-1907)	8.43	10.26	5.24	62.23	3.41	40.45	1.84	21.78	0.01	76.73	2.85	11.40	62.47	58.34
T02869	Whites Creek to Windmill Point (1907-1908)	1.13	1.10	0.94	82.70	0.97	85.69	-0.03	-2.99	0.02	28.66	5.09	47.42	19.06	15.03
T02957	Ingrams Bay to Little Bay (1908-1909)	2.87	1.95	1.01	34.97	1.93	67.12	-0.92	-32.15	0.03	20.38	11.77	58.46	21.34	15.87
T03243	York River (1911)	10.92	10.48	2.23	20.45	2.67	24.47	-0.44	-4.03	0.04	31.91	11.32	51.20	48.85	54.15
T03254	Mattaponi River - West Point to Scotland Landing (1912)	18.01	17.18	1.70	9.43	2.52	14.00	-0.82	-4.57	0.04	7.04	18.04	62.45	61.36	80.15
T03256	Mattaponi River - Scotland Landing to Dunkirk (1912)	4.81	4.08	1.11	23.14	1.84	38.28	-0.73	-15.14	0.05	11.17	17.43	60.17	34.67	21.5
T00199	Swan Creek to Eastern Neck Inlet (1854)	1.85	1.42	0.67	36.48	1.10	59.60	-0.43	-23.12	0.06	24.10	68.10	247.10	17.5	22.52
T00215	Wades Point to Lows Point (1846-1847)	2.87	3.60	2.96	102.88	2.23	77.62	0.73	25.25	0.04	20.11	56.58	11.92	37.92	45.51
T00225	Choptank River (1850)	2.20	1.71	1.22	55.41	1.71	77.59	-0.49	-22.18	0.04	21.32	63.19	7.55	22.12	38.94

T-sheet #	T-sheet Name and Year	Marsh Area in T-sheet (km^2)	Marsh Area in Modern (km^2)	Migration (km^2)	Migration (%)	Erosion (km^2)	Erosion (%)	Net Change (km^2)	Net Change (%)	Slope	Urban Area (%)	Agriculture Area (%)	Forested Area (%)	Shoreline length (marsh-water) (km)	Shoreline length (marsh-forest) (km)
T00251	Sharps Island (1848)	0.30	0.00	0.00	0.00	0.30	100.00	-0.30	-100.00					0	0
T00253	Choptank River (1848)	4.37	3.32	1.47	33.68	2.52	57.77	-1.05	-24.10	0.09	15.58	63.66	15.88	28.69	58.25
T00254	Choptank River (1848-1849)	15.71	12.41	1.67	10.66	4.97	31.64	-3.30	-20.98	0.10	8.15	64.01	26.75	68.93	75.15
T00255	Tar Bay and Upper Part of Honga River (1848)	23.17	31.15	13.14	56.70	5.17	22.30	7.97	34.40	0.01	65.53	16.11	5.79	98.28	146.15
T00266	Nanticoke River (1849)	25.46	25.25	4.24	16.64	4.45	17.47	-0.21	-0.83	0.01	3.19	45.34	46.46	126.39	64.04
T00268-1	Head of Tangier Sound including the Wicomico River (1854)	29.24	29.18	4.21	14.40	4.27	14.59	-0.06	-0.19	0.03	34.77	16.76	30.25	67.98	34.18
T00270	Deils Island and Manokin River (1849)	14.76	13.40	1.61	10.93	2.98	20.18	-1.36	-9.24	0.02	51.43	32.03	10.27	64.08	13.76
T00307	Nandua Creek (1853)	7.02	8.08	3.44	48.96	2.37	33.81	1.06	15.15	0.00	10.12	41.59	13.91	48.85	30.4
T00308	Chesconessex and Onancock Creeks (1850)	16.09	14.38	3.93	24.45	5.64	35.07	-1.71	-10.62	0.00	26.78	38.93	12.56	115.74	43.31
T00451	Meekins Neck (1854)	0.62	0.17	0.07	11.01	0.52	83.27	-0.45	-72.26	0.01	31.46	64.04	0.00	1.66	3.2
T01203	E.Shore of Virginia (1869-1870)	6.15	7.97	4.36	71.01	2.54	41.34	1.82	29.67	0.00	16.81	1.61	27.54	34.14	153.44

T-sheet #	T-sheet Name and Year	Marsh Area in T-sheet (km^2)	Marsh Area in Modern (km^2)	Migration (km^2)	Migration (%)	Erosion (km^2)	Erosion (%)	Net Change (km^2)	Net Change (%)	Slope	Urban Area (%)	Agriculture Area (%)	Forested Area (%)	Shoreline length (marsh-water) (km)	Shoreline length (marsh-forest) (km)
T01534i	Terminus of the N.-Y.P. & N.R.R. (1886)	0.21	0.05	0.04	17.25	0.19	94.32	-0.16	-77.08	0.01	31.17	43.51	0.00	1.19	1.13
T02675	Cape Charles and Vicinity (1905)	3.21	8.99	6.55	204.12	0.77	23.95	5.78	180.17	0.01	14.34	0.09	20.54	37.09	29.95
T02695	Tangier and Watts Islands (1905)	6.45	2.71	0.26	4.03	4.00	62.00	-3.74	-57.97	0.00	50.89	3.29	1.41	33.22	9.02
Simple average		**8.79**	**9.09**	**2.99**	**51.81**	**2.69**	**47.98**	**0.30**	**3.84**	**0.03**	**28.74**	**24.95**	**37.83**	**48.93**	**46.4**
std dev		**8.02**	**8.47**	**2.81**	**75.10**	**1.86**	**25.95**	**2.19**	**79.42**	**0.02**	**19.65**	**21.79**	**40.51**	**37.68**	**41.24**
Total		**311.95**	**318.63**	**100.9**	**32.34**	**94.39**	**30.25**	**6.84**	**2.19**	**0.023**	**25.90**	**22.17**	**40.74**	**2055.12**	**1948.72**

CHAPTER 2

Accelerating rates of forest retreat and marsh migration

ABSTRACT

Accelerated sea level rise is leading to rapid coastal transgression, where coastal treelines are retreating and forests are being replaced by encroaching salt marshes. In coastal forests, frequent flooding and salt stress lead to seedling mortality and allow new marshland to form along gently sloped, undeveloped landscapes. We reconstructed the position of the marsh-forest boundary through time at 5 study sites along the U.S. mid-Atlantic coast to identify long- and short- term drivers of coastal forest retreat, and how they vary with topographic slope and the rate of relative sea level rise. Historical maps and aerial photographs were used to quantify rates of forest retreat on decadal timescales over the last century, and compared to stratigraphy based estimates of forest retreat over century to millennial timescales. 20th century migration rates are 2-14 times faster than pre-industrial rates (< 1875 CE), and have generally accelerated throughout the last century. Together, these observations suggest that marshes migrate into terrestrial forests as a response to sea level rise on broad spatial and temporal scales, and that the onset of recent accelerations in forest retreat rates (1695 – 1915 CE) is closely tied to the onset of rapid increases in relative sea level rise.

INTRODUCTION

Global climate change assessments predict rates of relative sea level rise to increase, leading to enhanced inundation of low-lying coastal regions and a 20 – 50 % decline in salt marsh area by 2100 (Craft et al. 2009; Barbier et al. 2011). Tidal salt marshes provide important ecosystem services with an estimated value of approximately 10,000 US$ per hectare (Barbier et al. 2011). As sea level continues to rise, these critical benefits are increasingly threatened (Torio and Chmura 2013). Sea level began accelerating in the late 19th to early 20th century due to enhanced thermal expansion and ice melting (Church and White 2011). Local changes in relative sea level rise are considerably higher than global estimates, where current relative sea level rise rates along the U.S. mid-Atlantic coast in particular are three to four times faster than the global average due to changes in ocean circulation and regional subsidence (Kemp et al. 2009; Ezer and Corlett 2012; Sallenger et al. 2012; Church et al. 2013; Kemp et al. 2013). Sea level will continue to rise even if greenhouse gas emissions are reduced or halted (Church and White 2011). Previous work has mainly evaluated marsh resilience to relative sea level rise through rates of vertical accretion rather than changes in their lateral boundaries (Stevenson et al. 1986; Brinson et al 1995; Kirwan et al 2010; Kirwan et al. 2016a). The survival of coastal ecosystems however largely depends on their ability to migrate landward, allowing marshes to offset potential losses due to erosion at the seaward edge (Kirwan et al. 2016b).

The morphology of tidal salt marshes is largely controlled by feedbacks between sediment supply, vegetative growth and relative sea level in order to reach a dynamic equilibrium (Reed 1995; Friedrichs and Perry 2001; Cahoon et al. 2006; Kirwan et al. 2010 Kirwan and Megonigal 2013). Coastal marshes are predicted to drown under conditions of rapid sea level rise unless sufficient sediment supply and biological alterations of physical environments allow marshes to maintain equilibrium in the vertical dimension (Kirwan et al.

2010). Inadequate sediment supply leads to wetland deterioration, as salt marshes are particularly vulnerable to erosion processes, depending on the strength of wave power, marsh elevation relative to water elevation, and the presence of wave-mitigating vegetation (Fagherazzi et al. 2013). Marsh-edge erosion is a primary driver of marsh loss, and typically ranges from ~0.1 to > 3 m yr^{-1} (Day et al. 1998; Schwimmer 2001; Marani et al. 2011; Fagherazzi et al. 2013).

Marsh migration is more sensitive to increases in relative sea level than marsh erosion, so that increasing rates of RSLR may ultimately lead to marsh expansion in low-lying coastal regions (Kirwan et al. 2016a). Histosols form along flat, low-energy shorelines as low-lying terrestrial soils become permanently inundated (Friedrichs and Perry 2001; Hussein 2009). Frequent flooding and salt stress lead to the failure of tree regeneration, and are often accompanied by mortality of mature trees that requires punctuated disturbance events (Clark 1986; Williams et al. 1999; Kirwan et al. 2007). Subsequent marsh encroachment into terrestrial forests along gently sloped uplands leads to the migration of coastal forests to higher elevations, and is indicated by the creation of ghost forests and the remains of dead trees (Kirwan et al. 2007). Forest retreat has been observed along many undeveloped coastal margins along the U.S. Atlantic coast (Clark 1986; Williams et al. 1999; Raabe and Stumpf 2016; Kirwan et al. 2016b), and is considered an important factor in evaluating the resilience of coastal and estuarine ecosystems to sea level rise. Previous work suggests that the location of coastal ecosystems changes rapidly on century timescales (Raabe and Stumpf 2016; Schieder et al. 2018), and that rates of marsh migration into retreating forests may increase with increasing rates of relative sea level rise (Kirwan et al. 2016a). Here, we test the hypothesis that marshes migrate rapidly into terrestrial forests in parallel with faster sea level rise rates on century timescales, and that

ecological interactions may not allow shifts in coastal vegetation on annual to decadal timescales until major events occur.

METHODS

This work focuses on long- and short- term drivers of forest retreat relative to late-Holocene sea level rise. We reconstructed the historical marsh-forest boundary through time at five study sites along the U.S. mid-Atlantic coast to identify stratigraphic and modern patterns of marsh migration into terrestrial uplands. We developed a time series of forest retreat at all sites with different slopes and rates of relative sea level rise (Fig. 1). We reconstructed forest retreat over the last 150 years from historical maps and aerial photographs. Millennial time-scale retreat has already been reconstructed for four sites (Young 1995; Hussein 2009), and we reconstructed forest movement from sediment cores at one site (Goodwin Island).

Remote sensing

To determine how forest retreat rates responded to increasing rates of relative sea level rise during the last 150 years, we located the position of the marsh-forest boundary on recent aerial photographs and historical maps at each study site. We established a geodatabase of approximately ten maps or images per study site from the years 1849 to 2014 to identify the spatial distribution of tidal salt marshes and coastal forests within each time step. Historical maps included 1:20,000 scale NOS topographic sheets (T-sheets), 1:80,000 scale coast charts from the Office of Coast Survey's Historical Map and Chart Collection, and 1:24,000 to 1:125,000 scale USGS topographic maps (Table 1). USGS topographic maps were available as GeoPDF layers, and were converted to GeoTIFF, using the Geospatial Data Abstraction Library (GDAL) (www.gdal.org). We compared the aerial extent of marshland that was previously occupied by

terrestrial forest from 19th century maps to modern aerial photographs (U.S. Geological Survey Digital Orthophoto Quadrangles (DOQ), National Aerial Photography Program (NAPP), National Agriculture Imagery Program (NAIP), High Resolution Orthoimagery, Aerial Photo Single Frames, and 2013 ESRI World Imagery. 4-band NAIP images were viewed as false color infrared (CIR) images for simplified analyses of the marsh-forest boundary. On CIR films, dense forested areas appear red, whereas sparse vegetation and wetlands are shown as blue or gray, and dark gray or black areas, respectively (U.S. Geological Survey 2001; Walker et al. 2005). We georeferenced each map and aerial photograph to the 2013 ESRI World Imagery in ArcGIS by aligning at least five control points (e.g. road intersections) in all sets of images and visually fitting with 1st or 2nd order polynomials. The root mean square error (RMSE) of aerial photographs averaged 3 – 4 m and the RMSE of historical maps was 6 – 7 m, and is similar to previous mapping approaches (~4.6 m (Raabe and Stumpf 2016), 6 – 7 m (Schieder et al. 2018)).

To determine the elevation and distance from the modern marsh-forest boundary and rates of forest retreat on annual to decadal timescales, we manually located the transition point from terrestrial forest to salt marsh in each map or photograph along a transect established by Hussein (2009) at the Hell Hook and Cedar Creek, MD sites, a transect established by Young (1995) at the Cedar Island and Long Shoal River, NC sites, and a transect at Goodwin Island, VA at a scale of 1:1,000. We defined the elevation of the buried marsh-forest boundary for each image source by extrapolating the underlying topography of nearby core locations. RTK-GPS generally measures surface elevation in NAVD 88, and we were careful to convert coastal elevations from different frameworks to a common vertical datum by subtracting a correction factor from the source datum (https://vdatum.noaa.gov/vdatumweb/). Simple comparisons of core- and aerial imagery-based measurements of elevation and distance from the modern marsh-

forest boundary suggest that both approaches show similar changes in the coastal treeline, and are indeed comparable in order to reconstruct forest retreat through time (Fig. 2, Fig. 3).

Actual measurements of the vertical position of the marsh-forest boundary by Young (1995) exceed modern estimates by more than 1 meter, and are higher than reported elevation estimates within the same region (Poulter 2005; Kemp et al. 2009). We therefore adjusted stratigraphic elevation measurements by Young (1995) to fit the vertical position of the modern marsh-forest boundary by subtracting a consistent elevation difference (1.3 m) between the oldest aerial photograph/map (1872 CE) and the most recent core (1805 ± 70 CE) at Cedar Island and Long Shoal River. There may be many reasons responsible for potential errors with this procedure, but our corrections are likely sensitive to the alignment of elevations derived from aerial photos and core data. We were uncertain about the exact transect locations chosen by Young (1995), and therefore assumed that the T-sheet boundary corresponded to a sediment core with a similar ^{14}C age in an attempt to align modern and historic changes. However, we were unable to detect reported Mid-Wisconsin peat layers (10,000 – 20,000 years old) underlying the modern marsh peat, and we were also unable to find a similar peat thickness at the 1872 T-sheet boundary (52 cm) compared to the 1805 core (23 cm) (Young 1995). Reported non-calibrated ^{14}C dates involve further issues because the actual age of the marsh-forest boundary at the selected core location may potentially be much older or younger than the T-sheet boundary. Nevertheless, we merely used stratigraphic elevations by Young (1995) to identify the timing of acceleration at Cedar Island and Long Shoal River, which was independent of the correction factor.

Linear forest retreat rates were derived by dividing the length of the movement by the differences between the year 2013 and the year of the image source. To determine additional,

spatially averaged rates of forest retreat, we digitized the areal extent of tidal marshes between the upland and seaward boundary. Depending on the resolution of the aerial photograph, we delineated the modern marshes at a scale of 1:1,000 to 1:2,500. We summarized changes in forest retreat area between two consecutive time periods by calculating non-overlapping sections of marsh area along the upland edge. Linear rates of retreat refer to the change in retreat area divided by the number of years between the two time intervals and the length of the marsh-forest boundary. The length of the marsh-forest boundary is directly calculated from the most recent marsh polygon between two time steps. We then compared both approaches of modern retreat rates derived from aerial photographs (i.e. along a single transect and spatially averaged) with stratigraphic retreat rates based on sediment coring and radiometric dating.

Field work

To determine the slope of the underlying topography, and to reconstruct retreat rates on centennial timescales, we collected sediment cores along a transect at Goodwin Island, VA (Appendix Fig. 1; Appendix Fig. 2). Sediment cores at our Cedar Creek and Hell Hook, MD study sites have already been collected by Hussein (2009), and cores at Cedar Island and Long Shoal River, NC were obtained by Young (1995). We collected a total of 20 cores (Appendix Fig. 3 – 17) with a distance of approximately 20 m between each core location along a northeast-directed transect at Goodwin Island. The transect starts close to the modern marsh-forest boundary, and proceeds into marsh that increases in age. We collected cores using a 1-meter Russian peat corer with a 5 cm diameter half cylinder core chamber to reconstruct the buried marsh-forest boundary. Each core reached the base of the peat and penetrated at least 10 cm into terrestrial soil. We then segmented each core into 5 cm increments, except close to the visually

determined historic marsh-forest boundary, which we divided into 2 cm portions in the field and stored in Ziploc bags. The visual interpretation of the marsh-forest boundary was based on changes in color, density, and amount of organic material, where marsh soil was characterized by a dark brown, soft, and organic-rich layer, and terrestrial soil was defined as a gray, dense, and mineral-rich layer. We collected four additional cores (i.e. G4, G17, G13, and G20 with increasing distance from the modern marsh-forest boundary) to prepare for radiometric dating, using a large-diameter push corer, and packed them in PVC pipes with plastic wrap. We brought all cores to the lab for further analyses. Latitude, longitude and elevation of the modern marsh-forest boundary, and each core location were recorded using a Topcon Hiper V RTK-GPS with a vertical and horizontal error of 4 cm (Appendix Table 1).

Lab work

We analyzed each core for bulk density and percent organic matter to determine the depth of the marsh-forest boundary. We dried each increment in a drying oven and then weighed them to measure bulk density. Bulk density was obtained, using the following equation

$$Bulk\ density = \frac{w_d}{\frac{1}{2}(d_2 - d_1) * \pi * r^2} \ ,$$

where w_d is the dry weight (g), d_1 is the upper depth of each increment (cm), d_2 is the lower depth of each increment (cm), and r is the radius of the Russian peat corer (cm). To prepare the cores for loss on ignition (LOI), we ground every increment with a mortar and pestle and coffee grinder, combusted the homogenized soil samples for 8 hours in a muffle furnace at 550°C, and weighed the ashed sediment. We then used measurements of percent organic matter

and bulk density to determine the depth of the marsh-forest boundary within each core, where we classified layers with percent organic matter > 10 % and bulk density < 0.5 g cm^{-3} as marsh soil. For each core location, we compared the established peat thickness and RTK-GPS elevation measurements to the distance from the modern marsh-forest boundary to create a vertical profile of the antecedent topography, and used linear regression to calculate an average buried slope.

We used cores taken with a large diameter push corer to calculate marsh vertical accretion rates and the timing of upland to wetland conversion. During this process, we divided the core into 1 cm increments up to 20 cm, and into 2 cm from 20 cm to the bottom of the core (~50 cm). The individual samples were then weighed, dried and weighed again to determine percent water content and bulk density. We followed the same procedure that was used to analyze the Russian peat cores, grinding the samples and combusting them to obtain percent organic matter. We then filled petri dishes with homogenized samples, and sealed them with tape and paraffin wax. After thirty days, we used a Canberra gamma counter to obtain unsupported ^{210}Pb activity and ^{137}Cs concentrations of twenty increments per core. We were careful to measure concentrations for seventeen increments that were evenly distributed within the marsh peat and three additional increments that covered top, middle and bottom sections of the terrestrial layers within each core. We then read off net peak area and associated count error percent for gamma photopeaks of ^{210}Pb and ^{137}Cs at 46.5 keV and 661 keV, respectively, gamma photopeaks of ^{214}Pb and ^{214}Bi to determine background activities, and corrected for attenuation in ^{210}Pb and affiliated isotopes.

^{210}Pb is a product of the uranium decay series, where ^{266}Ra decays to ^{222}Rn within Earth's crust and a portion of ^{222}Rn decays to ^{210}Pb from atmospheric fallout (half-life = 22.3 years) (Donnelly and Bertness 2001; Allison et al. 2005). We derived excess ^{210}Pb activity by

subtracting the background value (i.e. the in situ product of the continuous decay of parent nuclides (Clark 1986; Allison et al. 2005)) from the total ^{210}Pb activity, which decreases exponentially with depth during the decay process (Donnelly and Bertness 2001; Allison et al. 2005; Hussein 2009). We derived accretion rates by multiplying the slope of the excess ^{210}Pb activity and core depth with the ^{210}Pb radioactive decay constant, assuming constant accumulation through time (0.03114 yr^{-1}) (Donnelly and Bertness 2001; Hussein 2009), and age of the buried marsh-forest boundary by multiplying accretion rates with the previously determined peat thickness.

We compared accretion rates and age of the marsh-forest boundary derived from ^{210}Pb activity with results from the ^{137}Cs dating method. Nuclear weapon testing started in ~1954 and created a peak fallout deposition of ^{137}Cs on Earth's surface in 1963 (half-life = 30 years) (Pennington et al. 1976; Allison et al. 2005). We plotted ^{137}Cs activity against depth, and determined onset and maximum ^{137}Cs concentrations in each core. We used these markers to calculate sediment accretion rates by dividing the depth of the peak by the differences of the years 2017 to 1954 and 2017 to 1963, respectively. Accretion rates based on ^{210}Pb were similar to rates derived from ^{137}Cs peak analyses, and generally increased with increasing distance from the marsh-forest boundary (Table 2). ^{210}Pb vertical accretion rates and the depth of the marsh-forest boundary were used to determine the year of marsh to forest transition (Appendix Fig. 18 – 21). We then related the age of the marsh-forest boundary to the lateral distance between individual cores to calculate forest retreat rates, which were highly variable along the transect.

RESULTS AND DISCUSSION

Elevation of coastal treelines

The elevation of coastal treelines based on core and imagery analyses gradually increased through time at all sites until ~1875 CE, and increased at more rapid rates afterwards (Fig. 4). Our findings suggest that coastal forests occupied elevations of about -2.3 m below modern mean sea level more than 2,000 years ago, whereas coastal trees now occupy elevations of approximately 0.6 m above mean sea level. Here, coastal treelines in the studied portions of the U.S. mid-Atlantic coast were generally higher than the vertical position of relative sea level at elevations that were approximately 0.3 m above the historic position of relative sea level. Field observations in North Carolina salt marshes suggest that relative sea level rose from -2.58 m to -0.01 m during the same time period (Kemp et al. 2011).

Breakpoint analyses of coastal elevations along individual transects suggest that the onset of recent accelerations in forest retreat rates is closely tied to the onset of rapid increases in relative sea level rise. We defined the breakpoint for each site as the point at which the second derivative was at its maximum (i.e. the change in elevation change rate). Breakpoints were 1695 CE (Long Shoal River), 1808 CE (Hell Hook), 1825 CE (Cedar Island), 1906 CE (Cedar Creek), and 1916 CE (Goodwin Island) (Table 3), and corresponded well to the timing of acceleration reported for sea level rise, both globally and along the U.S. mid-Atlantic coast. Abrupt changes in rates of relative sea level rise were observed for Nova Scotia (1900 - 1920 CE) (Gehrels et al. 2005), Connecticut (1850 – 1900 CE) (Donnelly et al. 2004), North Carolina (1865 – 1915 CE) (Kemp et al. 2009; Kemp et al. 2011), New Jersey (1830 – 1873 CE) (Kemp et al. 2013), and globally (late 18th century – 1900 CE) (Church and White 2006; Jevrejeva et al. 2008; Church and White 2011). Although our reported timing of acceleration is generally consistent with the previously estimated timing of sea level rise acceleration, small discrepancies between both

approaches are likely due to our smaller sample size (n = 8 – 17) relative to previous work (n = 184 (Kemp et al. 2009)) that does not allow for a more accurate estimation of recent forest retreat acceleration. The onset of acceleration at Long Shoal River therefore pre-dates previous estimates of the timing of sea level rise accelerations due to missing data points between 1695 and 1982. Nevertheless, the majority of our breakpoints lie well within the range of sea level rise breakpoints, and simple comparisons between both breakpoints indicate that accelerations in forest retreat rates along the studied portions of the U.S. mid-Atlantic coast were initiated around 1875 CE.

Our findings showed that measured rates of forest elevation change were similar to historic relative sea level rise rates for the same time periods. Average rate of change in coastal treeline elevation at all sites was 0.8 mm yr^{-1} prior to ~1875 CE, and nearly tripled after the onset of acceleration (2.3 mm yr^{-1}). Similar rates and trends in relative sea level rise have been observed along coastal landscapes of the U.S. Atlantic coast and globally (Donnelly et al. 2004; Gehrels et al. 2005; Church and White 2006; Jevrejeva et al. 2008; Kemp et al. 2009; Church and White 2011; Kemp et al. 2011; Kemp et al. 2013). Reported rates of relative sea level rise in North Carolina were approximately 1 mm yr^{-1} until 1865 – 1915 CE, and 2.1 – 3.3 mm yr^{-1} after the breakpoint, resulting in a threefold increase in the rate of relative sea level rise since the onset of acceleration (Kemp et al. 2009; Kemp et al. 2011). Consistency in the magnitude and timing of accelerated sea level rise and forest retreat suggests that coastal forest retreat closely follows climate induced sea level rise.

Accelerating rates of lateral forest retreat

Comparisons between forest retreat rates pre and post ~1875 CE were based on linear regression between time and lateral distance from the modern forest edge along individual transects at each site, and showed that modern retreat rates (1875 to 2016 CE) were 2 to 14 times faster than historic rates (65 BC to 1875 CE) (Table 3). Forest retreat rates were positive in each time step pre- and post- 1875 CE and location, indicating that encroaching marshland steadily replaced retreating coastal upland. Though core analyses along transects provide excellent long-term records of the transgression history, this approach is sensitive to changes in slope and site-specific disturbance events that would be particularly problematic for finer time steps. Here, other ecological factors may create a lag between habitat change and sea level rise along coastal landscapes that may limit expected patterns of ecosystem transgression at the salt marsh ecotone (Clark 1986; Young 1995). Therefore, large-scale spatially averaged measurements of forest retreat may average out the effect of local disturbance and variations in slope, so that relative sea level rise impacts are isolated. Previous field work suggests that salt tolerant trees are generally resilient to sea level rise to the effect that a punctuated disturbance event (e.g. major storm, fire, etc.) is required for coastal forest retreat to occur (Clark 1986; Young 1995; Williams et al. 1999; Kirwan et al. 2007). This finding is in contrast with the general assumption of landscape models that forest retreat takes place instantly as soon as the land is inundated (Feagin et al. 2010; Cadol et al. 2016; Kirwan et al. 2016a). However, we found evidence for both approaches as forest retreat is largely influenced by the upland topography and localized disturbance events on annual to decadal timescales, but follows sea level rise when averaged over large spatial and temporal scales.

Spatially averaged rates indicate that modern forest retreat rates continuously increased throughout the 20th and 21st century, and are higher than pre-1875 CE rates (Fig. 5). Historic forest retreat rate at Goodwin Island is higher than modern forest retreat rates because uncertainties associated with ^{210}Pb did not allow to accurately calculate the age of the buried marsh-forest boundary and therefore forest retreat rates. Our retreat rates generally increased in each time interval at all sites in parallel with recent accelerations in sea level rise, which is consistent with previous estimates for Goodwin Island, and support models that assume marsh migration into uplands follows relative sea level rise (Kirwan et al. 2016a). Our spatially averaged retreat rates (0.07 – 3.8 m yr^{-1}) are similar to mapped rates along the U.S. Atlantic coast (Hussein 2009; Smith 2013; Raabe and Stumpf 2016; Kirwan et al. 2016a; Schieder et al. 2018). Forest retreat rates during the last century were measured in the Big Bend region of the Florida Gulf Coast (2.3 m yr^{-1}) (Raabe and Stumpf 2016), the Delaware Bay (1.8 m yr^{-1}) (Smith 2013), the Chesapeake Bay (0.49 m yr^{-1}) (Schieder et al. 2018), and the eastern shore of Maryland (3.51 – 6.78 m yr^{-1}) (Hussein 2009). Discrepancies between our rates and previously estimated rates are likely due to differences in chosen methods because previous work generally compared changes in forest extent between two time steps (Smith 2013; Raabe and Stumpf 2016; Schieder et al. 2018) or along a single transect (Hussein 2009), whereas our work uniquely combines long-term records along individual transects and mapped retreat rates averaged over broad regions.

Forest retreat is widely considered to be a function of topographic slope and rates of sea level rise (Brinson et al. 1995; Hussein 2009; Raabe and Stumpf 2016; Kirwan et al. 2016a). Previous work suggests that forest retreat lags behind sea level rise because mature trees are resistant to impacts of flooding and salinity, and therefore require a punctuated disturbance event

in order to migrate further landward (Young 1995; Kirwan et al. 2007). Woody plants with higher tolerance to flooding and salinity may temporarily survive sea level rise or develop morphological, anatomical, and physiological adaptations (e.g., hypertrophied lenticels, aerenchyma tissue, and adventitious roots) to cope with flooding stress (Kozlowski 1997; Poulter et al. 2008) to the effect that the coastal treeline retreats stepwise following disturbance-induced mortality (Kirwan et al. 2007). Short-term analyses of marsh response to sea level rise indicate coastal transgression events are strongly influenced by changes in the physical environment, and therefore do not strictly follow Redfield's basic transgression model (Clark 1986). Redfield's model suggests that a ~8 m rise in relative sea level during the last ~4,000 years has led to widespread upland drowning and the creation of new marshland (Redfield 1972). We therefore spanned our work over a large temporal (> 2,000 years) and spatial (~80 km^2) scale to eliminate potential influences of changes in slope and disturbance events on a small area, and found that forest retreat is fundamentally tied to rates of relative sea level rise. Our approach of combining two fundamentally different methods (i.e. long-term coring and spatially averaged mapping analyses) uniquely emphasizes that forest retreat is not an artifact of disturbance events, and that sea level rise is the major driver of long-term habitat change along coastal landscapes.

Implications

Previous work has commonly focused on the movement of different portions of the landscape in response to climate change. Recent accelerations in sea level rise have created a history of transgression events of adjacent ecosystems (e.g. barrier islands, salt marshes, coastal forests) along many coastal margins. Barrier islands and their associated backbarrier environments migrate landwards, as sea level rise promotes complex ecogeomorphic feedbacks that allow

barrier islands to increase their elevation in order to maintain their position in the tidal frame (Walters et al. 2014; Deaton et al. 2017). Backbarrier marshes then migrate into shallow bays, and bays in turn inundate adjacent uplands (Walters et al. 2014). Our work is part of this coupled transgression where marsh migration into adjacent uplands may have compensated for potential marsh loss. Coastal forestland in the studied portions of the U.S. mid-Atlantic coast declined by ~25 km^2 over the last 150 years (~30 % of study area), allowing encroaching marshes to occupy higher elevations and maintain their position relative to sea level rise. Previous mapping efforts showed that approximately 100,000 acres (400 km^2) of coastal forest were lost by upland drowning in the Chesapeake region alone, and that forest retreat can potentially lead to marsh stability in the face of sea level rise (Raabe and Stumpf 2016; Schieder et al. 2018).

However, the stability of tidal wetlands is greatly threatened by anthropogenic activities and their impacts on coastal processes through alterations of climate, nutrient inputs, sediment delivery and subsidence rates (Kirwan and Megonigal 2013). Human activities (e.g. coastal barriers, destructions of wetlands, and/or reduced sediment supply due to dams) exacerbate impacts of relative sea level rise on coastal landscapes, and mitigate potential adaptations of coastal ecosystems to environmental changes (Nicholls and Cazenave 2010). Hardened structures such as dykes and seawalls built at the upper boundary of salt marshes in order to protect coastal properties reduce the ability of marsh migration to compensate for the effects of shoreline erosion on salt marsh extent (Van der Wal and Pye 2004; Kirwan and Megonigal 2013). Our findings therefore highlight how sea level rise has led to widespread loss of coastal forests and the creation of large acreages of tidal salt marshes, and that their survival largely depends on management decisions to exploit the ability of marshes to quickly adapt to environmental changes.

There is ongoing scientific debate over how coastal ecosystems respond to changes in sea level rise. Simple transgression models assume that forest retreat is directly linked to changes in sea level rise (Kirwan et al. 2016a), whereas previous field observations suggest that ecological factors create a lag between sea level rise and forest retreat so that retreat of coastal treelines ultimately occurs through punctuated disturbance events (Young 1995). We unequivocally found that forest retreat responds directly to sea level rise, which is consistent at all five sites along the U.S. mid-Atlantic coast. The elevation of coastal treelines relative to sea level was similar throughout the last 2,000 years, and rates of treeline elevation change and rates of relative sea level rise were nearly identical for the same time periods before and after the onset of acceleration. Breakpoint analyses showed that the timing of forest retreat acceleration corresponds well to the onset of sea level rise acceleration. Together, these observations suggest that marshes migrate into terrestrial forests as a response to sea level rise on broad spatial and temporal scales, and that the onset of recent acceleration in forest retreat is closely tied to the onset of rapid acceleration in relative sea level rise.

LITERATURE CITED

Allison, M.A., A. Sherement, M.A. Goni, and G.W. Stone. 2005. Storm layer deposition on the Mississippi-Atchafalaya subaqueous delta generated by Hurricane Lili in 2002. *Continental Shelf Research* 25: 2213 – 2232.

Barbier, E. B., S.D. Hacker, C. Kennedy, E.W. Koch, A.C. Stier, and B.R. Silliman. 2011. The value of estuarine and coastal ecosystem services. *Ecological Monographs* 81: 169 – 193.

Brinson, M.M., R.R. Christian, and L. K. Blum.1995. Multiple states in the sea-level induced transition from terrestrial forest to estuary. *Estuaries* 18: 648 – 659.

Cadol, D., A. Elmore, S. Guinn, K.A.M. Engelhardt, and G. Sanders. 2016. Modeled tradeoffs between developed land protection and tidal habitat maintenance during rising sea levels. *PLoS ONE* 11(10): e0164875. Doi:10.1371/journal.pone.0164875.

Cahoon, D.R., P.F. Hensel, T. Spencer, D.J. Reed, and N.S. McKee. 2006. Coastal vulnerability to relative sea-level rise: Wetland elevation trends and process controls. *Ecological Studies* 190: 271 – 292.

Church, J.A., and N.J. White. 2006. A 20th century acceleration in global sea-level rise. *Geophysysical Research Letters* 33: L01602.

Church, J.A., and N.J. White. 2011. Sea-level rise from the late 19th to the early 21st century. *Survey Geophysics.* 32: 585 – 602.

Church, J.A., P.U. Clark, A. Cazenave, J.M. Gregory, S. Jevrejeva, A. Levermann, M.A. Merrifield, G.A. Milne, R.S. Nerem, P.D. Nunn, A.J. Payne, W.T. Pfeffer, D. Stammer, and A.S. Unnikrishnan. 2013. Sea level change. In: Climate Change 2013: The physical

science basis. Contribution of working group I to the fifth assessment report of the Intergovernmental Panel on Climmate Change [Stocker, T.F., D. Qin, G.-K. Plattner, M. Tignor, S.K. Allen, J. Boschung, A. NAuels, Y. Xia, V. Bex, and P.M. Midgley (eds.)]. Cambridge University Press, Cambridge, United Kingdom and New York, NY, USA.

Clark, J.S. 1986. Coastal forest tree populations in a changing environment, southeastern Long Island, New York. *Ecological Monographs* 56: 259 – 277.

Craft, C., J. Clough, J. Ehman, S. Joye, R. Park, S. Pennings, H. Guo, and M. Machmuller. 2009. Forecasting the effects of accelerated sea-level rise on tidal marsh ecosystem services. *Frontiers in Ecology and Environment* 7: 73 – 38.

Day, J.W., F. Scarton, A. Rismondo, and D. Are. 1998. Rapid deterioration of a salt marsh in Venice Lagoon, Italy. *Journal of Coastal Research* 14: 583 – 590.

Deaton, C.D., C.J. Hein, and M.L. Kirwan. 2017. Barrier island migration dominates ecogeomorphic feedbacks and drives salt marsh loss along the Virginia Atlantic Coast, USA. *Geology* 45: 123 – 126.

Donnelly, J.P., and M.D. Bertness. 2001. Rapid shoreward encroachment of salt marsh cordgrass in response to accelerated sea-level rise. *Proceedings of the National Academy of Sciences* 98: 14218 – 14223.

Donnelly, J.P., P. Cleary, P. Newby, and R. Ettinger. 2004. Coupling instrumental and geological records of sea-level change: Evidence from southern New England of an increase in the rate of sea-level rise in the late 19th century. *Geophysical Research Letters* 31: L05203.

Ezer, T. and W. B. Corlett. 2012. Is sea level rise accelerating in the Chesapeake Bay? A demonstration of a novel new approach for analyzing sea level data. *Geophysical Research Letters* 39: L19605.

Fagherazzi, S., Mariotti, G., Wiberg, P., and McGlathery, K. 2013. Marsh collapse does not require sea level rise. *Oceanography* 26: 70 -77.

Feagin, R., M. Martinez, G. Mendoza-Gonzalez, and R. Costanza. 2010. Salt marsh zonal migration and ecosystem service change in response to global sea level rise: A case study from an urban region. *Ecology and Society:* 15(4): 14. www.ecologyandsocity.org/vol15/iss4/art14/.

Friedrichs, C.T., and J.E. Perry. 2001. Tidal salt marsh morphodynamics: A synthesis. *Journal of Coastal Research:* 7 – 37.

Gehrels, W.R., J.R. Kirby, A. Prokoph, R.M. Newnham, E.P. Achterberg, H. Evans, S. Black, and D.B. Scott. 2005. Onset of recent rapid sea-level rise in the western Atlantic Ocean. *Quaternary Science Reviews* 24: 2083 – 2100.

Hussein, A.H. 2009. Modeling of sea-level rise and deforestation in submerging coastal ultisols of Chesapeake Bay. *Soil Science Society of America Journal* 73: 185.

Jevrejeva, S., J.C. Moore, A. Grinsted, and P.L. Woodworth. 2008. Recent global sea level acceleration started over 200 years ago? *Geophysical Research Letters* 35: L08715.

Kemp, A.C., B.P. Horton, S.J. Culver, R. Corbett, O. van de Plassche, W.R. Gehrels, B.C. Douglas, and A.C. Parnell. 2009. Timing and magnitude of recent accelerated sea-level rise (North Carolina, United States). *Geology* 37: 1035 – 1038.

Kemp, A.C., B.P. Horton, J.P. Donnelly, M.E. Mann, M. Vermeer, and S. Rahmstorf. 2011. Climate related sea-level variations over the past two millennia. *Proceedings of the National Academy of Science* 108: 11017 – 11022.

Kemp, A.C., B.P. Horton, C.H. Vane, C.E. Bernhardt, D.R. Corbett, S.E. Engelhart, S.C. Anisfeld, A.C. Parnell, and N. Cahill. 2013. Sea-level change during the last 2500 years in New Jersey, USA. *Quaternary Science Reviews* 81: 90 – 104.

Kirwan, M.L., J.L. Kirwan, and C.A. Copenheaver. 2007. Dynamics of an estuarine forest and its response to rising sea level. *Journal of Coastal Research* 232: 457 – 463.

Kirwan, M.L., GlR. Guntenspergen, A. D'Alpaos, J.T. Morris, S.M. Mudd, and S. Temmermann. 2010. Limits on the adaptability of coastal marshes to rising sea level. *Geophysical Research Letters* 37, L23401.

Kirwan, M.L., and J.P. Megonigal. 2013. Tidal wetland stability in the face of human impacts and sea-level rise. *Nature* 504: 53 – 60.

Kirwan, M.L., D.C. Walters, W. Reay, and J.A. Carr. 2016a. Sea level driven marsh expansion in a coupled model of marsh erosion and migration: Sea level driven marsh expansion. *Geophysical Research Letters* 43: 4366 – 4373.

Kirwan, M.L., S. Temmerman, E.E. Skeehan, G.R. Guntenspergen, and S. Fagherazzi. 2016b. Overestimation of marsh vulnerability to sea level rise. *Nature Climate Change* 6: 253 – 260.

Kozlowski, T. 1997. Responses of woody plants to flooding and salinity. *Tree Physiology* 17: 490.

Marani, M., A. D'Alpaos, S. Lanzoni, and M. Santalucia. 2011. Understanding and predicting wave erosion of marsh edges. *Geophysical Research Letters* 38: L21401.

Nicholls, R.J., and A. Cazenave. 2010. Sea-level rise and its impact on coastal zones. *Science* 328: 1517 – 1520.

Pennington, W., R.S. Cambray, J.D. Eakins, and D.D. Harkness. 1976. Radionuclide dating of the recent sediments of Blelham Tarn. *Freshwater Biololgy* 6: 317 – 331.

Poulter, B. 2005. Interactions between landscape disturbance and gradual environmental change: Plant community migration in response to fire and sea level rise. elibrary.ru/item.asp?id=9348557

Poulter, B., N.L. Christensen, and S.S. Qian. 2008. Tolerance of *Pinus taeda* and *Pinus serotine* to low salinity and flooding: Implications for equilibrium vegetation dynamics. *Journal of Vegetation Science* 19: 15 – 22.

Raabe, E.A., and R.P. Stumpf. 2016. Expansion of tidal marsh in response to sea-level rise: Gulf Coast of Florida, USA. *Estuaries and Coasts* 39: 145 – 157.

Redfield, A. 1972. Development of a New England Salt Marsh. *Ecological Monographs* 42: 201 – 237.

Reed, D.J. 1995. The response of coastal marshes to sea-level rise: Survival or submergence? *Earth Surface Processes and Landforms* 20: 39 – 48.

Sallenger, A.H.S., K.S. Doran, and P.A. Howd. 2012. Hotspot of accelerated sea-level rise on the Atlantic coast of North America. *Nature Climate Change* 2, 884 – 888.

Schieder, N.W., D.C. Walters, and M.L. Kirwan. 2018. Massive upland to wetland conversion compensated for historical marsh loss in Chesapeake Bay, USA. *Estuaries and Coasts.* In press. https://doi.org/10.1007/s12237-017-0336-9.

Schwimmer, R.A. 2001. Rates and processes of marsh shorelines erosion in Rehoboth Bay, Delaware, U.S.A. *Journal of Coastal Research* 17: 672 – 683.

Smith, J.A.M. 2013. The role of *Phragmites australis* in mediating inland salt marsh migration in a mid-Atlantic estuary. *PLoS ONE* 8: e65091.

Stevenson, J.C., L.G. Ward, and M.S. Kearney. 1986. Vertical accretion in marshes with varying rates of sea level rise. *Estuarine Variability I:* 241 – 259.

Torio, D.D. and G.L. Chmura. 2013. Assessing coastal squeeze of tidal wetlands. *Journal of Coastal Research:* 1049 – 1061.

U.S. Geological Survey. 2001. Understanding color-infrared photographs. *USGS Fact Sheet*129. pubs.er.usgs.gov/publication/fs12901.

Van der Wal, D., and K. Pye. 2004. Patterns, rates and possible causes of saltmarsh erosion in the Greater Thames area (UK). *Geomorphology* 61: 373 – 381.

Walker, D.A., M.K. Raynolds, F.J.A. Daniels, E. Einarsson, A. Elvebakk, W.A. Gould, A.E. Katenin, S.S. Kholod, C.J. Markon, E.S. Melnikov, N.G. Moskalenko, S.S. Talbot, and B.A. Yurtsev. 2005. The circumpolar Arctic vegetation map. *Journal of Vegetation Science* 16: 267 – 282.

Walters, D.C., L.J. Moore, O. Duran Vinent, S. Fagherazzi, and G. Mariotti. 2014. Interactions between barrier islands and backbarrier marshes affect island system response to sea level

rise: Insights from a coupled model. *Journal of Geophysical Research: Earth Surface* 119: 2014JF003091.

Williams, K., K.C. Ewel, R.P. Stumpf, F.E. Putz, and T.W. Workman. 1999. Sea-level rise and coastal forest retreat on the west coast of Florida, USA. *Ecology* 80: 2045 – 2063.

Young, R.S. 1995. Coastal wetland dynamics in response to sea-level rise: Transgression and erosion. Dissertation. *Duke University*.

FIGURES

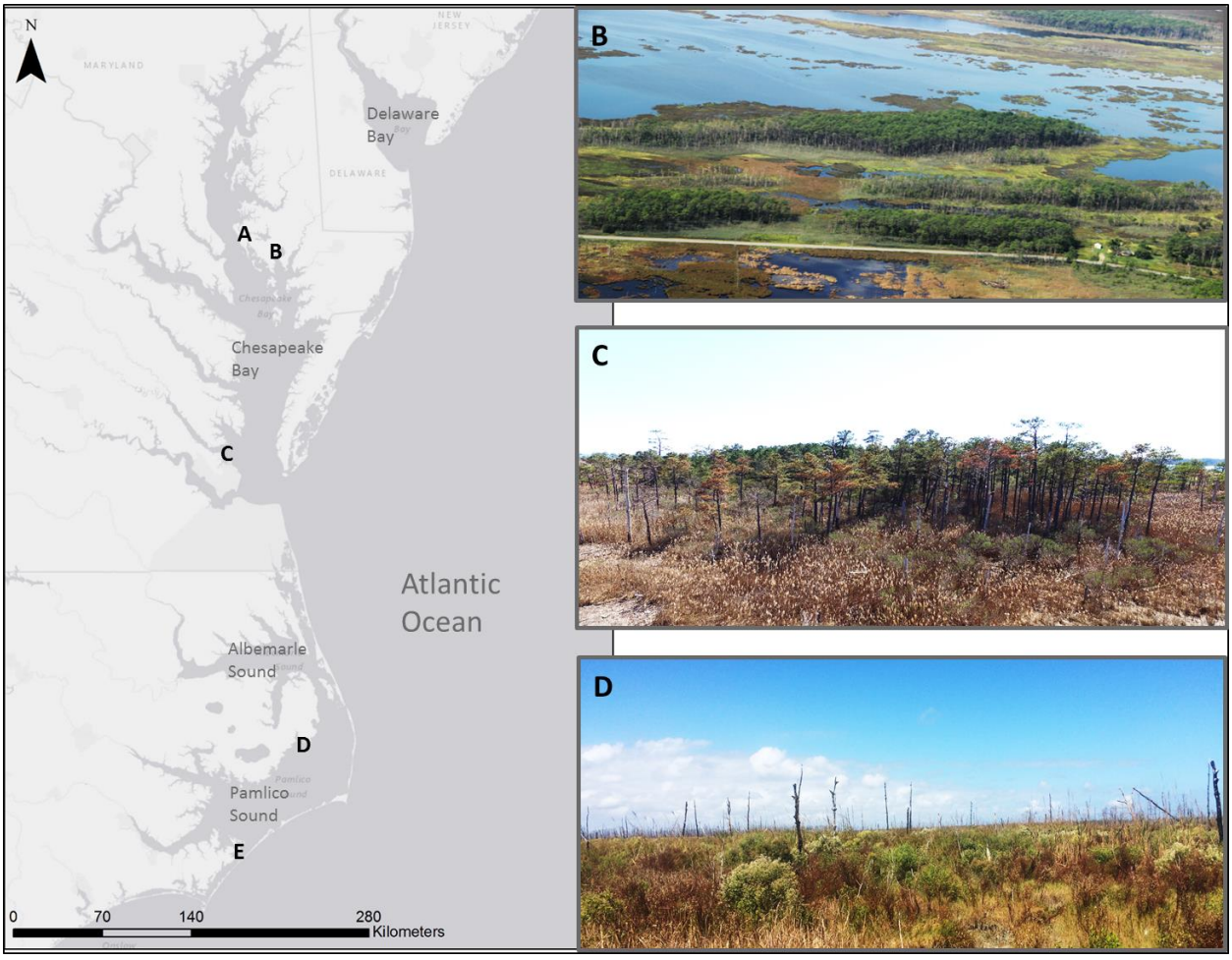

Fig. 1 | Map of study sites along the U.S. Mid-Atlantic coast. *From north to south: (A) Hell Hook, MD; (B) Cedar Creek, MD; (C) Goodwin Island, VA; (D) Long Shoal River, NC; (E) Cedar Island, NC. Drowning of terrestrial uplands leads to the creation of ghost forests along the marsh-forest transition zone. Ghost forests were present in all five study sites (shown: (B) Cedar Creek, MD, (C) Goodwin Island, and (D) Long Shoal River, NC).*

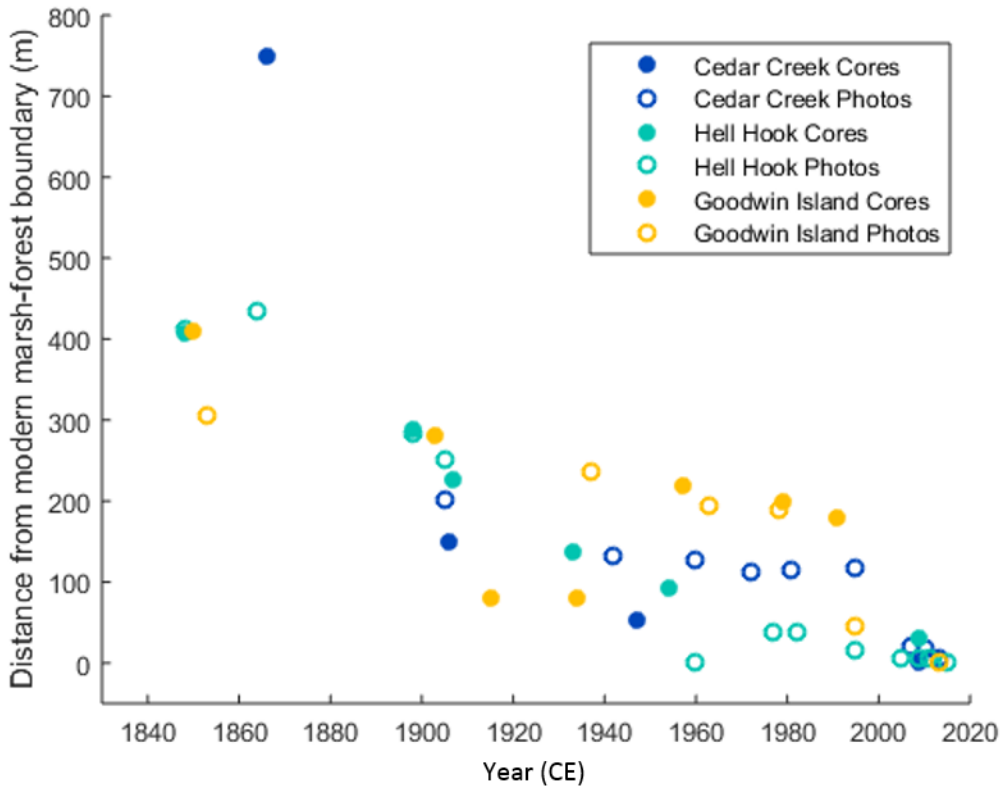

Fig. 2 | Distance from the modern marsh-forest boundary through time. *Sediment core (solid circles) and map/photo (open circles) derived positions of the marsh-forest boundary through time, where distance represents the distance along a transect from the modern marsh-forest boundary. Core data from Cedar Creek and Hell Hook were derived from re-analyses of Hussein (2009). Cedar Island and Long Shoal River sites were not included because the timing of core and map/photo data did not overlap. Distance from the modern marsh-forest boundary generally decreased through time, and was similar between both methods.*

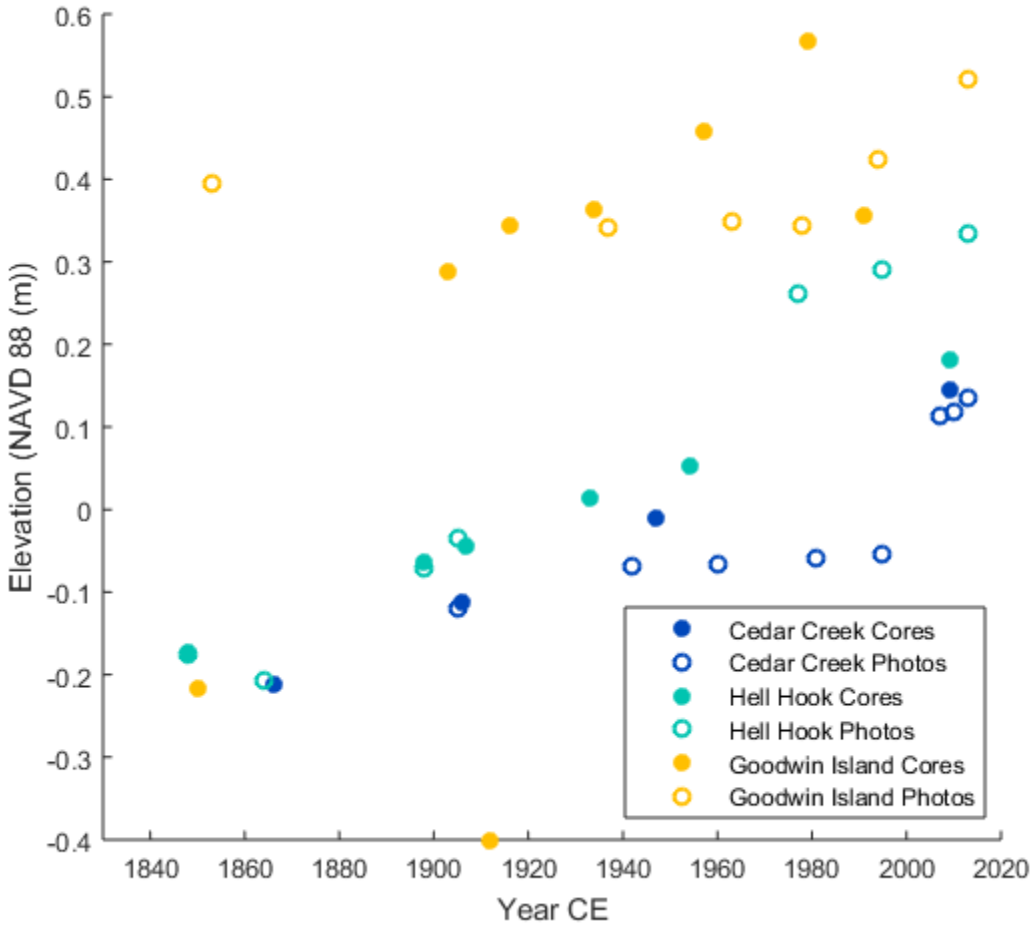

Fig. 3 | Elevation of the marsh-forest boundary through time. *Core-derived treeline elevation (solid circles) was compared to elevation derived from aerial images (open circles). Core data from Cedar Creek and Hell Hook were derived from re-analyses of Hussein (2009). Data from Cedar Island and Long Shoal River were not included because the timing of core and map/photo data did not overlap. Elevation of the coastal treeline generally increased through time, and was similar between both methods. Elevation of Goodwin Island core G20 (1915 CE) differs substantially from the remaining treeline elevations due to uncertainties associated with* ^{210}Pb

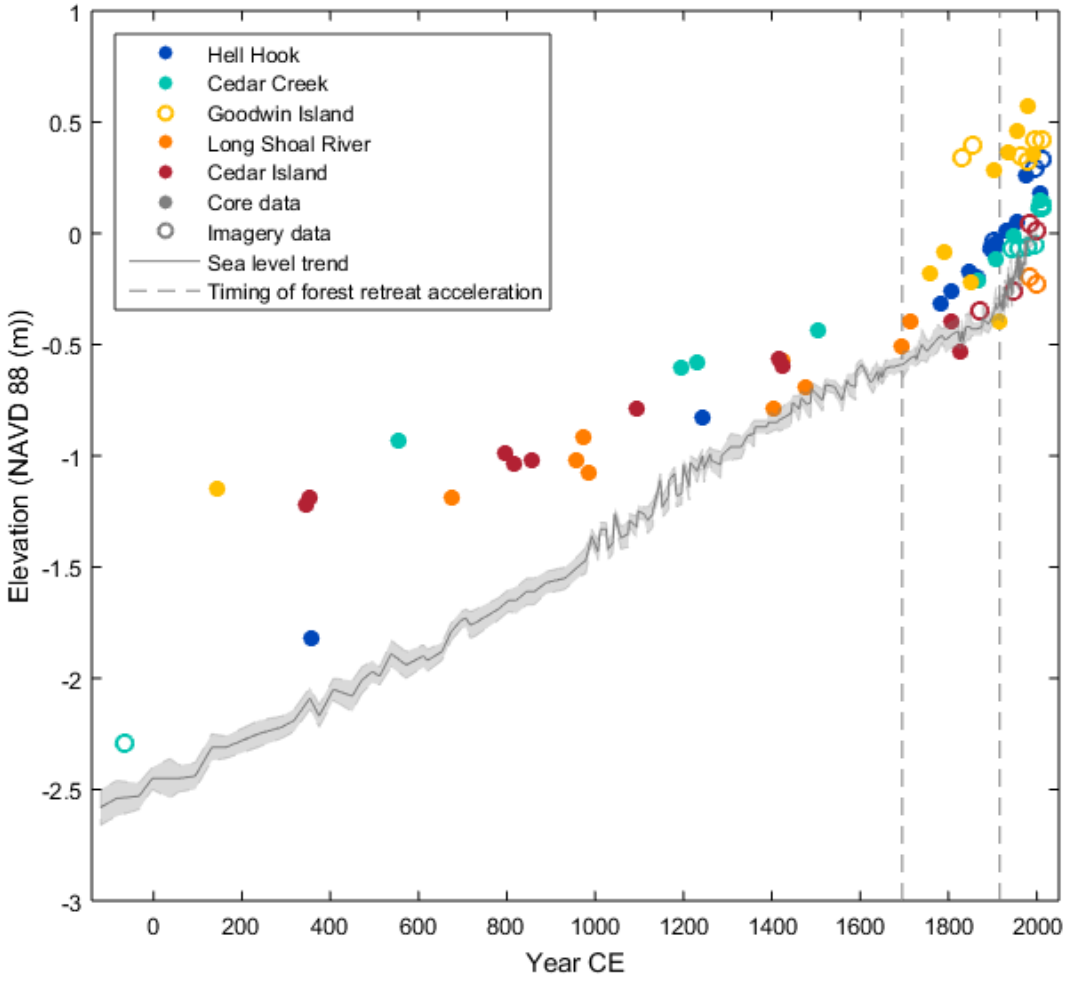

Fig. 4 | Effects of relative sea level rise on coastal treeline elevation. *Long-term relative sea level trend (gray line) is based on paleo-marsh analyses in North Carolina (Kemp et al. 2011). Core-derived elevation of the marsh-forest boundary at Cedar Island and Long Shoal River, as well as Hell Hook and Cedar Creek sites are based on re-analyses of Young (1995) and Hussein (2009), respectively. The remaining data were derived from aerial photographs, sediment cores and RTK-GPS. Core derived relative elevations at Cedar Island and Long Shoal River were adjusted to match absolute elevations measured in the field. Elevation of the marsh-forest transition zone slowly increased through time until ~1875 CE, and increased at faster rates afterwards.*

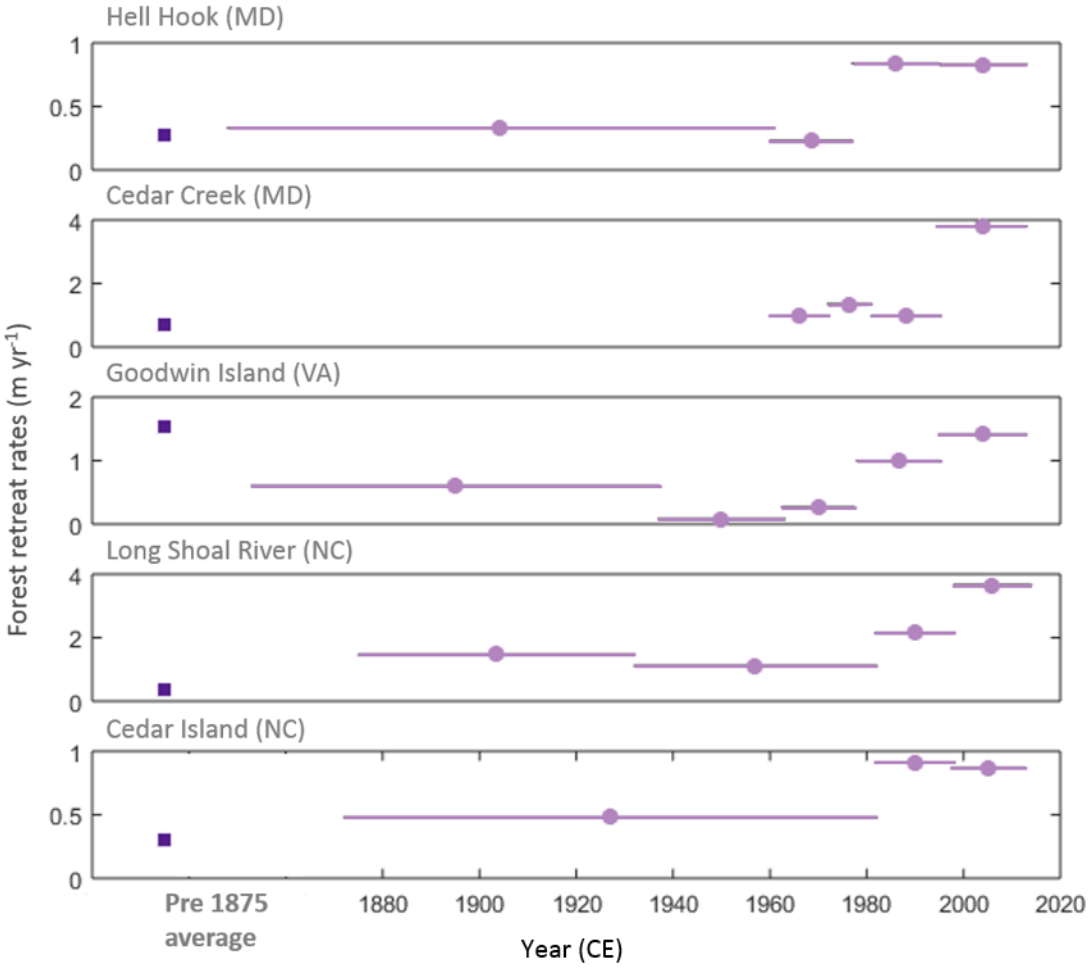

Fig. 5 | Lateral forest retreat rates through time. *20th century forest retreat rates (light purple circles) were compared to pre 1875 CE rates (dark purple square). Forest retreat rates before 1875 are based on linear regression analyses of time and distance to the modern marsh-forest boundary, derived from historical maps and sediment cores. Stratigraphic analyses at Hell Hook, Cedar Creek, Long Shoal River, and Cedar Island are based on re-analyses of Hussein (2009) and Young (1995). Modern rates of lateral forest retreat are based on spatially averaged aerial image analysis, where lateral retreat rate represents the area of forest loss divided by the length of the marsh-forest treeline. Modern forest retreat rates exceed historic rates, and generally increase through time. Historic forest retreat rate at Goodwin Island is higher than modern forest retreat rates because uncertainties associated with ^{210}Pb did not allow to accurately calculate the age of the buried marsh-forest boundary and therefore forest retreat rates.*

Table 1| Sources of aerial images for every location and time step*. Aerial imageries were used for spatially averaged forest retreat analyses as well as transect-based treeline elevation and distance from the modern marsh-forest boundary. Images are organized by location and include further information on the year, type of image, resolution and weblink.*

Year (CE)	Location	Source	Resolution	Weblink
1848	Hell Hook	NOAA Shoreline Data Explorer	1:20,000	https://www.ngs.noaa.gov/NSDE/
1864	Hell Hook	NOAA Historical Map & Chart Collection	1:80,000	https://historicalcharts.noaa.gov/
1898	Hell Hook	United States Geological Survey	1:125,000	https://store.usgs.gov/map-locator
1905	Hell Hook	United States Geological Survey	1:62,500	https://store.usgs.gov/map-locator
1938	Hell Hook	U.S. Agricultural Stabilization and Conservation Service	1:20,000	http://jhir.library.jhu.edu/handle/1774.2/36444
1942	Hell Hook	United States Geological Survey	1:24,000	https://store.usgs.gov/map-locator
1952	Hell Hook	U.S. Agricultural Stabilization and Conservation Service	1:20,000	http://jhir.library.jhu.edu/handle/1774.2/36544
1960	Hell Hook	Aerial Photo Single Frames	1:60,000	https://earthexplorer.usgs.gov/
1977	Hell Hook	Aerial Photo Single Frames	1:80,000	https://earthexplorer.usgs.gov/
1978	Hell Hook	Aerial Photo Single Frames	1:10,000	https://earthexplorer.usgs.gov/
1982	Hell Hook	National High Altitude Photography	1:58,000	https://earthexplorer.usgs.gov/
1994	Hell Hook	Digital Orthophotoquadrangle	1:12,000	https://earthexplorer.usgs.gov/
2005	Hell Hook	National Agriculture Imagery Program GEOTIFF	N/A	https://earthexplorer.usgs.gov/
2009	Hell Hook	National Agriculture Imagery Program GEOTIFF	N/A	https://earthexplorer.usgs.gov/
2011	Hell Hook	National Agriculture Imagery Program GEOTIFF	N/A	https://earthexplorer.usgs.gov/
2013	Hell Hook	ESRI World Imagery	1:280	N/A
2015	Hell Hook	National Agriculture Imagery Program GEOTIFF	N/A	https://earthexplorer.usgs.gov/
1849	Cedar Creek	NOAA Shoreline Data Explorer	1:20,000	https://www.ngs.noaa.gov/NSDE/
1898	Cedar Creek	United States Geological Survey	1:125,000	https://store.usgs.gov/map-locator
1905	Cedar Creek	United States Geological Survey	1:62,500	https://store.usgs.gov/map-locator
1938	Cedar Creek	U.S. Agricultural Stabilization and Conservation Service	1:20,000	http://jhir.library.jhu.edu/handle/1774.2/36444
1942	Cedar Creek	United States Geological Survey	1:24,000	https://store.usgs.gov/map-locator
1952	Cedar Creek	U.S. Agricultural Stabilization and Conservation Service	1:20,000	http://jhir.library.jhu.edu/handle/1774.2/36544
1960	Cedar Creek	Aerial Photo Single Frames	1:60,000	https://earthexplorer.usgs.gov/
1972	Cedar Creek	Aerial Photo Single Frames	1:76,000	https://earthexplorer.usgs.gov/

1981	Cedar Creek	National High Altitude Photography	1:58,000	https://earthexplorer.usgs.gov/
1995	Cedar Creek	Digital Orthophotoquadrangle	1:12,000	https://earthexplorer.usgs.gov/
2005	Cedar Creek	National Agriculture Imagery Program GEOTIFF	N/A	https://earthexplorer.usgs.gov/
2007	Cedar Creek	High Resolution Orthoimagery	N/A	https://earthexplorer.usgs.gov/
2009	Cedar Creek	National Agriculture Imagery Program GEOTIFF	N/A	https://earthexplorer.usgs.gov/
2011	Cedar Creek	National Agriculture Imagery Program GEOTIFF	N/A	https://earthexplorer.usgs.gov/
2013	Cedar Creek	ESRI World Imagery	1:280	N/A
1853	Goodwin Island	NOAA Shoreline Data Explorer	1:20,000	https://www.ngs.noaa.gov/NSDE/
1937	Goodwin Island	Virginia Institute of Marine Science Shoreline Studies Program	N/A	N/A
1963	Goodwin Island	Virginia Institute of Marine Science Shoreline Studies Program	N/A	N/A
1978	Goodwin Island	Virginia Institute of Marine Science Shoreline Studies Program	N/A	N/A
1994	Goodwin Island	Digital Orthophotoquadrangle	1:12,000	https://earthexplorer.usgs.gov/
2013	Goodwin Island	ESRI World Imagery	1:280	N/A
1872	Long Shoal River	NOAA Shoreline Data Explorer	1:20,000	https://www.ngs.noaa.gov/NSDE/
1932	Long Shoal River	Natural Resources Conservation Service, Plymouth, NC	~1:10,000	N/A
1952	Long Shoal River	United States Geological Survey	1:24,000	https://store.usgs.gov/map-locator
1982	Long Shoal River	National High Altitude Photography	1:58,000	https://earthexplorer.usgs.gov/
1998	Long Shoal River	Digital Orthophotoquadrangle	1:12,000	https://earthexplorer.usgs.gov/
2013	Long Shoal River	ESRI World Imagery	1:280	N/A
2014	Long Shoal River	National Agriculture Imagery Program GEOTIFF	N/A	https://earthexplorer.usgs.gov/
1872	Cedar Island	NOAA Shoreline Data Explorer	1:20,000	https://www.ngs.noaa.gov/NSDE/
1949	Cedar Island	United States Geological Survey	1:24,000	https://store.usgs.gov/map-locator
1952	Cedar Island	Doug Newcomp at Raleigh Ecological Services Office	1:20,000	N/A
1982	Cedar Island	National High Altitude Photography	1:58,000	https://earthexplorer.usgs.gov/
1998	Cedar Island	Digital Orthophotoquadrangle	1:12,000	https://earthexplorer.usgs.gov/
2013	Cedar Island	ESRI World Imagery	1:280	N/A

Table 2 | Accretion rates and forest retreat rates at Goodwin Island (VA). *Accretion rates are based on ^{137}Cs peak (1963) and onset (1954), and excess ^{210}Pb. Depth of the marsh-forest boundary was determined using thresholds of organic matter and bulk density (10 % and 0.5 g cm^{-3}). Year of marsh to forest transition was calculated based on the depth of the marsh-forest boundary and ^{210}Pb accretion rates. Distance and retreat rates were calculated between core locations (e.g. distance of 220 m and retreat rate of 4.31 – 7.59 m yr^{-1} were calculated between cores G17 and G4). Retreat rate for G20 is missing due to conflicting year of marsh to forest transition (CE) (Appendix Fig. 1).*

	Accretion Rate (cm yr^{-1})							
Core	^{137}Cs peak	^{137}Cs onset	^{210}Pb	Depth of marsh-forest boundary (cm)	Age of marsh-forest boundary	Year of marsh to forest transition (CE)	Distance (m)	Retreat Rate (m yr^{-1})
G4	0.17-0.19	0.3	0.09	16-17	178-189	1824-1838	80	0.42-0.45
G17	0.09-0.17	0.5	0.14	31-32	221-229	1787-1795	220	4.31-7.59
G13	0.24-0.28	0.37	0.11	48-54	244-274	1742-1772	70	1.32-4.67
G20	0.42-0.53	0.66	0.52	45-59	87-113	1903-1929	40	

Table 3 | Forest retreat rates pre and post breakpoint. *Breakpoints were defined as the point where the second derivative was at its maximum (i.e. the change in elevation change rate). The onset of acceleration at Long Shoal River pre-dates previous estimates of the timing of sea level rise accelerations due to missing data points between 1695 and 1982. Retreat rates were based on linear regression analyses of time and distance from the modern marsh-forest boundary. Post 1875 retreat rates are 2-14 times faster than rates before 1875.*

Site	Breakpoint Year (CE)	Retreat rate (m yr^{-1}) < 1875	Retreat rate (m yr^{-1}) > 1875
Hell Hook	1808	0.27	2.18
Cedar Creek	1906	0.68	1.87
Goodwin Island	1916	1.53	3.3
Long Shoal River	1695	0.34	4.61
Cedar Island	1825 (1948/1949)	0.3	1.65

APPENDIX

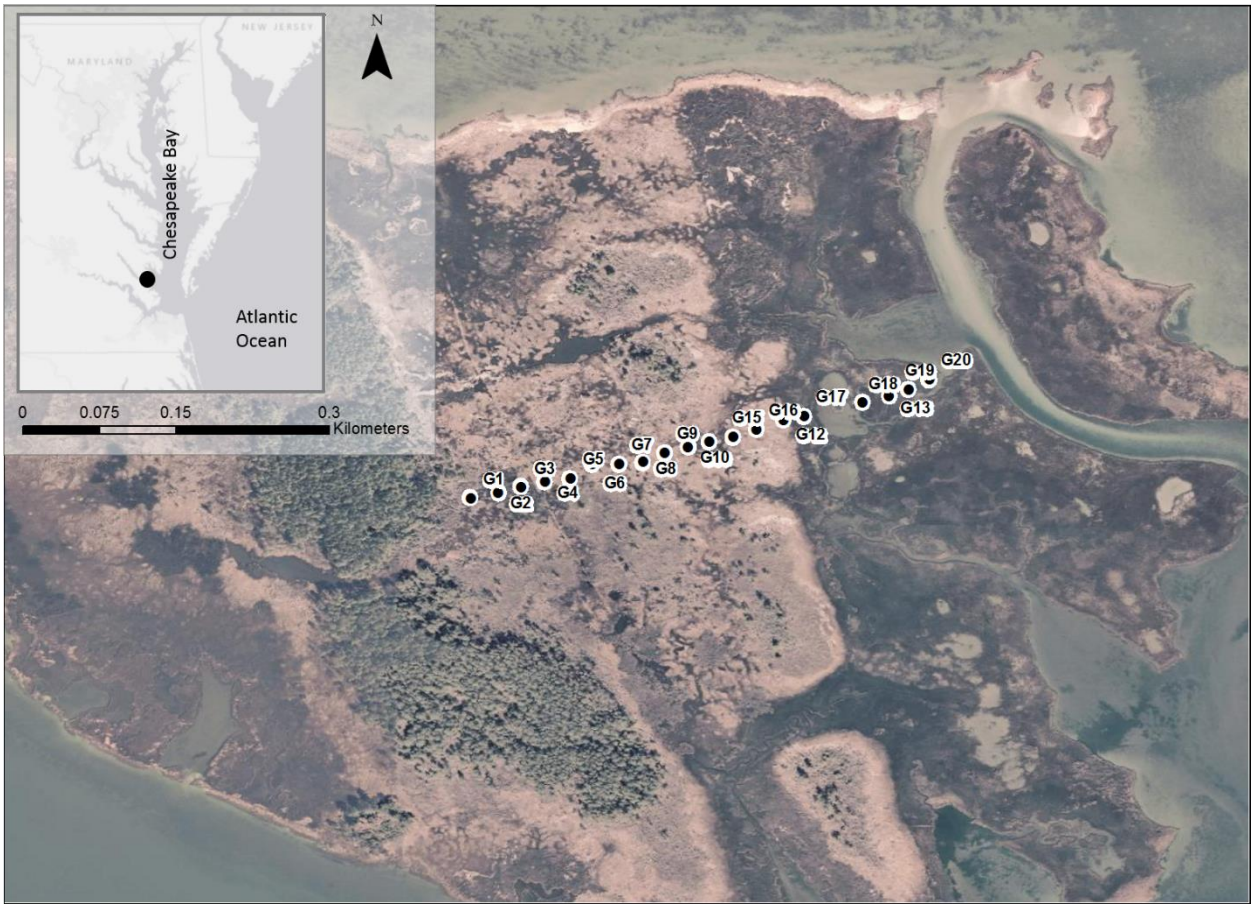

Appendix Fig. 1 | Goodwin Island core locations. *Black dot represents location of Goodwin Island within the Chesapeake Bay. Map shows exact locations of all twenty cores at Goodwin Island. Cores were taken with a Russian peat corer, and analyzed for bulk density and organic matter (Appendix Fig. 3 – 17). Four additional cores (G4, G17, G13, and G20) were taken with a large-diameter push corer to calculate the age of the historic marsh-forest boundary and vertical accretion rates (Appendix Fig. 18 – 21).*

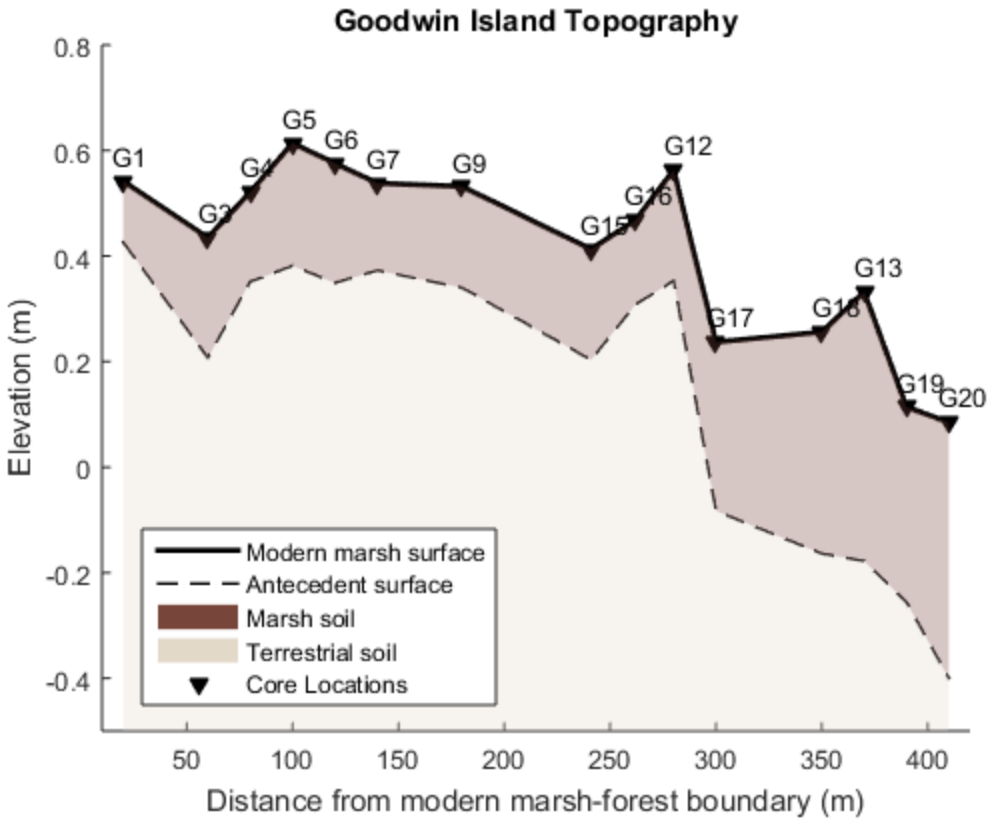

Appendix Fig. 2 | Vertical profile of Goodwin Island*. Profile shows vertical (exaggerated) and horizontal position of individual cores (triangles) and the antecedent surface (dashed line) along a transect (Appendix Fig. 1). Following core profiles (Appendix Fig. 3 – 17) and ^{210}Pb and ^{137}Cs profiles (Appendix Fig. 18 – 21) are ordered according to their position along the transect (i.e. increasing distance from the modern forest edge). The reconstructed antecedent surface was used to determine the elevation from aerial images. The underlying topography is gently sloped (0.0019), and the peat thickness (dark brown) generally increases with increasing distance from the modern forest edge.*

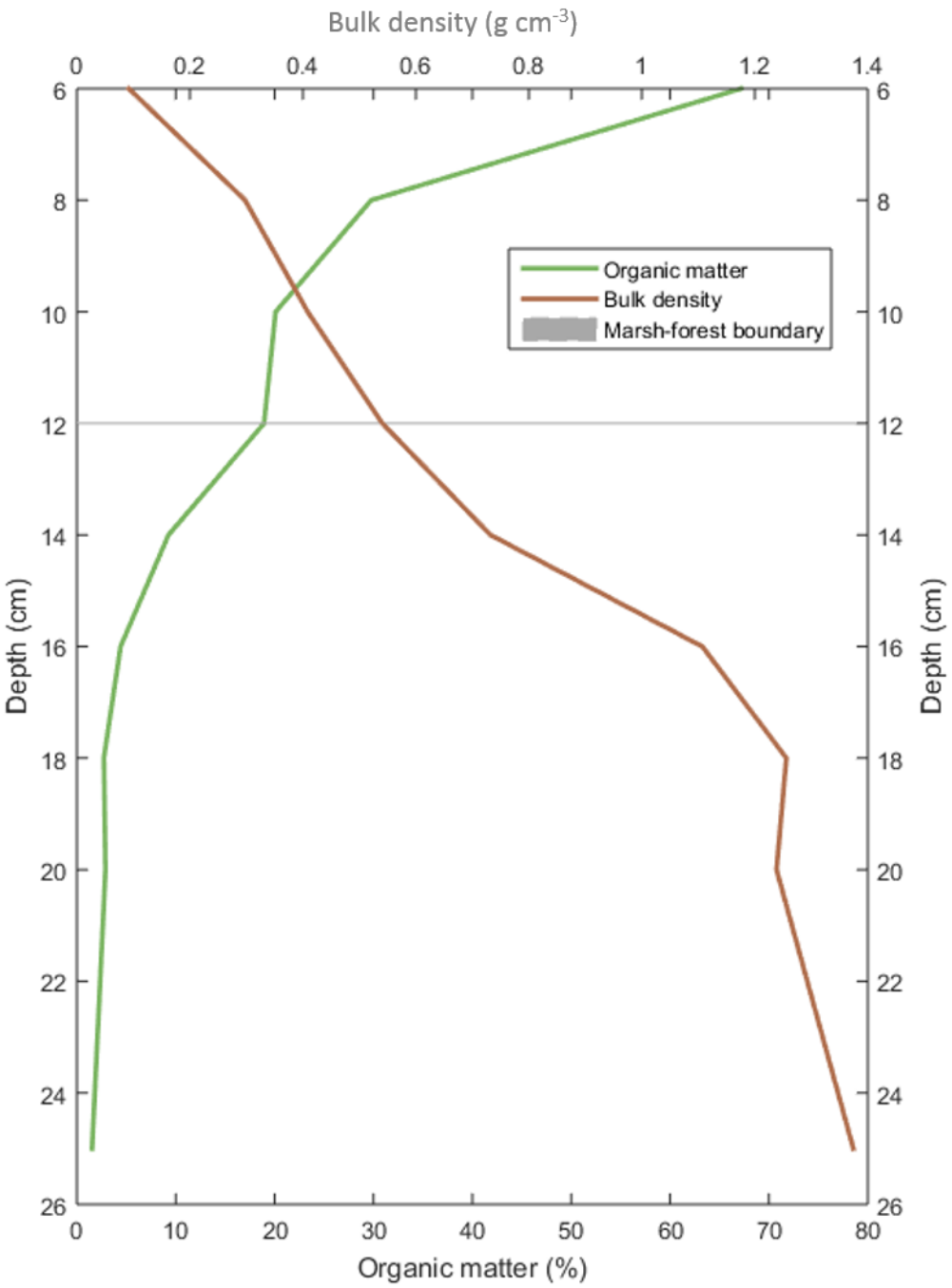

Appendix Fig. 3 | G1 core profile (Goodwin Island). *Organic matter (%) (green) and bulk density (g cm^{-3}) (brown) were used to determine the depth of the historic marsh-forest boundary (gray envelope). Bulk density generally increased with depth, while organic matter decreased. We defined brown, high organic, mineral-poor soil as marsh (organic matter > 10%, bulk density < 0.5 g cm^{-3}), and gray, clay-rich, low organic soil as terrestrial (organic matter < 10%, bulk density > 0.5 g cm^{-3}). The gray envelope represents the upper and lower extend of marsh-forest boundary determined by organic matter and bulk density. A larger envelope indicates larger discrepancies between both methods. The average depth of the historic marsh-forest boundary at G1 is 12 cm.*

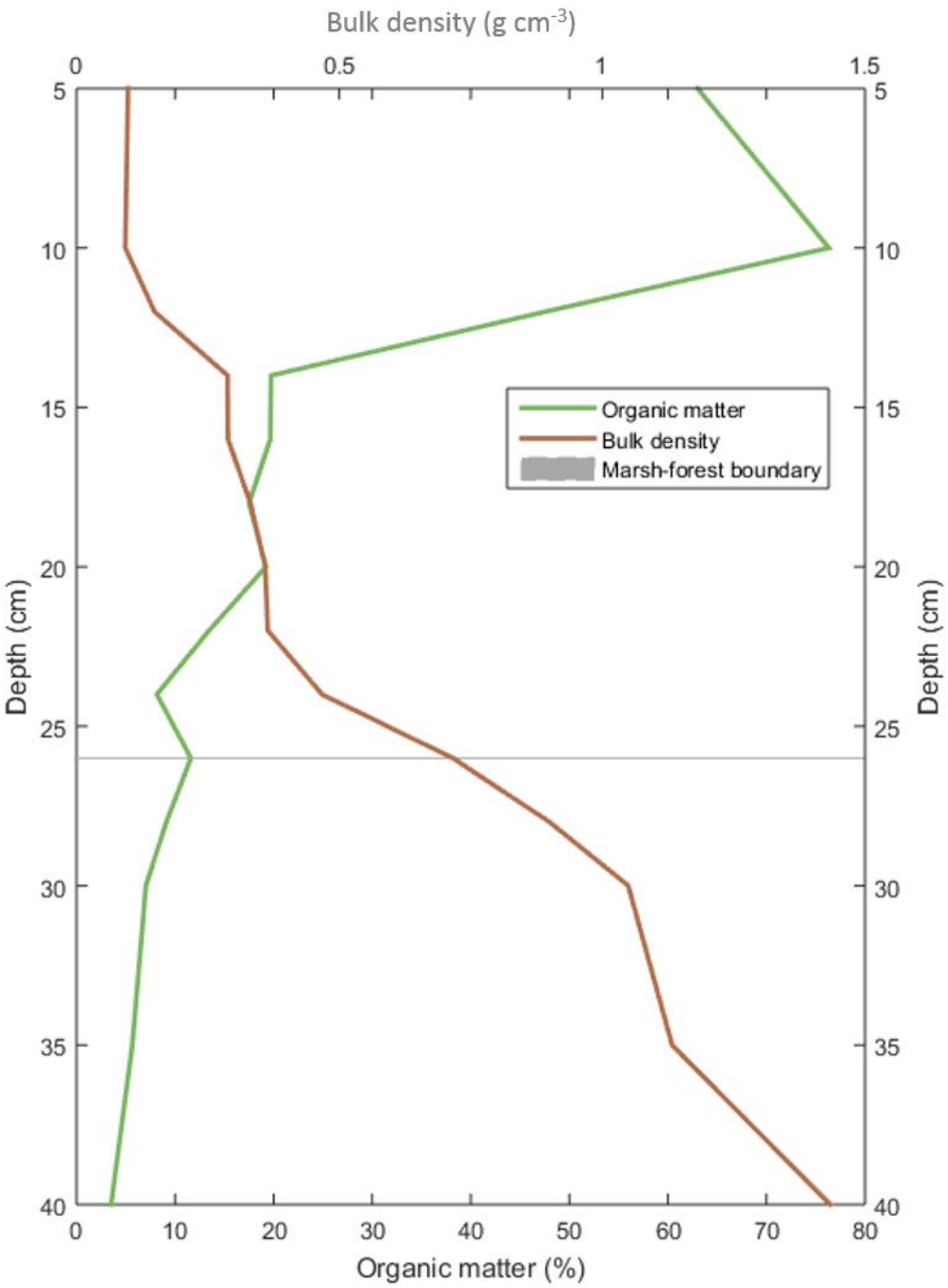

Appendix Fig. 4 | G3 core profile (Goodwin Island). *Organic matter (%) (green) and bulk density (g cm^{-3}) (brown) were used to determine the depth of the historic marsh-forest boundary (gray envelope). Bulk density generally increased with depth, while organic matter decreased. We defined brown, high organic, mineral-poor soil as marsh (organic matter > 10%, bulk density < 0.5 g cm^{-3}), and gray, clay-rich, low organic soil as terrestrial (organic matter < 10%, bulk density > 0.5 g cm^{-3}). The gray envelope represents the upper and lower extend of marsh-forest boundary determined by organic matter and bulk density. A larger envelope indicates larger discrepancies between both methods. The average depth of the historic marsh-forest boundary at G3 is 26 cm.*

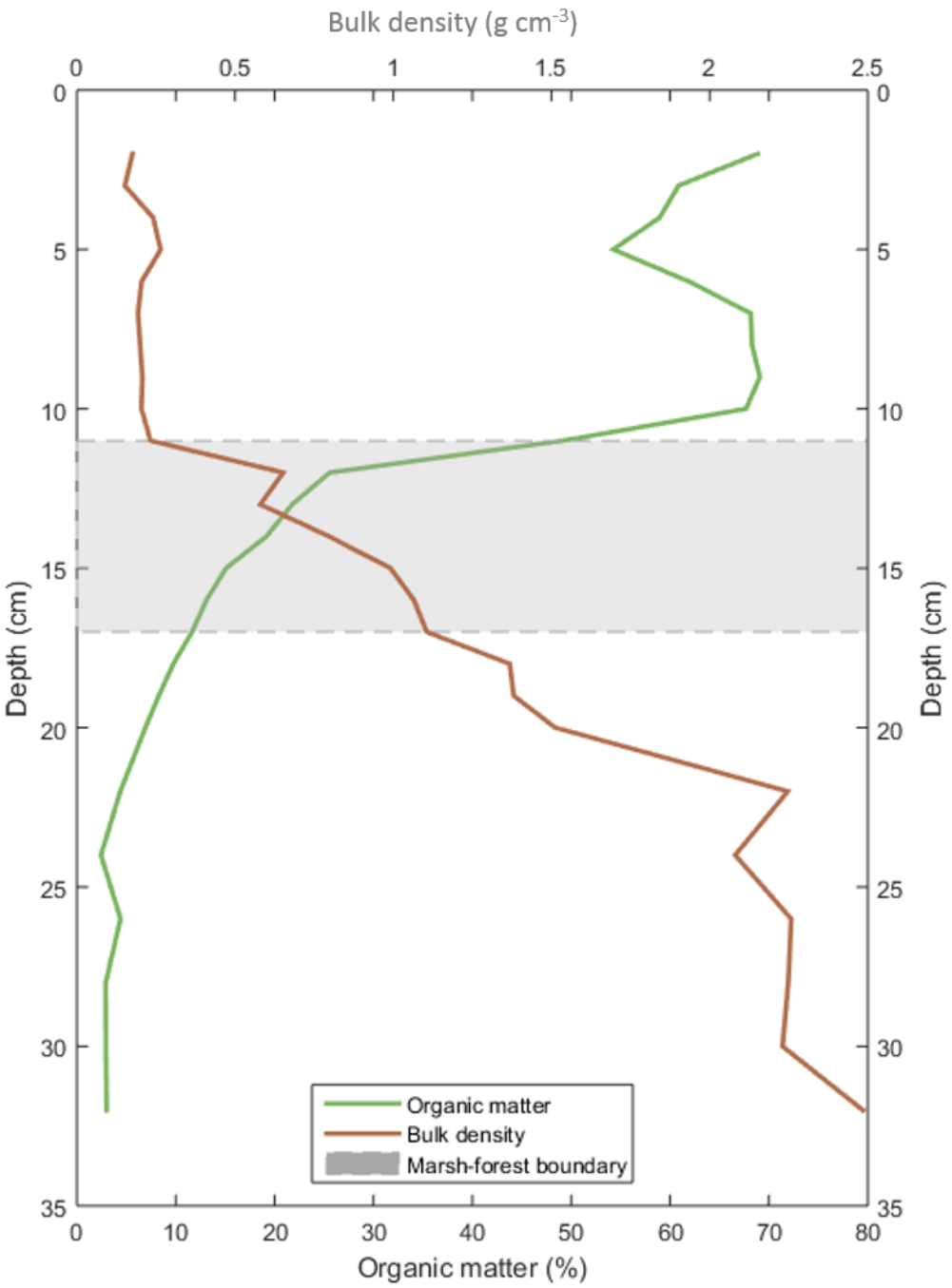

Appendix Fig. 5 | G4 core profile (Goodwin Island). *Organic matter (%) (green) and bulk density (g cm^{-3}) (brown) were used to determine the depth of the historic marsh-forest boundary (gray envelope). Bulk density generally increased with depth, while organic matter decreased. We defined brown, high organic, mineral-poor soil as marsh (organic matter > 10%, bulk density < 0.5 g cm^{-3}), and gray, clay-rich, low organic soil as terrestrial (organic matter < 10%, bulk density > 0.5 g cm^{-3}). The gray envelope represents the upper and lower extend of marsh-forest boundary determined by organic matter and bulk density. A larger envelope indicates larger discrepancies between both methods. The average depth of the historic marsh-forest boundary at G4 is 14 cm.*

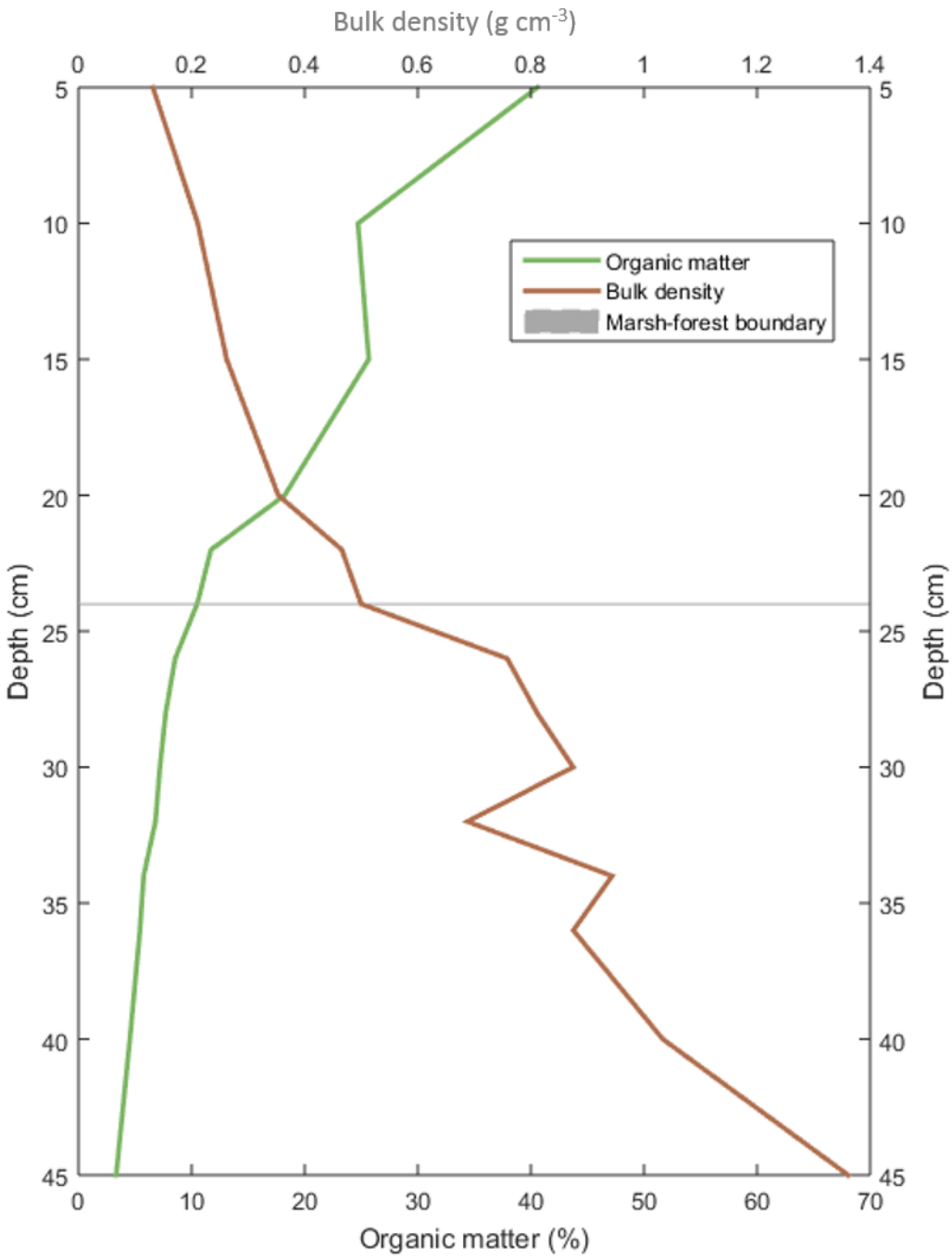

Appendix Fig. 6 | G5 core profile (Goodwin Island). *Organic matter (%) (green) and bulk density (g cm^{-3}) (brown) were used to determine the depth of the historic marsh-forest boundary (gray envelope). Bulk density generally increased with depth, while organic matter decreased. We defined brown, high organic, mineral-poor soil as marsh (organic matter > 10%, bulk density < 0.5 g cm^{-3}), and gray, clay-rich, low organic soil as terrestrial (organic matter < 10%, bulk density > 0.5 g cm^{-3}). The gray envelope represents the upper and lower extend of marsh-forest boundary determined by organic matter and bulk density. A larger envelope indicates larger discrepancies between both methods. The average depth of the historic marsh-forest boundary at G5 is 24 cm.*

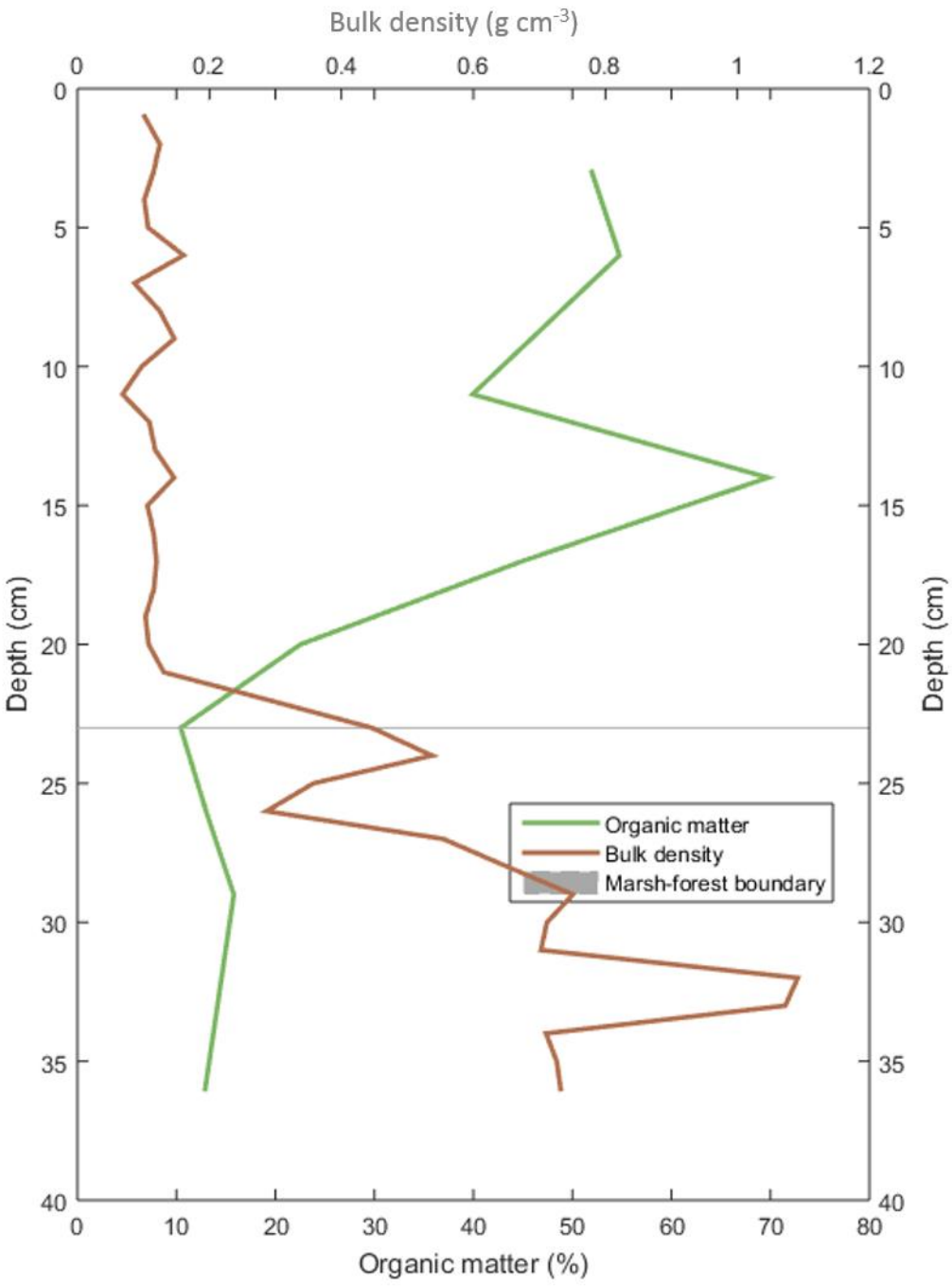

***Appendix Fig. 7 | G6 core profile (Goodwin Island)**. Organic matter (%) (green) and bulk density (g cm^{-3}) (brown) were used to determine the depth of the historic marsh-forest boundary (gray envelope). Bulk density generally increased with depth, while organic matter decreased. We defined brown, high organic, mineral-poor soil as marsh (organic matter > 10%, bulk density < 0.5 g cm^{-3}), and gray, clay-rich, low organic soil as terrestrial (organic matter < 10%, bulk density > 0.5 g cm^{-3}). The gray envelope represents the upper and lower extend of marsh-forest boundary determined by organic matter and bulk density. A larger envelope indicates larger discrepancies between both methods. The average depth of the historic marsh-forest boundary at G6 is 23 cm.*

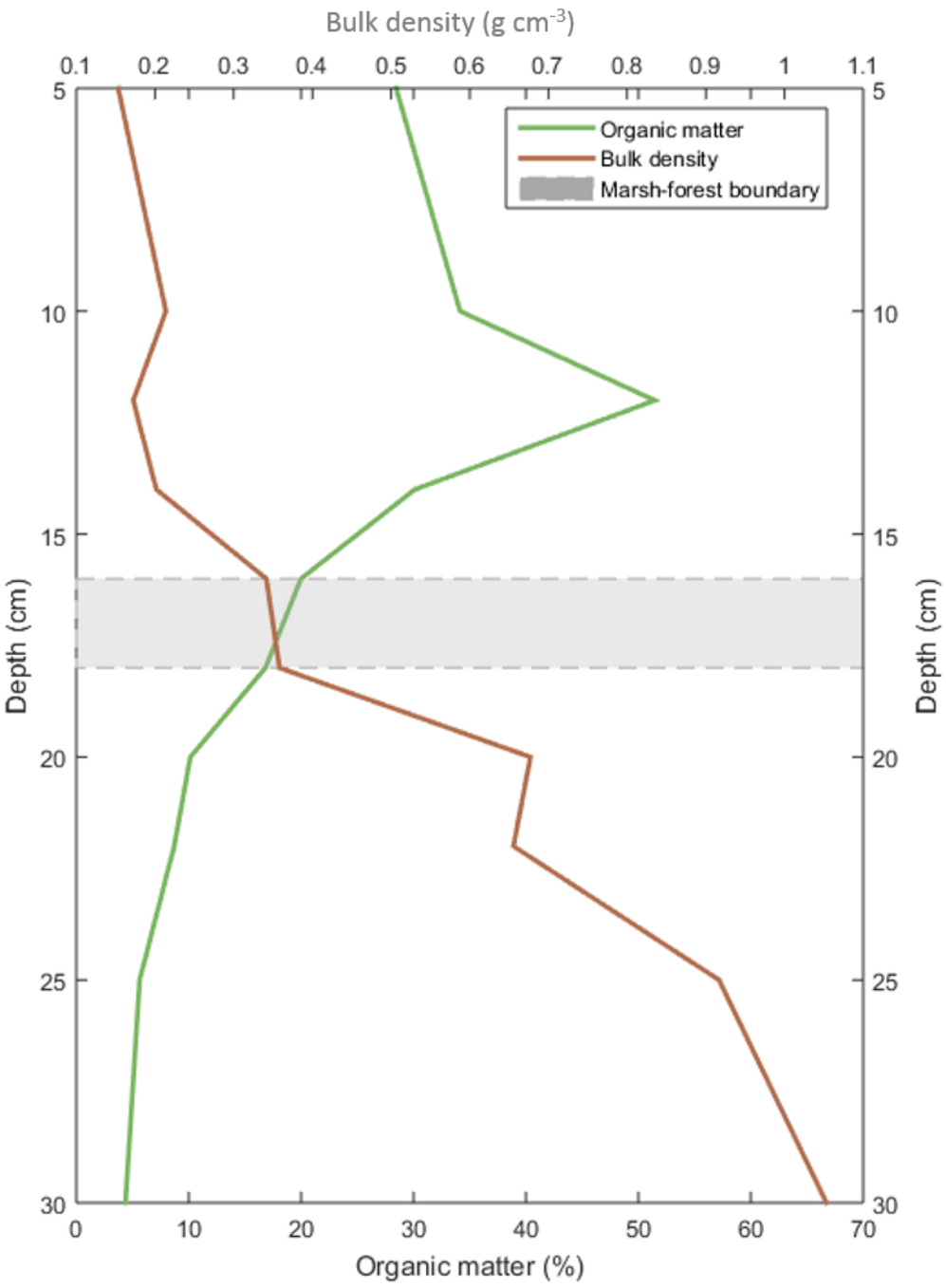

Appendix Fig. 8 | G7 core profile (Goodwin Island). *Organic matter (%) (green) and bulk density (g cm^{-3}) (brown) were used to determine the depth of the historic marsh-forest boundary (gray envelope). Bulk density generally increased with depth, while organic matter decreased. We defined brown, high organic, mineral-poor soil as marsh (organic matter > 10%, bulk density < 0.5 g cm^{-3}), and gray, clay-rich, low organic soil as terrestrial (organic matter < 10%, bulk density > 0.5 g cm^{-3}). The gray envelope represents the upper and lower extend of marsh-forest boundary determined by organic matter and bulk density. A larger envelope indicates larger discrepancies between both methods. The average depth of the historic marsh-forest boundary at G7 is 17 cm.*

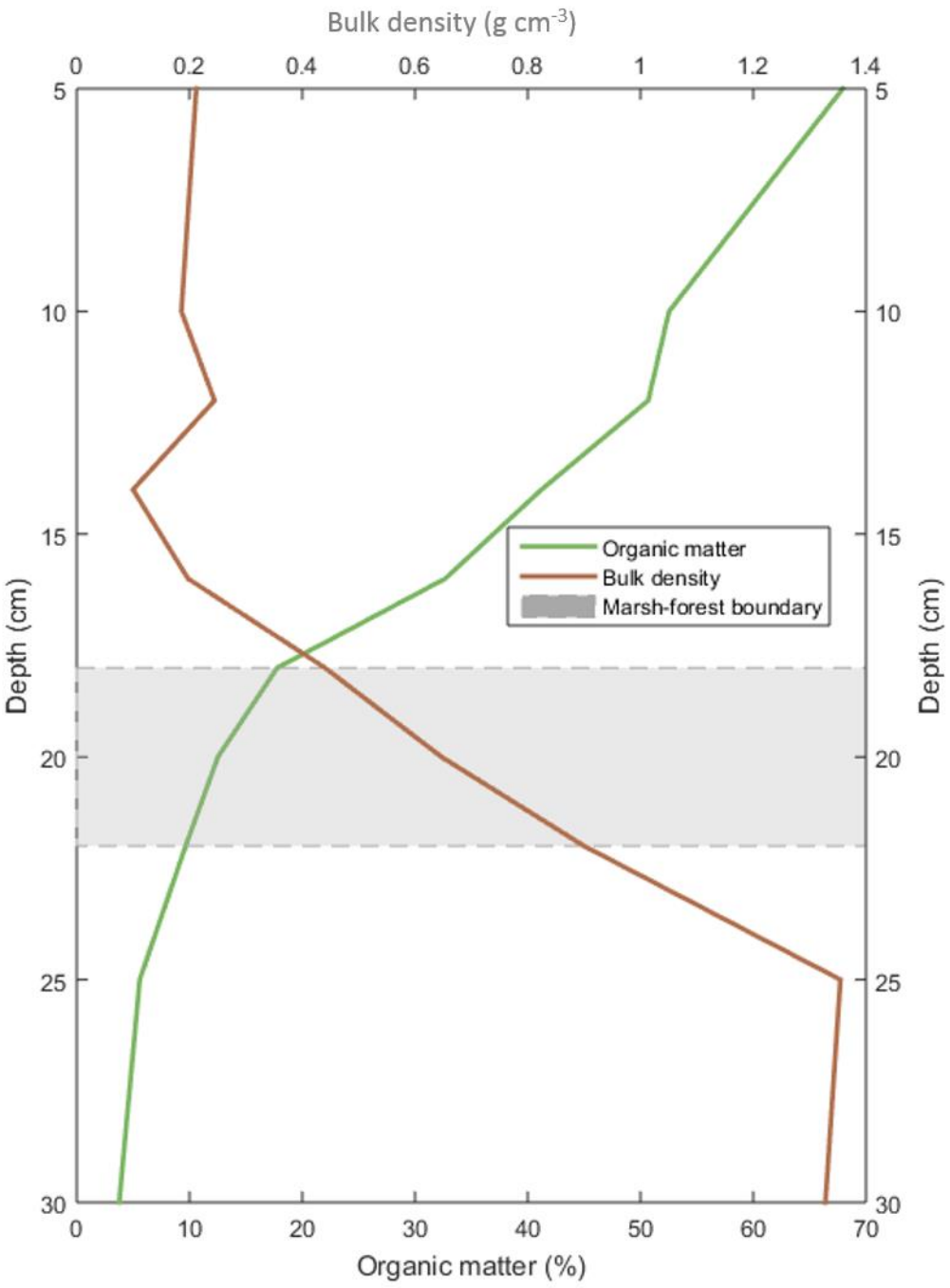

Appendix Fig. 9 | G9 core profile (Goodwin Island). *Organic matter (%) (green) and bulk density (g cm^{-3}) (brown) were used to determine the depth of the historic marsh-forest boundary (gray envelope). Bulk density generally increased with depth, while organic matter decreased. We defined brown, high organic, mineral-poor soil as marsh (organic matter > 10%, bulk density < 0.5 g cm^{-3}), and gray, clay-rich, low organic soil as terrestrial (organic matter < 10%, bulk density > 0.5 g cm^{-3}). The gray envelope represents the upper and lower extend of marsh-forest boundary determined by organic matter and bulk density. A larger envelope indicates larger discrepancies between both methods. The average depth of the historic marsh-forest boundary at G9 is 18 cm.*

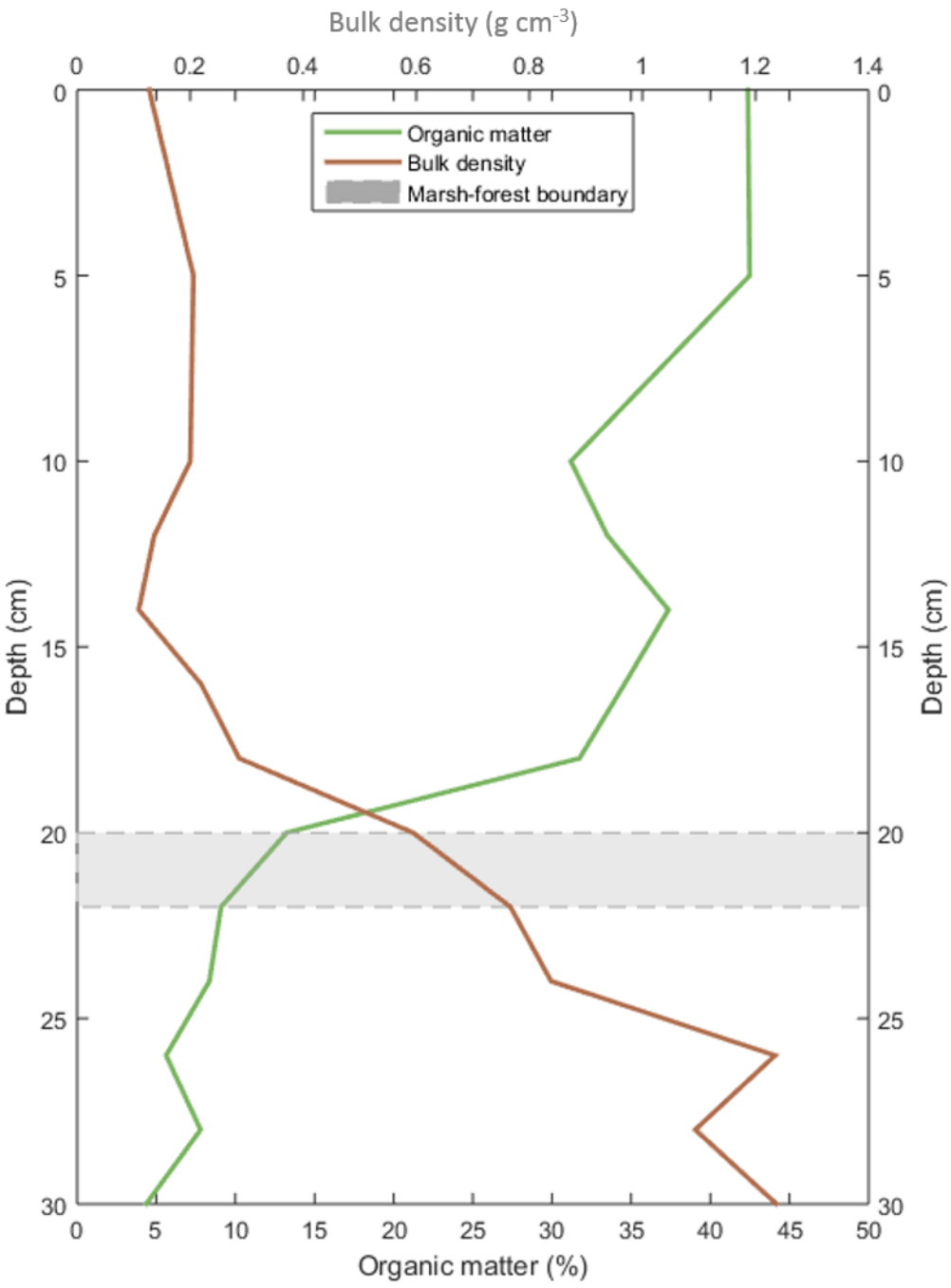

Appendix Fig. 10 | G15 core profile (Goodwin Island). *Organic matter (%) (green) and bulk density (g cm^{-3}) (brown) were used to determine the depth of the historic marsh-forest boundary (gray envelope). Bulk density generally increased with depth, while organic matter decreased. We defined brown, high organic, mineral-poor soil as marsh (organic matter > 10%, bulk density < 0.5 g cm^{-3}), and gray, clay-rich, low organic soil as terrestrial (organic matter < 10%, bulk density > 0.5 g cm^{-3}). The gray envelope represents the upper and lower extend of marsh-forest boundary determined by organic matter and bulk density. A larger envelope indicates larger discrepancies between both methods. The average depth of the historic marsh-forest boundary at G15 is 21 cm.*

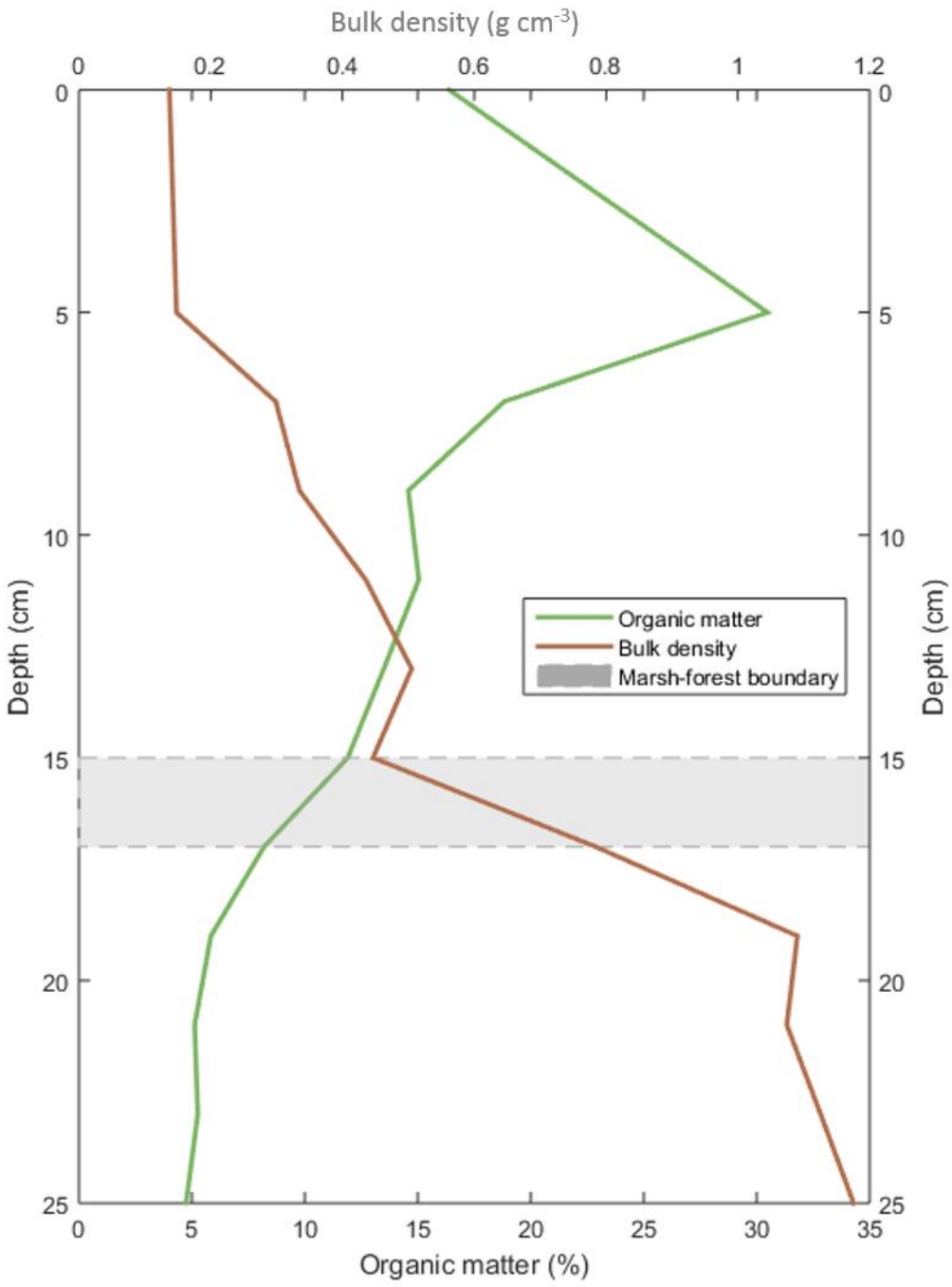

Appendix Fig. 11 | G16 core profile (Goodwin Island). *Organic matter (%) (green) and bulk density (g cm^{-3}) (brown) were used to determine the depth of the historic marsh-forest boundary (gray envelope). Bulk density generally increased with depth, while organic matter decreased. We defined brown, high organic, mineral-poor soil as marsh (organic matter > 10%, bulk density < 0.5 g cm^{-3}), and gray, clay-rich, low organic soil as terrestrial (organic matter < 10%, bulk density > 0.5 g cm^{-3}). The gray envelope represents the upper and lower extend of marsh-forest boundary determined by organic matter and bulk density. A larger envelope indicates larger discrepancies between both methods. The average depth of the historic marsh-forest boundary at G16 is 16 cm.*

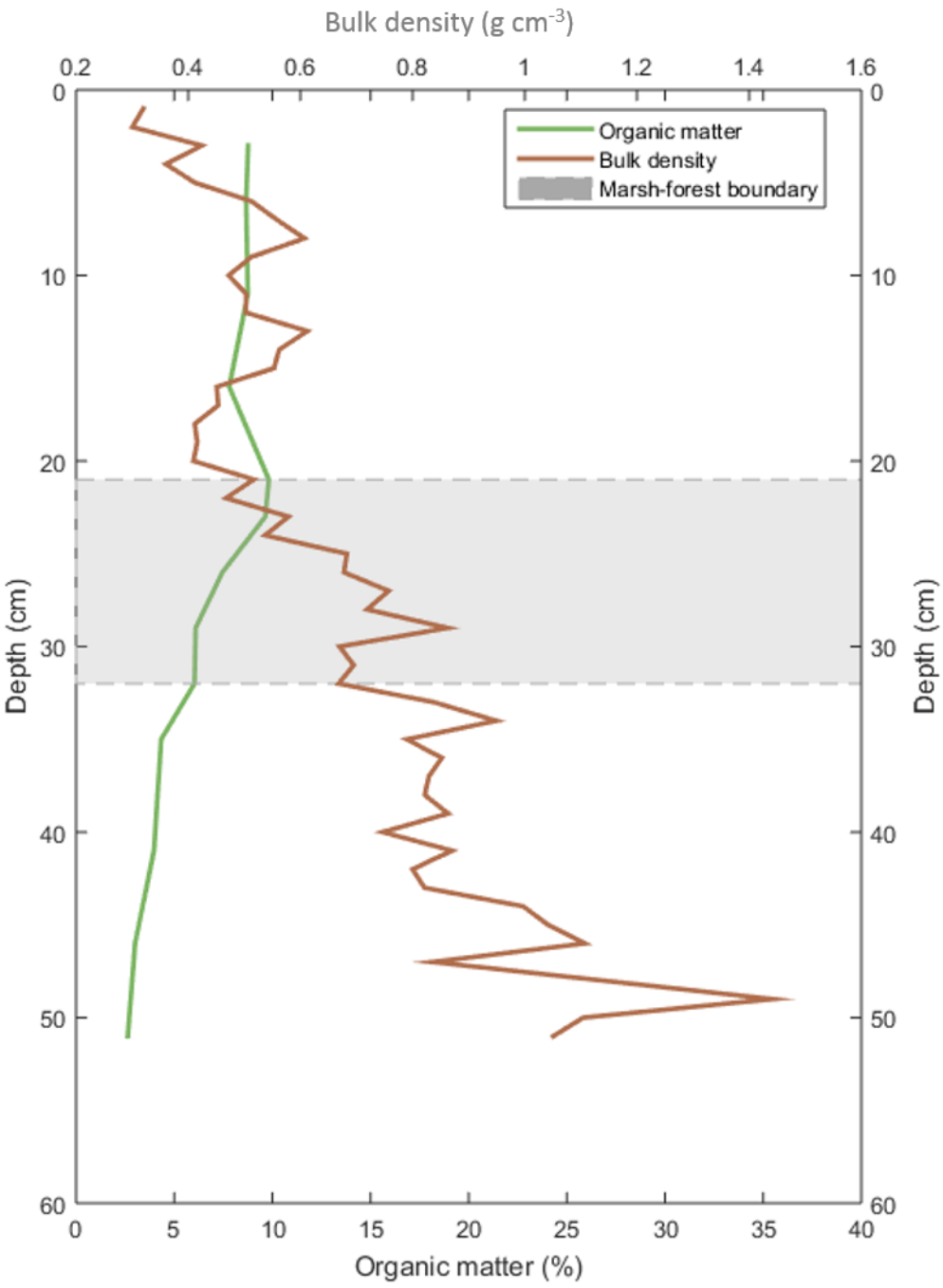

Appendix Fig. 12 | G12 core profile (Goodwin Island). *Organic matter (%) (green) and bulk density (g cm^{-3}) (brown) were used to determine the depth of the historic marsh-forest boundary (gray envelope). Bulk density generally increased with depth, while organic matter decreased. We defined brown, high organic, mineral-poor soil as marsh (organic matter > 10%, bulk density < 0.5 g cm^{-3}), and gray, clay-rich, low organic soil as terrestrial (organic matter < 10%, bulk density > 0.5 g cm^{-3}). The gray envelope represents the upper and lower extend of marsh-forest boundary determined by organic matter and bulk density. A larger envelope indicates larger discrepancies between both methods. The average depth of the historic marsh-forest boundary at G21 is 27 cm.*

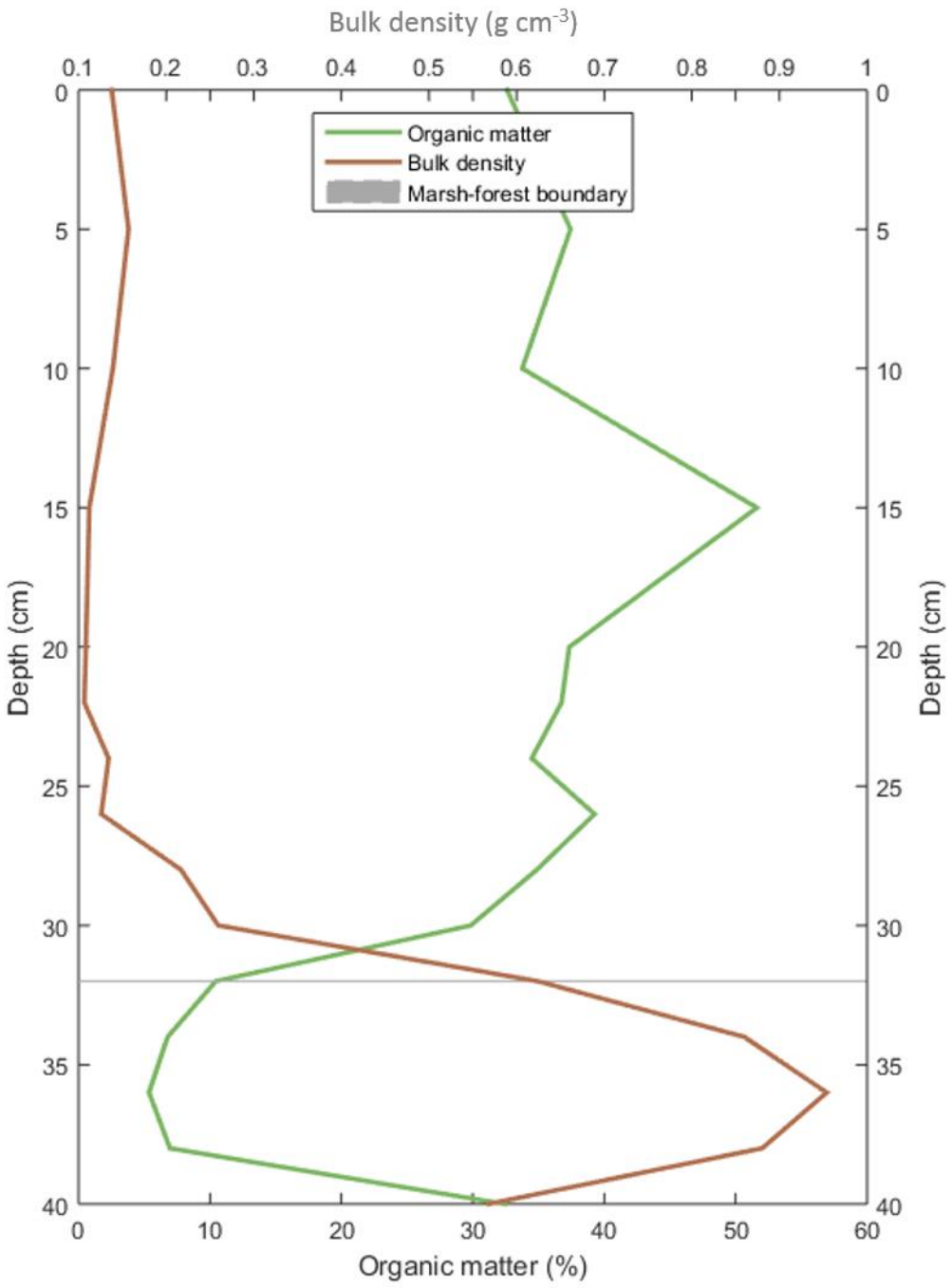

Appendix Fig. 13 | G17 core profile (Goodwin Island). *Organic matter (%) (green) and bulk density (g cm^{-3}) (brown) were used to determine the depth of the historic marsh-forest boundary (gray envelope). Bulk density generally increased with depth, while organic matter decreased. We defined brown, high organic, mineral-poor soil as marsh (organic matter > 10%, bulk density < 0.5 g cm^{-3}), and gray, clay-rich, low organic soil as terrestrial (organic matter < 10%, bulk density > 0.5 g cm^{-3}). The gray envelope represents the upper and lower extend of marsh-forest boundary determined by organic matter and bulk density. A larger envelope indicates larger discrepancies between both methods. The average depth of the historic marsh-forest boundary at G17 is 32 cm.*

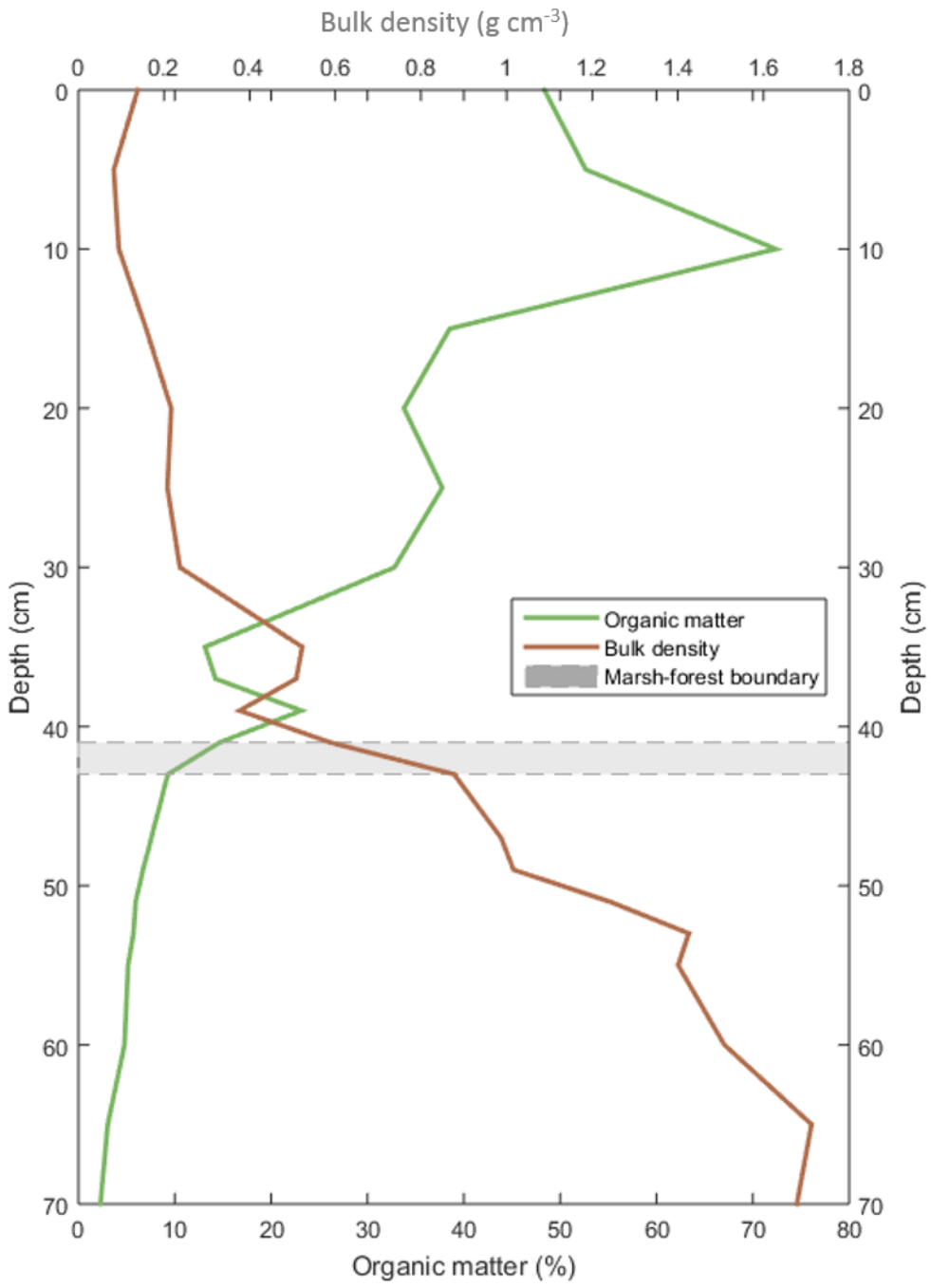

Appendix Fig. 14 | G18 core profile (Goodwin Island). *Organic matter (%) (green) and bulk density (g cm^{-3}) (brown) were used to determine the depth of the historic marsh-forest boundary (gray envelope). Bulk density generally increased with depth, while organic matter decreased. We defined brown, high organic, mineral-poor soil as marsh (organic matter > 10%, bulk density < 0.5 g cm^{-3}), and gray, clay-rich, low organic soil as terrestrial (organic matter < 10%, bulk density > 0.5 g cm^{-3}). The gray envelope represents the upper and lower extend of marsh-forest boundary determined by organic matter and bulk density. A larger envelope indicates larger discrepancies between both methods. The average depth of the historic marsh-forest boundary at G18 is 43 cm.*

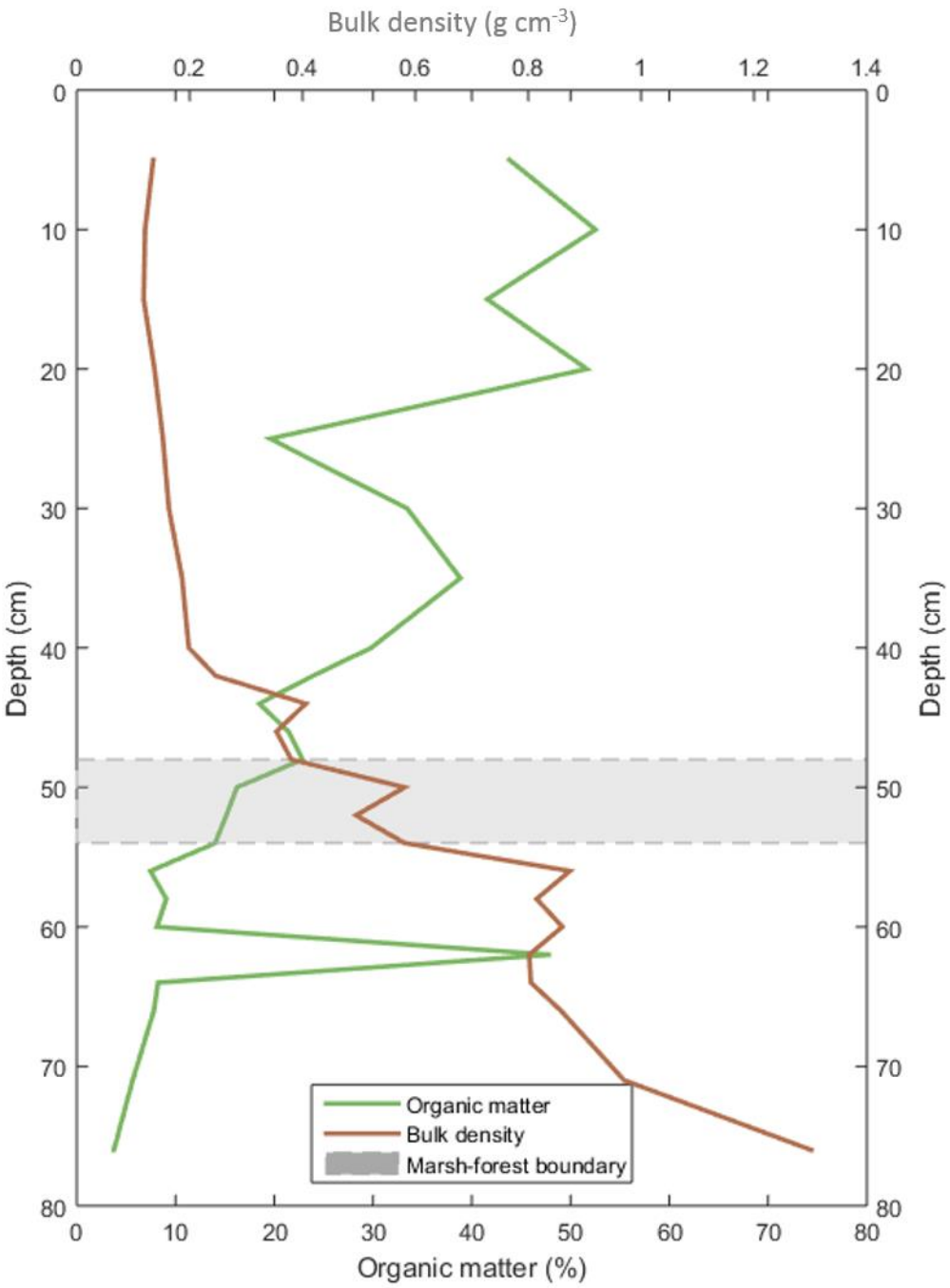

Appendix Fig. 15 | G13 core profile (Goodwin Island). *Organic matter (%) (green) and bulk density (g cm^{-3}) (brown) were used to determine the depth of the historic marsh-forest boundary (gray envelope). Bulk density generally increased with depth, while organic matter decreased. We defined brown, high organic, mineral-poor soil as marsh (organic matter > 10%, bulk density < 0.5 g cm^{-3}), and gray, clay-rich, low organic soil as terrestrial (organic matter < 10%, bulk density > 0.5 g cm^{-3}). The gray envelope represents the upper and lower extend of marsh-forest boundary determined by organic matter and bulk density. A larger envelope indicates larger discrepancies between both methods. The average depth of the historic marsh-forest boundary at G13 is 51 cm.*

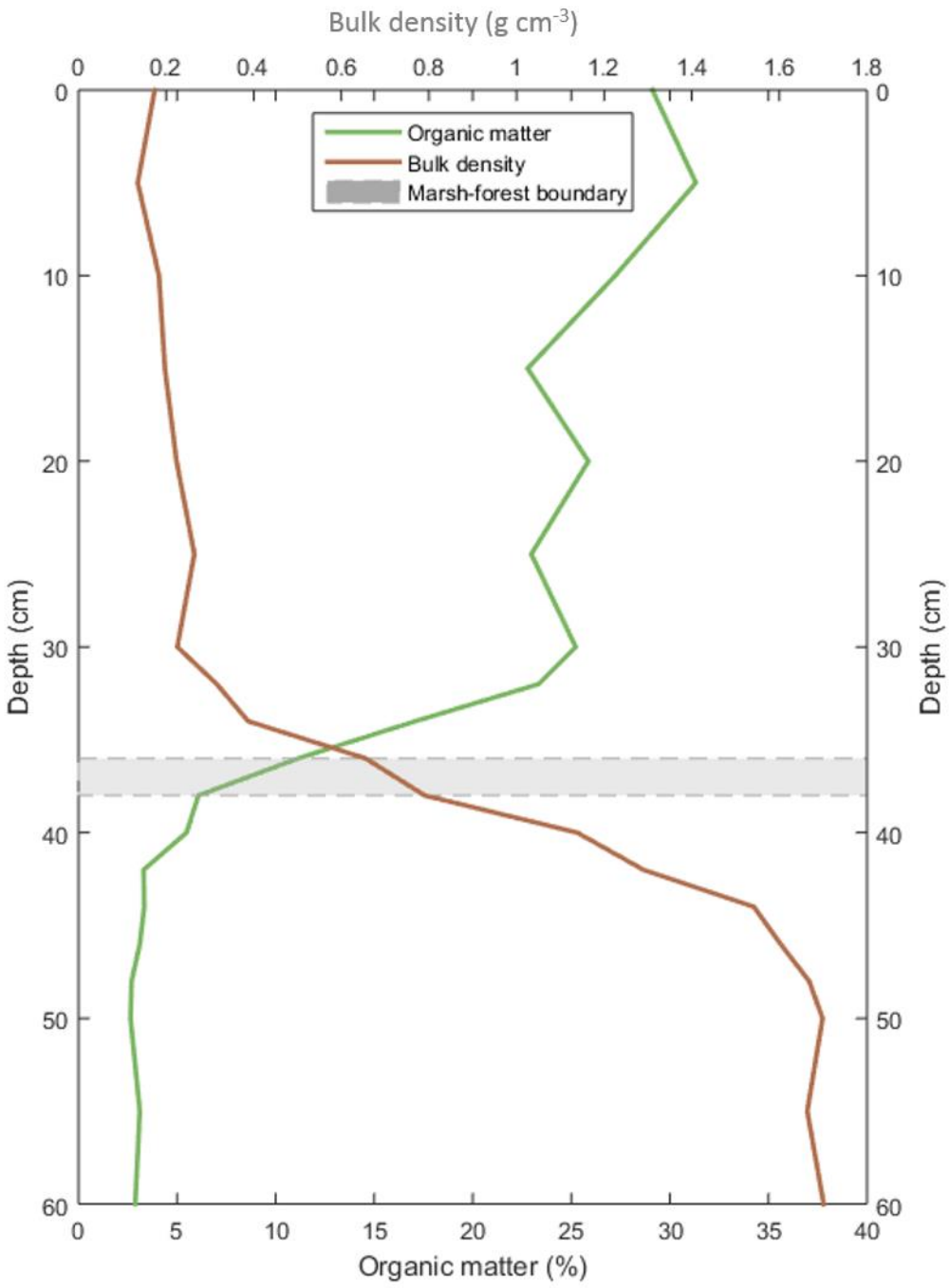

Appendix Fig. 16 | G19 core profile (Goodwin Island). *Organic matter (%) (green) and bulk density (g cm^{-3}) (brown) were used to determine the depth of the historic marsh-forest boundary (gray envelope). Bulk density generally increased with depth, while organic matter decreased. We defined brown, high organic, mineral-poor soil as marsh (organic matter > 10%, bulk density < 0.5 g cm^{-3}), and gray, clay-rich, low organic soil as terrestrial (organic matter < 10%, bulk density > 0.5 g cm^{-3}). The gray envelope represents the upper and lower extend of marsh-forest boundary determined by organic matter and bulk density. A larger envelope indicates larger discrepancies between both methods. The average depth of the historic marsh-forest boundary at G19 is 38 cm.*

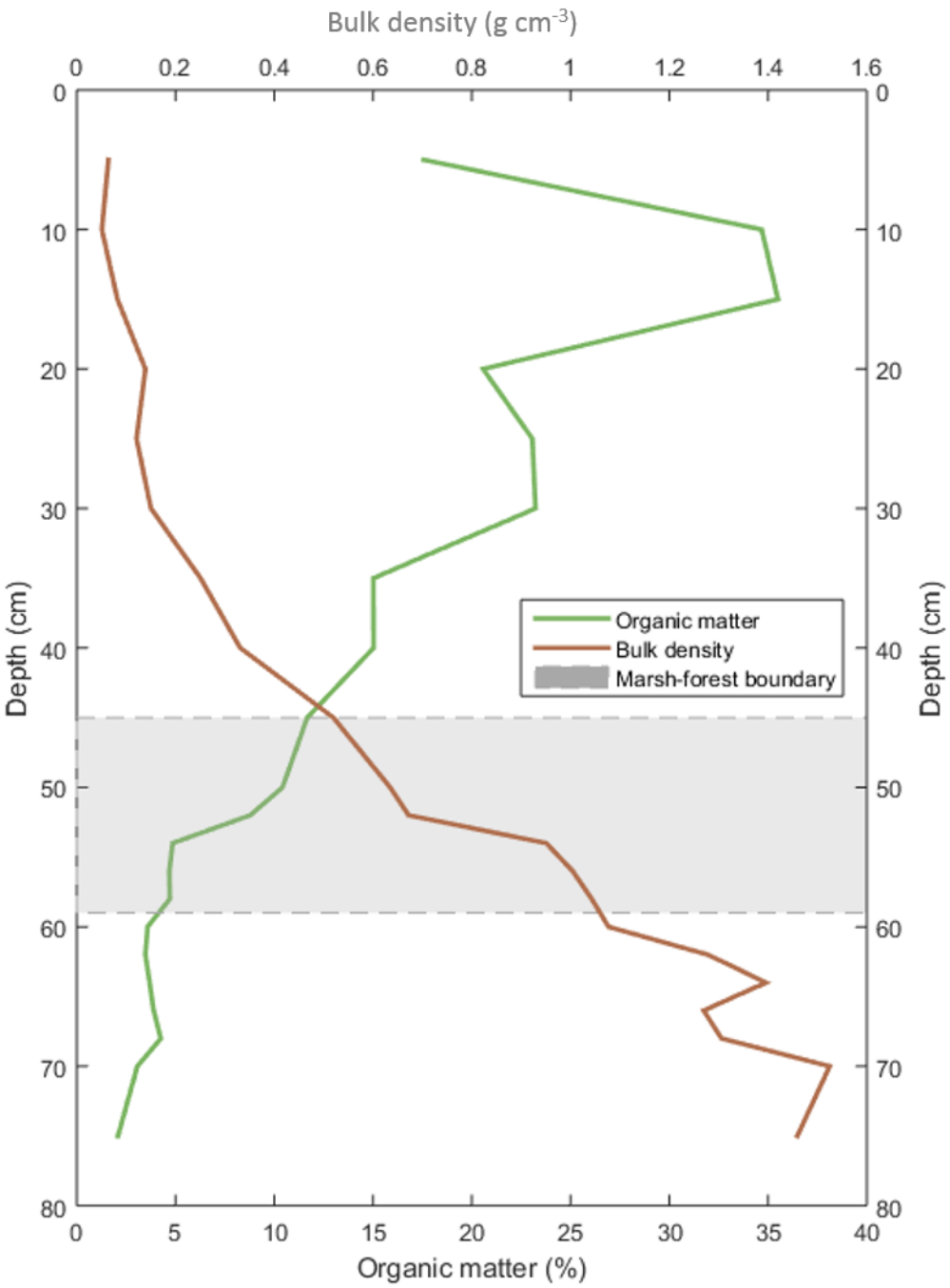

Appendix Fig. 17 | G20 core profile (Goodwin Island). *Organic matter (%) (green) and bulk density (g cm^{-3}) (brown) were used to determine the depth of the historic marsh-forest boundary (gray envelope). Bulk density generally increased with depth, while organic matter decreased. We defined brown, high organic, mineral-poor soil as marsh (organic matter > 10%, bulk density < 0.5 g cm^{-3}), and gray, clay-rich, low organic soil as terrestrial (organic matter < 10%, bulk density > 0.5 g cm^{-3}). The gray envelope represents the upper and lower extend of marsh-forest boundary determined by organic matter and bulk density. A larger envelope indicates larger discrepancies between both methods. The average depth of the historic marsh-forest boundary at G20 is 52 cm.*

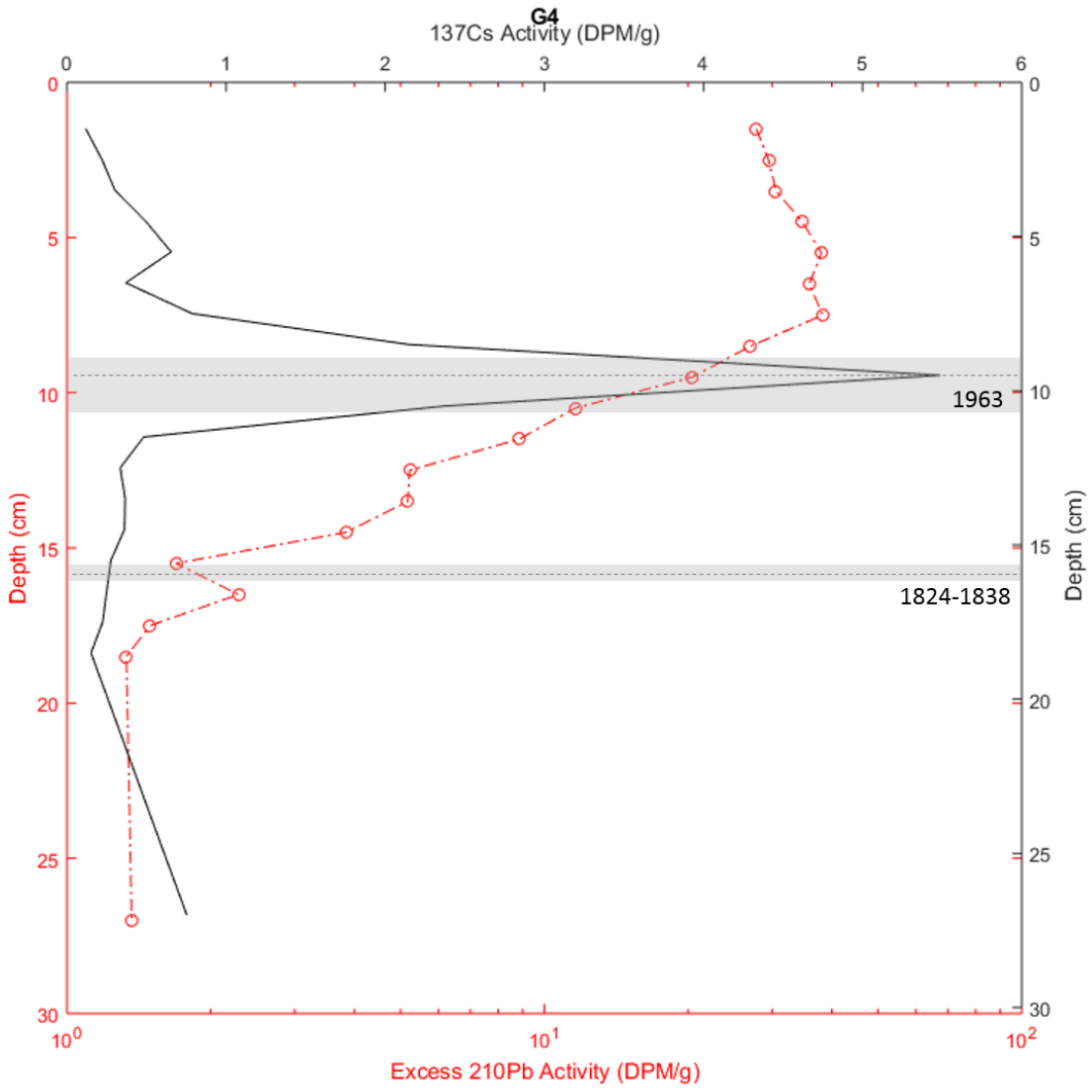

Appendix Fig. 18 | G4 ^{210}Pb and ^{137}Cs profile (Goodwin Island). *Excess ^{210}Pb activity (red) and ^{137}Cs activity (black) were measured for each core. Nuclear weapon testing started in ~1954 and created a peak fallout deposition of ^{137}Cs on Earth's surface in 1963 (Pennington et al. 1976; Allison et al. 2005). Peak ^{137}Cs concentrations indicate the year 1963, and accretion rates are calculated by dividing the depth of the ^{137}Cs peak (cm) by 53 years (i.e. the years that have passed since 1963 and core collection). ^{210}Pb accretion rates were derived by multiplying the slope of the excess ^{210}Pb activity and core depth with the ^{210}Pb radioactive decay constant, assuming constant accumulation through time (0.03114 yr^{-1}) (Donnelly and Bertness 2001; Hussein 2009), and age of the buried marsh-forest boundary was derived by multiplying accretion rates with the previously determined peat thickness (Appendix Fig. 5). The gray envelope represents uncertainties associated with ^{137}Cs, ^{210}Pb measurements, and the depth of the marsh-forest boundary.*

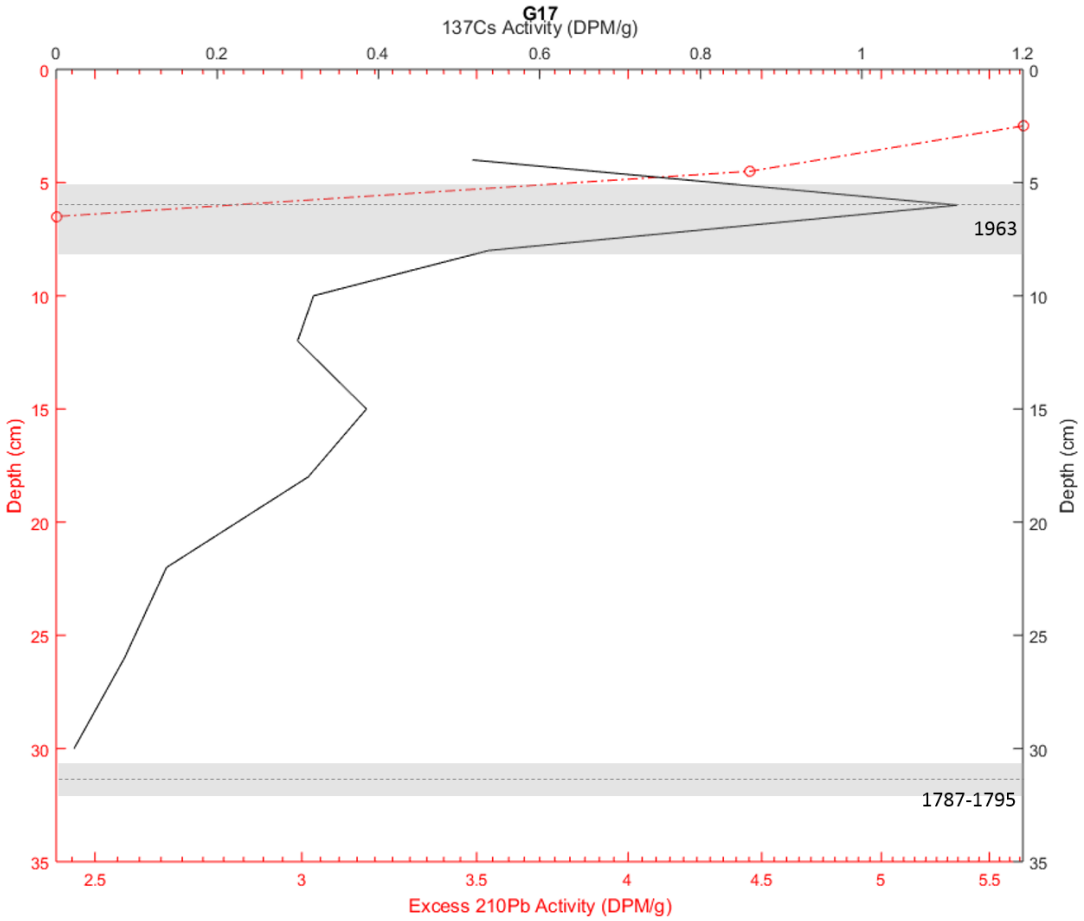

Appendix Fig. 19 | G17 ^{210}Pb and ^{137}Cs profile (Goodwin Island). *Excess ^{210}Pb activity (red) and ^{137}Cs activity (black) were measured for each core. Nuclear weapon testing started in ~1954 and created a peak fallout deposition of ^{137}Cs on Earth's surface in 1963 (Pennington et al. 1976; Allison et al. 2005). Peak ^{137}Cs concentrations indicate the year 1963, and accretion rates are calculated by dividing the depth of the ^{137}Cs peak (cm) by 53 years (i.e. the years that have passed since 1963 and core collection). ^{210}Pb accretion rates were derived by multiplying the slope of the excess ^{210}Pb activity and core depth with the ^{210}Pb radioactive decay constant, assuming constant accumulation through time (0.03114 yr^{-1}) (Donnelly and Bertness 2001; Hussein 2009), and age of the buried marsh-forest boundary was derived by multiplying accretion rates with the previously determined peat thickness (Appendix Fig. 13). The gray envelope represents uncertainties associated with ^{137}Cs, ^{210}Pb measurements, and the depth of the marsh-forest boundary.*

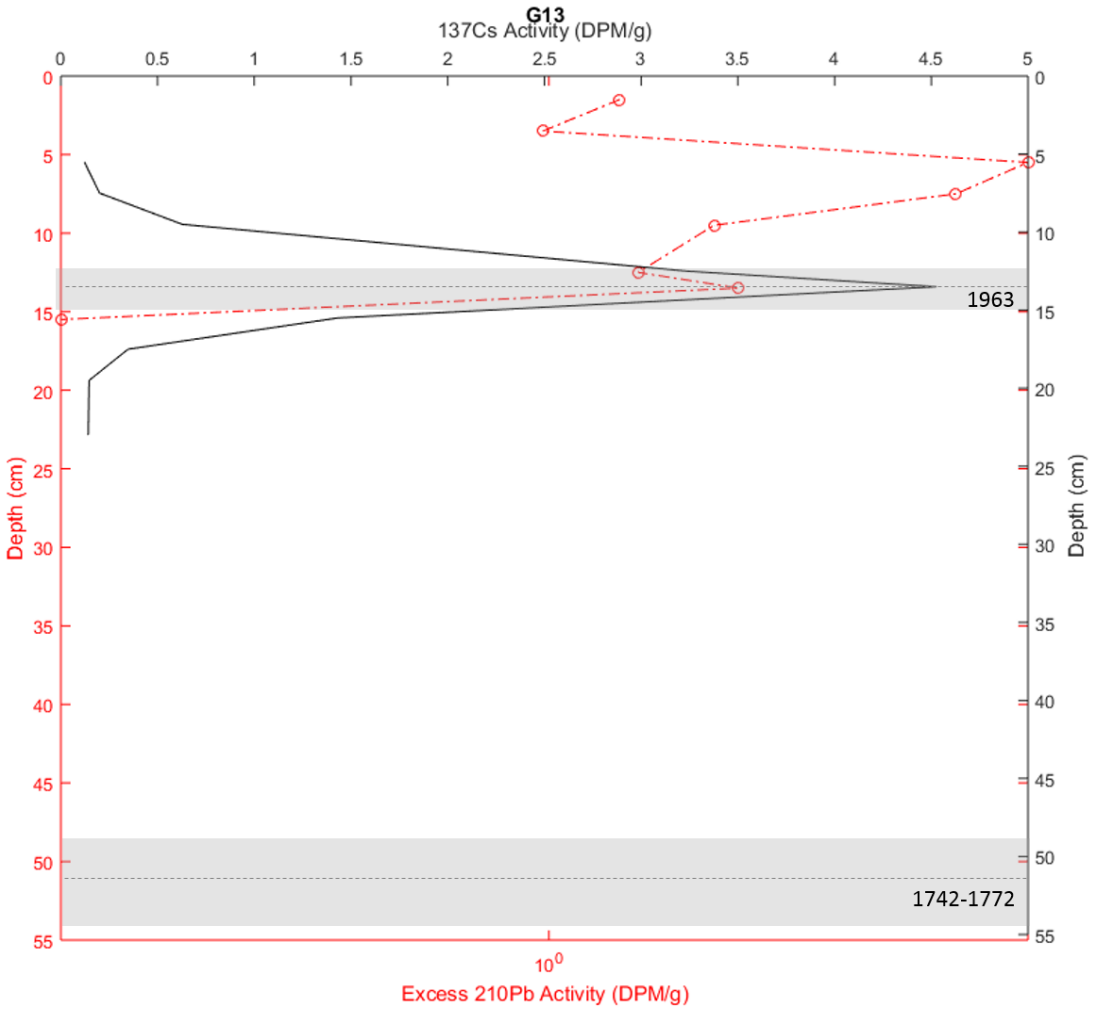

Appendix Fig. 20 | G13 ^{210}Pb and ^{137}Cs profile (Goodwin Island). *Excess ^{210}Pb activity (red) and ^{137}Cs activity (black) were measured for each core. Nuclear weapon testing started in ~1954 and created a peak fallout deposition of ^{137}Cs on Earth's surface in 1963 (Pennington et al. 1976; Allison et al. 2005). Peak ^{137}Cs concentrations indicate the year 1963, and accretion rates are calculated by dividing the depth of the ^{137}Cs peak (cm) by 53 years (i.e. the years that have passed since 1963 and core collection). ^{210}Pb accretion rates were derived by multiplying the slope of the excess ^{210}Pb activity and core depth with the ^{210}Pb radioactive decay constant, assuming constant accumulation through time (0.03114 yr^{-1}) (Donnelly and Bertness 2001; Hussein 2009), and age of the buried marsh-forest boundary was derived by multiplying accretion rates with the previously determined peat thickness (Appendix Fig. 15). The gray envelope represents uncertainties associated with ^{137}Cs, ^{210}Pb measurements, and the depth of the marsh-forest boundary.*

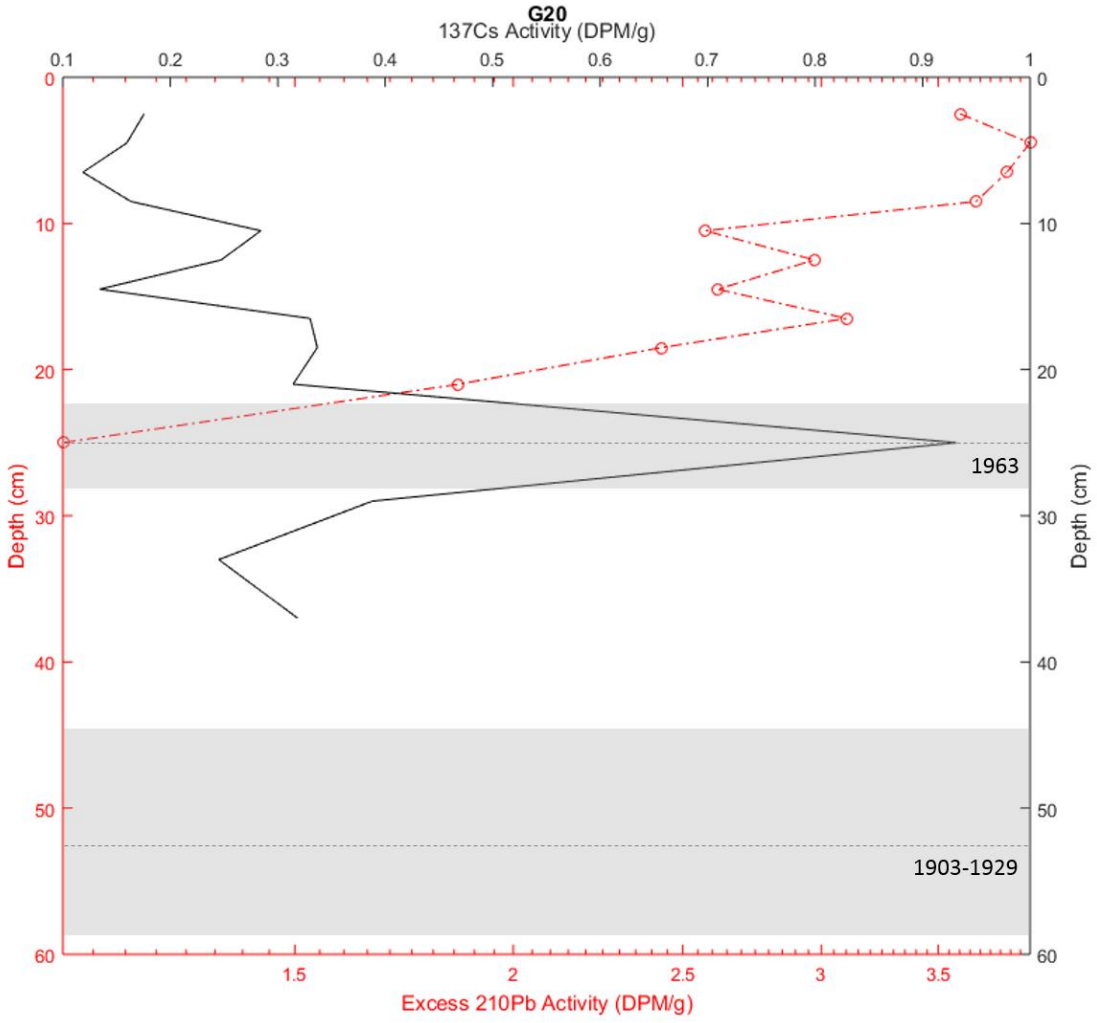

Appendix Fig. 21 | G20 ^{210}Pb and ^{137}Cs profile (Goodwin Island). *Excess ^{210}Pb activity (red) and ^{137}Cs activity (black) were measured for each core. Nuclear weapon testing started in ~1954 and created a peak fallout deposition of ^{137}Cs on Earth's surface in 1963 (Pennington et al. 1976; Allison et al. 2005). Peak ^{137}Cs concentrations indicate the year 1963, and accretion rates are calculated by dividing the depth of the ^{137}Cs peak (cm) by 53 years (i.e. the years that have passed since 1963 and core collection). ^{210}Pb accretion rates were derived by multiplying the slope of the excess ^{210}Pb activity and core depth with the ^{210}Pb radioactive decay constant, assuming constant accumulation through time (0.03114 yr^{-1}) (Donnelly and Bertness 2001; Hussein 2009), and age of the buried marsh-forest boundary was derived by multiplying accretion rates with the previously determined peat thickness (Appendix Fig. 17). The gray envelope represents uncertainties associated with ^{137}Cs, ^{210}Pb measurements, and the depth of the marsh-forest boundary.*

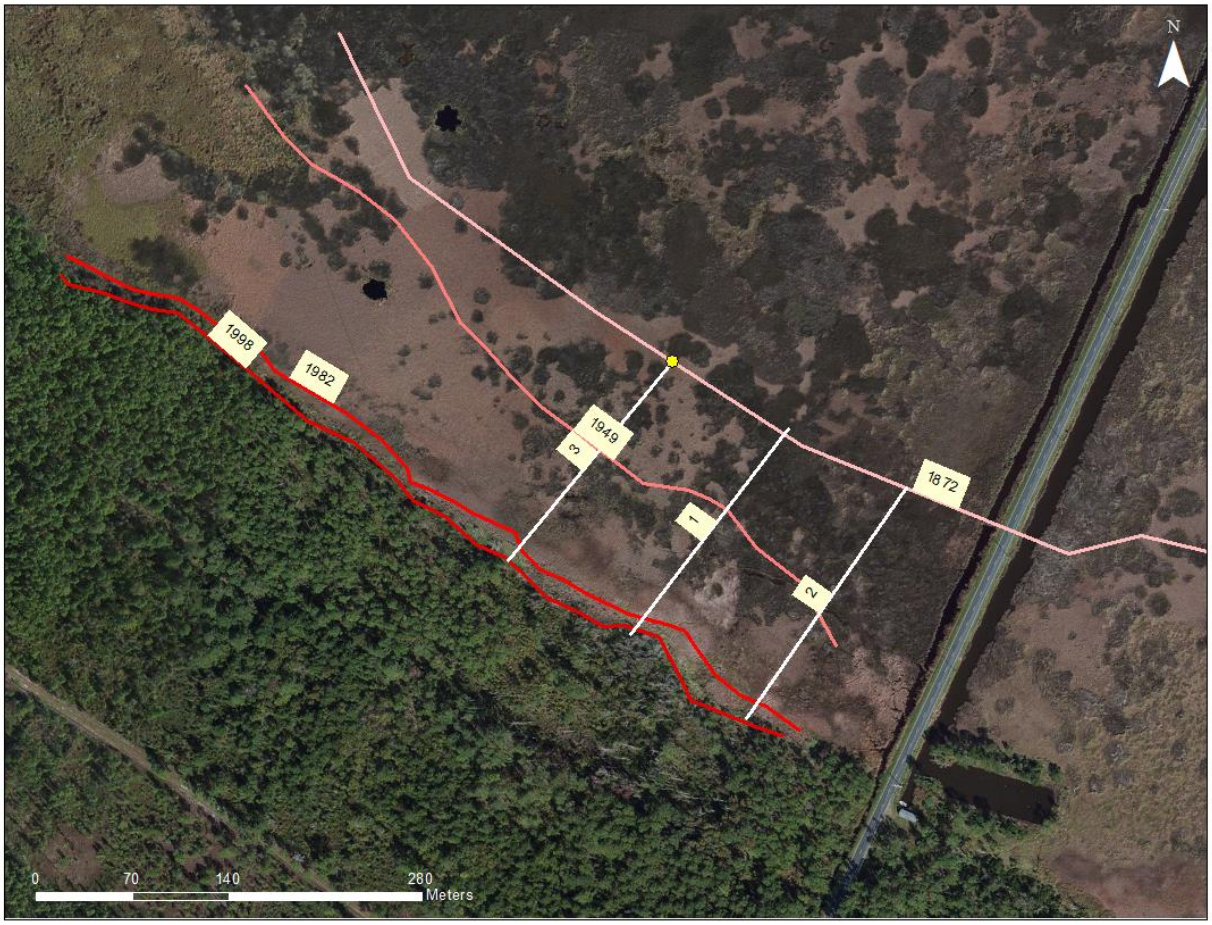

Appendix Fig. 22 | Transect locations at Cedar Island (NC). *To determine the historic elevation of the buried marsh-forest boundary from aerial images and historical maps, cores and elevation measurements were taken along 'modern' transects and compared to the topography based on Young (1995). Transect 1 was the main transect and compared to transect 2 and 3 as a reference (100 m distance). Transects were chosen to best fit previous transects by Young (1995). The lines represent the marsh-forest boundary based on T-sheets (1872), USGS maps (1949), and modern photographs (1982 and 1998). The marsh-forest boundary retreats gradually, with only little retreat since 1982.*

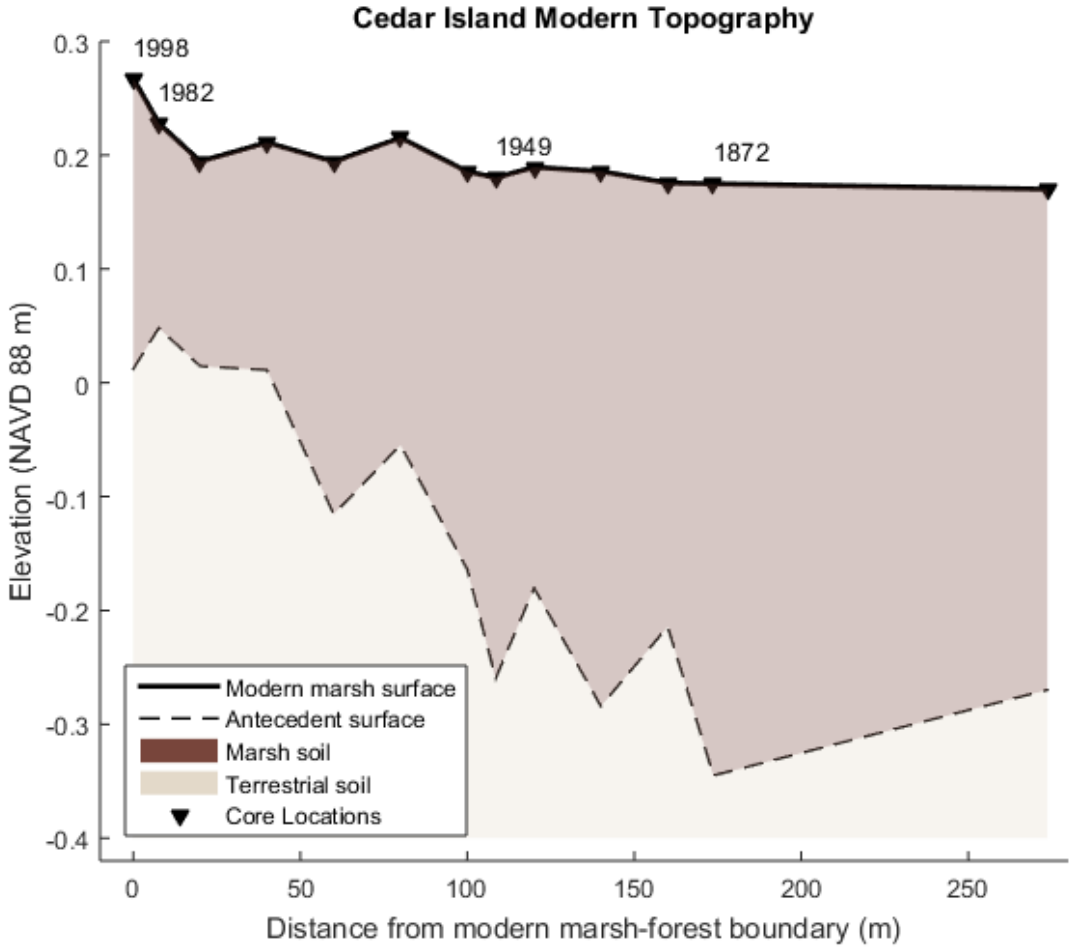

Appendix Fig. 23 | Vertical profile of Cedar Island*. Profile shows vertical (exaggerated) and horizontal position of individual cores (triangles) and the antecedent surface (dashed line) along a transect 1 (Appendix Fig. 22). The reconstructed antecedent surface was used to determine the elevation from aerial images. The underlying topography is gently sloped, and the peat thickness (dark brown) generally increases with increasing distance from the modern forest edge.*

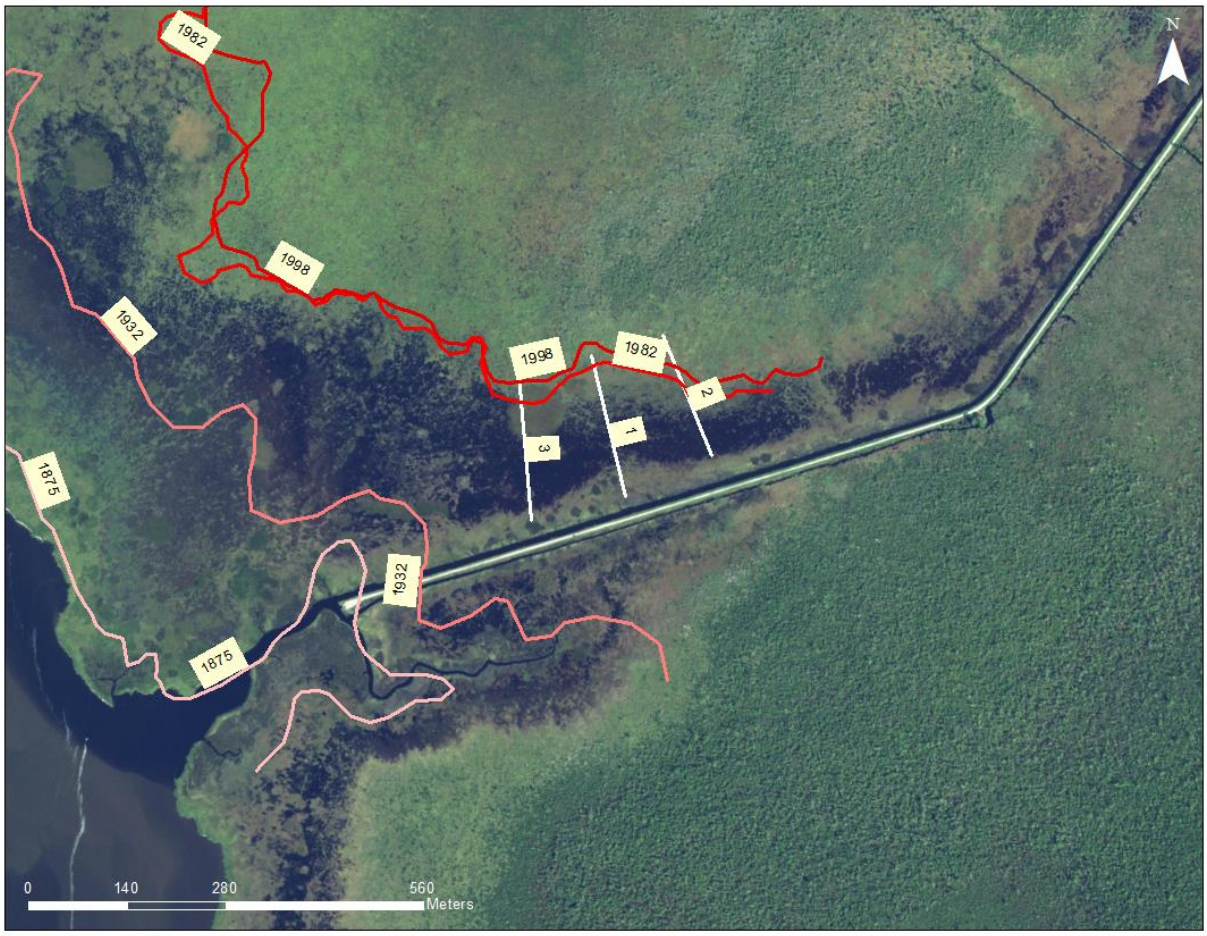

Appendix Fig. 24 | Transect locations at Long Shoal River (NC). *To determine the historic elevation of the buried marsh-forest boundary from aerial images and historical maps, cores and elevation measurements were taken along 'modern' transects and compared to the topography based on Young (1995). Transect 1 was the main transect and compared to transect 2 and 3 as a reference (100 m distance). Transects were chosen to best fit previous transects by Young (1995). The lines represent the marsh-forest boundary based on T-sheets (1875), and modern photographs (1932, 1982 and 1998). The marsh-forest boundary retreats gradually, with only little retreat since 1982.*

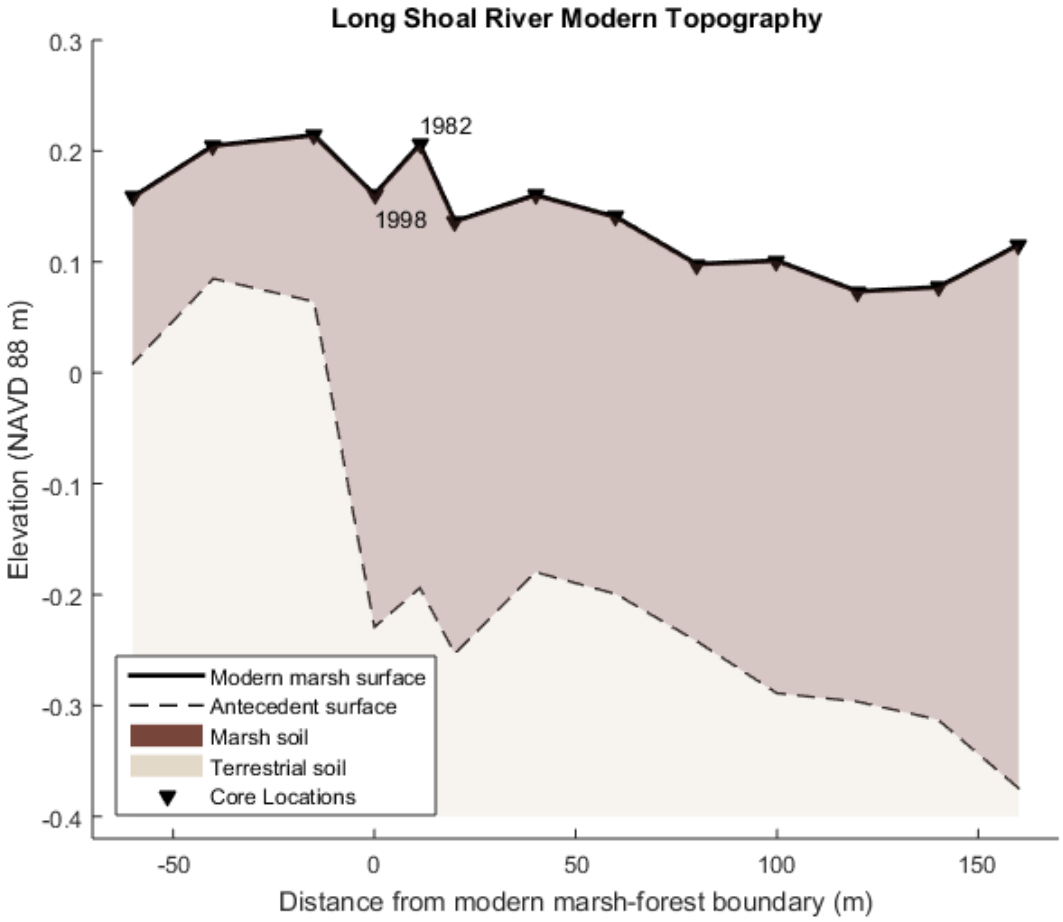

Appendix Fig. 25 | Vertical profile of Long Shoal River. *Profile shows vertical (exaggerated) and horizontal position of individual cores (triangles) and the antecedent surface (dashed line) along a transect 1 (Appendix Fig. 24). The reconstructed antecedent surface was used to determine the elevation from aerial images. The underlying topography is gently sloped, and the peat thickness (dark brown) generally increases with increasing distance from the modern forest edge.*

Appendix Table 1 | Goodwin Island core locations. *Longitude and latitude for each core at Goodwin Island are displayed. Cores are arranged according to location along the transect, with G1 being closest to the modern marsh-forest boundary and G20 being furthest away. Large-diameter push cores were taken for G4, G17, G13, and G20.*

Core	Longitude	Latitude	Elevation (NAVD 88 m)	Peat depth (m)
G1	-76.407367	37.21905	0.543	0.12
G2	-76.407117	37.2191	0.468	———
G3	-76.4069	37.21915	0.435	0.26
G4	-76.406683	37.2192	0.521	0.17
G5	-76.40645	37.21923	0.614	0.24
G6	-76.40625	37.21937	0.576	0.23
G7	-76.406	37.21937	0.538	0.17
G8	-76.405783	37.21938	0.549	0.22
G9	-76.405583	37.21947	0.532	0.18
G10	-76.405367	37.21952	0.568	———
G11	-76.405167	37.21957	0.459	———
G15	-76.404949	37.21962	0.413	0.21
G16	-76.404735	37.21968	0.468	0.16
G12	-76.404483	37.21977	0.563	0.27
G17	-76.404296	37.2198	0.237	0.32
G18	-76.403755	37.21993	0.256	0.43
G13	-76.403517	37.21998	0.332	0.51
G19	-76.403334	37.22004	0.114	0.38
G20	-76.403144	37.22014	0.085	0.52

Appendix Table 2 | Cedar Island core locations. *Longitude and latitude for each core at a historic marsh-forest boundary at Cedar Island are displayed. Cores are arranged according to location along the transect.*

Boundary	Longitude	Latitude	Elevation (NAVD 88 m)	Peat depth (m)
1998	-76.3719	34.91746	0.2672	0.26
1982	-76.3719	34.91752	0.2280	0.18
1949	-76.3713	34.9183	0.1802	0.44
1872	-76.3709	34.91873	0.1749	0.52

Appendix Table 3 | Long Shoal River core locations. *Longitude and latitude for each core at a historic marsh-forest boundary at Long Shoal River are displayed. Cores are arranged according to location along the transect.*

Boundary	Longitude	Latitude	Elevation (NAVD 88 m)	Peat depth (m)
1998	-75.8501	35.60108	0.1606	0.39
1982	-75.8500	35.60099	0.2059	0.40

THESIS CONCLUSION

Previous work predicts widespread marsh loss as a response to sea level rise, but underestimates the potential for marshes to migrate inland. Although anthropogenic barriers may locally prevent marsh migration into retreating coastal forests, my work finds that about 400 km^2 (100,000 acres) of uplands have converted to marshes in the Chesapeake region since the late 1800s, and that this process was responsible for the formation of about 1/3 of all marsh area. Beyond the Chesapeake, my work finds that forest retreat is fundamentally tied to the rate of sea level rise, accelerating through time. Therefore, management efforts that allow marshes to migrate into adjacent uplands may help preserve marshes by exploiting their ability to quickly adapt to environmental change.